2-1-2012

Nano-structured platinum-based catalysts for the complete oxidation of ethylene glycol and glycerol

Akinbayowa Falase

Akinbayowa Falase
Candidate

Chemical and Nuclear Engineering
Department

This dissertation is approved, and it is acceptable in quality and form for publication:

Approved by the Dissertation Committee:

Plamen Atanassov, Chairperson

Dimiter Petsev

Scott Calabrese-Barton

Carolin Lau

Nano-structured Platinum-based Catalysts for the Complete Oxidation of Ethylene Glycol and Glycerol

by

AKINBAYOWA FALASE

B.S. Chemical Engineering, University of New Mexico, 2005

DISSERTATION

Submitted in Partial Fulfillment of the
Requirements for the Degree of

Doctor of Philosophy
Engineering

The University of New Mexico
Albuquerque, New Mexico

December, 2011

DEDICATION

I dedicate this work to my grandparents, Emmanuel Akinrolabu and Janet Omolayo Falase, and Samuel Olawunmi and Esther Wuraola Erinle.

ACKNOWLEDGMENTS

I would like to thank my parents, Dr. Ekundayo and Oladapo Falase, for their love, support, and for providing me with everything I needed to succeed in life. I would like to thank my sisters, Oludolapo and Olutayo who have always believed in, supported, and encouraged me as I grew up. I would like to thank my extended family, my brother in law Seyi Ojo, my niece Ololade Ojo, my uncles, aunts, and my many cousins who have all provided a strong community of love and support.

I would like to thank Plamen Atanassov my advisor for taking me in as a graduate student at a time where I doubted myself in respect to finishing graduate school. I appreciate his frank honesty, his encouragement, and his words of wisdom. I would like to thank the rest of my committee, Drs. Petsev, Calabrese-Barton and Lau, for their time and instructive comments.

I owe many thanks to my friends that have helped me along the way: Andrew, Noel, Randy, Jared, Ulises, Rosalba, Anant, Claudia, Nick, Michelle C, Gustavo, Alexey, Barr, Pablo, Anne, Michelle M, and the rest of the Atanassov lab. Thank you Kristen for sticking with me and helping me to make my experiments work. Thank you for your dedication, your infectious happiness, and your willingness to spend 12 hours in the lab on a weekend for experiments that ultimately sometimes failed. I would like to thank Geoff, Hien, Damien, the CRLS staff, Trini, Lisa, Carson, and the ChNE office staff for providing help and support when I needed it.

I would also like to thank all of my friends that I have met through life that have provided distraction, fun, and a balance to the hectic life working in the lab as a graduate student.

Nano-structured Platinum-based Catalysts for Complete Oxidation of Ethylene Glycol and Glycerol

by

Akinbayowa Falase

B.S. CHEMICAL ENGINEERNG, UNIVERSITY OF NEW MEXICO, 2005
Ph.D., ENGINEERING, UNIVERSITY OF NEW MEXICO, 2011

ABSTRACT

Direct alcohol fuel cells are a viable alternative to the traditional hydrogen PEM fuel cell. Fuel versatility, integration with existing distribution networks, and increased safety when handling these fuels increases their appeal for portable power applications. In order to maximize their utility, the liquid fuel must be fully oxidized to CO_2 so as to harvest the full amount of energy. Methanol and ethanol are widely researched as potential fuels to power these devices, but methanol is a toxic substance, and ethanol has a much lower energy density than other liquids such as gasoline or glucose. Oxidation of complex fuels is difficult to realize, due to difficulty in breaking carbon-carbon bonding and poisoning of the catalysts by oxidative byproducts. In order to achieve the highest efficiency, an anode needs to be engineered in such a way as to maximize activity while minimizing poisoning effects of reaction byproducts. We have engineered an anode that uses platinum-based catalysts that is capable of completely oxidizing ethylene glycol and glycerol in neutral and alkaline media with little evidence of CO poisoning. We have

constructed a hybrid anode consisting of a nano-structured PtRu electrocatayst with an NAD-dependent alcohol dehydrogenase for improved oxidation of complex molecules.

A nano-structured PtRu catalyst was used to oxidize ethylene glycol and glycerol in neutral media. *In situ* infrared spectroscopy was used to verify complete oxidation via CO_2 generation. There was no evidence of poisoning by CO species. A pH study was performed to determine the effect of pH on oxidative current. The peak currents did not trend at 60 mV/pH unit as would be expected from the Nernst equation, suggesting that adsorption of fuel to the surface of the electrode is not an electron-transfer step.

We synthesized nano-structured PtRu, PtSn, and PtRuSn catalysts for oxidation of ethylene glycol and glycerol in alkaline media. The PtRu electrocatalyst the highest oxidative currents and highest stability compared to a nano-structured platinum, PtSn, and PtRuSn catalyst. *In situ* infrared spectroscopy showed complete oxidation of each fuel occurred by the presence of CO_2, with very little poisoning CO species present.

In order to increase oxidative performance in neutral media, a hybrid anode based on nano-structured PtRu and a NAD-dependent alcohol dehydrogenase for the oxidation of ethanol and ethylene glycol was developed. Steady state polarization showed that the hybrid anode had higher current densities than the enzyme or the PtRu electrocatalyst alone. The hybrid anode had higher current densities at concentrations up to 3 M while oxidizing ethanol and ethylene glycol.

The catalyst synthesis, characterization, and experimental results demonstrate the feasibility of fuel cells that can oxidize higher order fuels that platinum based catalysts or enzymes cannot oxidize alone. The cooperative mechanism from co-catalysis using

inorganic and organic catalysts will allow for deep oxidation and improved power generation.

Table of Contents

LIST OF FIGURES

LIST OF TABLES

Chapter 1 - Introduction

Energy security, production, and consumption are major global issues that will become gradually important as nations industrialize and populations increase. The United States Energy Information Administration (EIA) estimated in its' 2011 annual report that consumption of liquid fuels and petroleum in the United States was 36.62 quadrillion Btu per year in 2009, with projections increasing to 39.10 in 2015 and higher in the future[1]. Imports of crude oil, liquid fuels, natural gas and other energy accounted for over half of that figure at 29.53 quadrillion Btu per year in 2009. That figure is projected to fall in 2015 slightly to 29.41 quadrillion Btu per year as alternative energy sources are discovered and local renewable energy sources are discovered. These alternative energy sources utilize advancements in wind, solar, hydro, and chemical means of energy production. There has been a general push to increase utilization of these alternative energy sources as concerns of climate change, geopolitical instability, and cost become pressing issues with traditional energy sources.

The main categories of energy sources alternative to fossil fuels are solar, wind, hydro, nuclear, geothermal and fuel cells. Solar, wind and hydropower sources are intermittent sources of energy that depend on local weather conditions. Nuclear power is efficient, but generates hazardous radioactive waste that is difficult to dispose of and transport. Pollutants from deep earth can contribute to global warming, acid rain, and noxious smells if released from geothermal power plants. Fuel cells are safe to operate, and release water or CO_2 as waste. Hydrogen and direct alcohol fuel cells provide a balance of portability, reliability, and safety. These types of fuel cells can operate indefinitely regardless of local weather conditions as long as fuel is available. Waste products from electricity generation are water for hydrogen fuel cells, and carbon dioxide for

alcohol fuel cells. The defining characteristic of a fuel cell is its ability to convert chemical energy directly to electrical energy. This direct conversion provides higher conversion efficiencies than conventional thermo–mechanical systems, thus extracting more electricity from the same amount of fuel. Since they operate without combustion, they are virtually pollution free and have quieter operation since there are no moving parts[2].

1.1 - Operating principles of an electrochemical device

An aqueous electrochemical process is describes as the conversion of species involving an observable faradic transfer of electrons enabled by the separation of the reaction participants. This is described by an overall reaction

$$\boldsymbol{O + ne^{-} \leftrightharpoons R} \qquad \mathbf{1}$$

where O and R are the oxidized and reduced species participating in the transfer of atoms and electrons process as shown in Figure 1.1.

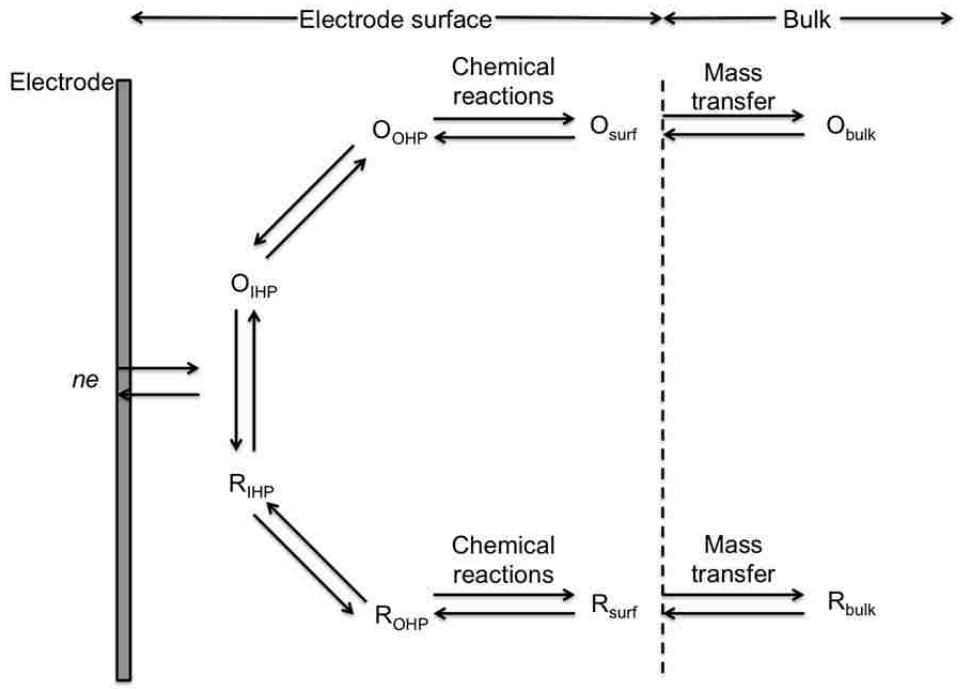

Figure 1.1: Oxidation reduction reactions on an electrode surface (Figure modified from Chou, 2007[3]).

Faradic processes involve the transfer of electrons across the metal-solution interface. This electron transfer is what causes the oxidation-reduction reaction to occur, and are governed by Faraday's law. Non-Faradic processes can occur where there are no charge-transfer reactions due to thermodynamically or kinetically unfavorable conditions, but adsorption or desorption processes can occur that changes the electrode-solution interface.

1.1.1 The Helmholtz layer

The species participating in the oxidation-reduction reaction are located in specific zones or layers. Closest to the surface of the electrode is the inner layer containing solvent molecules and

species that are adsorbed onto the electrode surface in order to compensate for excess electrode charge.

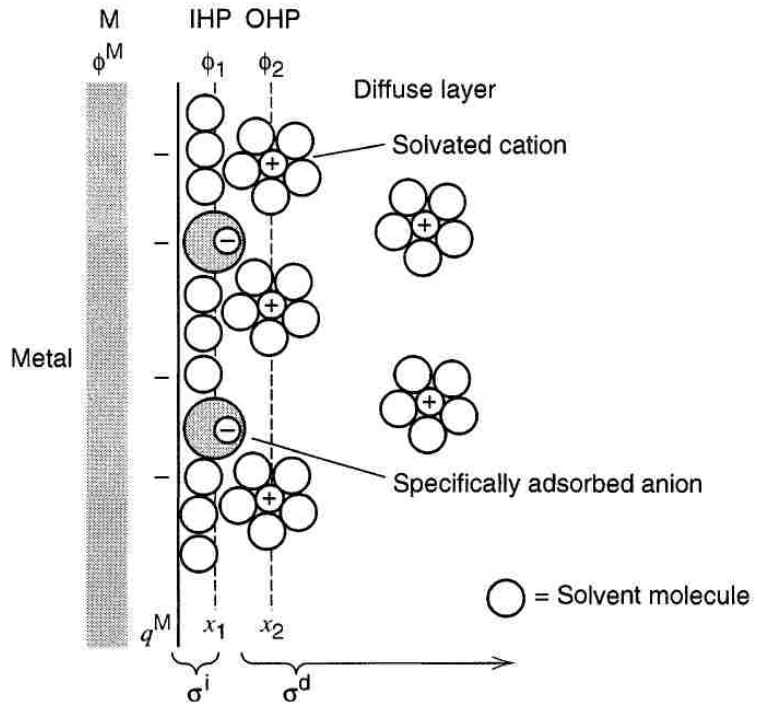

Figure 1.2: Model of double-layer region under conditions where anions are adsorbed[4]

This layer is described as the Helmholtz layer, and it can be further broken up into an inner Helmholtz plane at a distance that is the center of adsorbed ions, and the outer Helmholtz plane whose distance is defined as the distance from the electrode surface to the center of a solvated ion. If the electrode is negatively charged in an aqueous electrolyte, water molecules will orient to the surface to bring their positively charged hydrogen atoms oriented to the electrode, and the negatively charged oxygen atoms away from the surface. If the electrode is positively charged, the opposite situation will occur. The inner Helmholtz plane will pass through the center of these molecules. Molecules that orient themselves on top of the IHP, attracted by long-range coulombic forces constitute the outer Helmholtz plane.

The rate of an electrochemical reaction is governed by the rate of constituent processes such as mass transfer from the bulk to the electrode surface, the electron transfer rate at the surface of the electrode, chemical reactions that occur before or after electron transfer, and surface reactions such as adsorption and desorption from the electrode surface. Since the double layer is composed of ions from the electrolyte, the ionic concentration of the solution influences the thickness and structure of the double layer, which can affect the rates of reactions at the electrode. If there are very low concentrations of electroactive species, the charging current due to the electrolyte could be much larger than the faradic current from the oxido-reduction reaction.

1.1.2 Thermodynamic considerations of a fuel cell

The ultimate performance of a fuel cell is dictated by its polarization curve. A simple way to measure the efficiency of energy conversion of a fuel is to divide the voltage at a given current density by the voltage recorded under open circuit conditions. For a control volume, the change in energy is equal to the summation of the change in kinetic, potential, internal energy and work done on the system. This value is known as the enthalpy of the system. The work term for a fuel cell is due to the transport of electrons across a potential difference, which is related to the cell voltage and the amount of electricity transferred. These terms are bundled in equation 2,

$$\boldsymbol{W = -nFE} \qquad \mathbf{2}$$

where n is the number of electrons transferred, and F is Faraday's constant, 96,485 Coulombs per mol. The maximum amount of work in the system is represented by Gibbs free energy, which is

the change in enthalpy minus the entropy of the system. The unavailable energy that cannot be converted to useful work manifests as the entropy of the system. When describing the free energy of a chemical system, the chemical energy that is released in the fuel cell reaction can be described as the free energy of formation.

$$\Delta \boldsymbol{G}^{\circ} = \Delta \boldsymbol{G}^{\circ}_{\boldsymbol{Products}} - \Delta \boldsymbol{G}^{\circ}_{\boldsymbol{Reactants}} \qquad \mathbf{3}$$

The maximum voltage for a system can then be calculated from $\Delta \boldsymbol{G}^{\circ}$ as

$$\boldsymbol{E} = \frac{-\Delta \boldsymbol{G}^{\circ}}{\boldsymbol{nF}} \qquad \mathbf{4}$$

and for the anode (E^-) and cathode (E^+) reactions

$$\boldsymbol{E}^{\circ} = \boldsymbol{E}^{+} - \boldsymbol{E}^{-} = \frac{-\Delta \boldsymbol{G}_{\boldsymbol{f}}^{+}}{\boldsymbol{nF}} + \frac{-\Delta \boldsymbol{G}_{\boldsymbol{f}}^{-}}{\boldsymbol{nF}} \qquad \mathbf{5}$$

To illustrate this concept, consider a PEM hydrogen/oxygen fuel cell. By definition, the potential for the hydrogen anodic reaction is 0 V vs. a standard hydrogen electrode (SHE), while the potential for the cathode reaction is 1.229 V. The OCP (open circuit potential, E^0) for a hydrogen/oxygen fuel cell operating at standard conditions is 1.229 V vs. SHE. This is the maximum potential that is available in the system as defined by the Gibbs free energy of the system. In ideal conditions at thermodynamic equilibrium for a galvanic cell, the efficiency and

maximum amount of energy that can be used is based on ΔG^R. This value is related to the potential of the system as shown in Equation 4. This is in contrast to an energy source based on combustion where heat is taken from a heat source to expand a gas that then performs useful work. A combustion-based energy source's efficiency depends on the temperature and entropy.

Deviation from ΔG^R is referred to as overpotential. In a galvanic cell (a fuel cell), this term represents the difference in energy recovered vs. the expected energy that thermodynamics would predict at equilibrium. The anode is less negative and the cathode is less positive, resulting in both cathode and anode supplying less energy than thermodynamically possible. A useful exercise to visualize the overpotential is to construct a polarization curve.

The cell's potential is plotted vs. the current of the cell, usually given in terms of a current density. The y-axis signals 0 current and the potential measured is the open circuit potential. Polarization curves can be constructed for the anode and cathode solely, or for the combination of both.

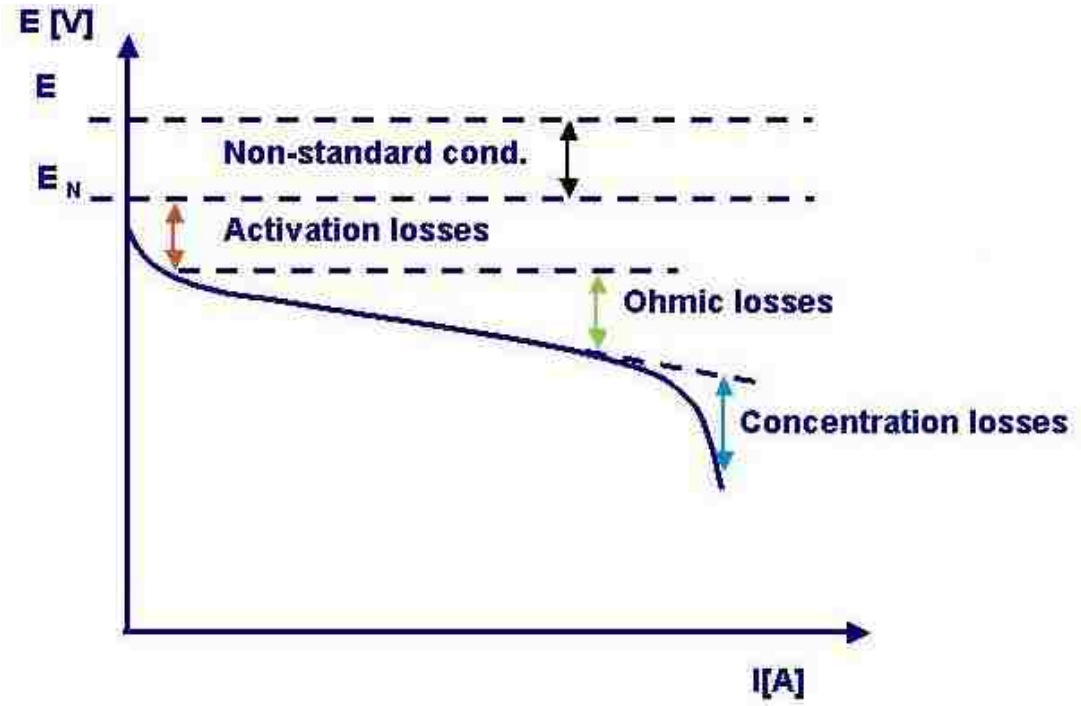

Figure 1.3: Polarization Curve for PEM fuel cell (figure adapted from Hogarth et al.[5])

For non-standard conditions (where the activity of components is not equal to 1), the equilibrium potential can be corrected according to the Nernst equation

$$E = E^{\circ} - \frac{RT}{nF} lnQ \qquad 6$$

where Q is the reaction quotient.

1.1.3 Kinetic considerations of a fuel cell

As soon as current begins to flow, different losses decrease the cell voltage from the expected thermodynamic value. The losses account for various areas in the operation of a fuel cell and can

have characteristic shapes. Operational losses are usually divided into three groups that can be combined to give the operating cell voltage.

$$\eta_{cell} = \eta_{activation} + \eta_{ohmic} + \eta_{concentration} \quad (7)$$

Activation losses occur in low current density regions and are associated with energy needed to force the reaction. This term combines energy associated with activated processes, charge transfer through the electrolyte, and kinetics of the reaction.

Activation losses are a function of the operating temperature and materials used to construct the fuel cell. The tafel equation is used to relate the rate of an electrochemical reaction to the voltage drop due to activation overpotential

$$\eta_{activation} = \beta \cdot ln\left(\frac{i}{i_0}\right) \quad (8)$$

where β (a constant) is the Tafel slope, i_0 is the exchange current density, or the current density where overvoltage increases from 0. The tafel slope is defined by

$$\beta = \frac{RT}{n\alpha F} \quad (9)$$

where R is the ideal gas constant, T is the temperature, and α is the charge transfer coefficient.

Ohmic losses are due to resistances associated with conducting protons through the electrolyte of PEM, and electrons through the electrode. As mentioned earlier, for a PEM fuel cell the conductivity is a function of the hydration state of the membrane. Ohmic losses are proportional to the current density and are defined as

$$\eta_{ohmic} = iR \qquad 10$$

Concentration losses occur in areas of high current densities and arise due to mass transport limitations. If fuel is not able to reach the electrode for reaction, a drop in potential is realized. From the Nerst equation (Equation 6)

$$\eta_{concentration} = \frac{RT}{nF} ln\left(\frac{i_{lim} - i}{i_{lim}}\right) \qquad 11$$

where i_{lim} is defined as

$$i_{lim} = nFD\left(\frac{C^0}{\delta}\right) \qquad 12$$

where D is the diffusion coefficient, δ is the Nerst diffusion layer, and C^0 is the bulk concentration of fuel.

The rate at which a reversible reaction proceeds depends on the surface concentration of species to be reduced or oxidized. For the forward reaction, this relation manifests itself as

$$r_f = k_f C_O(0,t) = \frac{i_c}{nFA} \quad (13)$$

and

$$r_b = k_b C_R(0,t) = \frac{i_a}{nFA} \quad (14)$$

for the backwards reaction, where ic and ia are the cathodic and anodic components of the current, respectively, and is k is the rate constant linking the reaction rate to the concentration at a distance from the surface at time t. Combining the rate expression for the forwards and backwards reaction gives

$$i = i_c - i_a = nFA\left[k_f C_O(0,t) - k_f C_O(0,t)\right] \quad (15)$$

Another way of describing the rates of reactions involves the activation energies of the system. When using this method, the free energy of the reaction can be controlled by the potential of the reaction due to equation 2. The Arrhenius type rate equations for the cathode and anode becomes

$$r_a = k_a C_R exp\left(\frac{-\Delta G_a}{RT}\right) = k_a C_R exp\left(\frac{nF(1-\beta)}{RT}V\right) \quad (16)$$

$$r_c = k_c C_O exp\left(\frac{-\Delta G_c}{RT}\right) = k_c C_O exp\left(\frac{nF(1-\beta)}{RT}V\right) \quad (17)$$

for the anode and cathode reactions, respectively, where β is the asymmetry factor. We can get the overall rate by subtracting the cathode reaction rate from the anode reaction rate. At equilibrium, the equilibrium potential, U is

$$\boldsymbol{U = \frac{RT}{nF} ln\left(\frac{k_c C_O}{k_a C_R}\right)} \qquad \textbf{18}$$

Subtracting the actual potential drop from the equilibrium potential drop gives us the surface overpotential

$$\boldsymbol{\eta_s = V - U} \qquad \textbf{19}$$

where V is the potential difference between electrode and electrolyte, and U is the equilibrium potential difference between the electrode and electrolyte. Substituting, we get

$$\boldsymbol{r = \frac{i}{nF} = k_a C_R exp\left(\frac{nF(1-\beta)}{RT}\eta_s\right) + (1-\beta) ln\left(\frac{k_c C_O}{k_a C_R}\right) - k_c C_O exp\left(\frac{-nF\beta)}{RT}\eta_s\right) - \beta ln\left(\frac{k_c C_O}{k_a C_R}\right)} \qquad \textbf{20}$$

or

$$i = i_0 \left[exp\left(\frac{nF(1-\beta)}{RT}\eta_s\right) - exp\left(\frac{-nF\beta)}{RT}\eta_s\right)\right] \quad 21$$

where

$$i_0 = nFk_a^{\beta}k_c^{1-\beta}C_R^{\beta}C_O^{1-\beta} \quad 22$$

When plotted we get Figure 1.4, where the solid curve shows the total current that is the sum of the dashed traces of the cathodic and anodic currents.

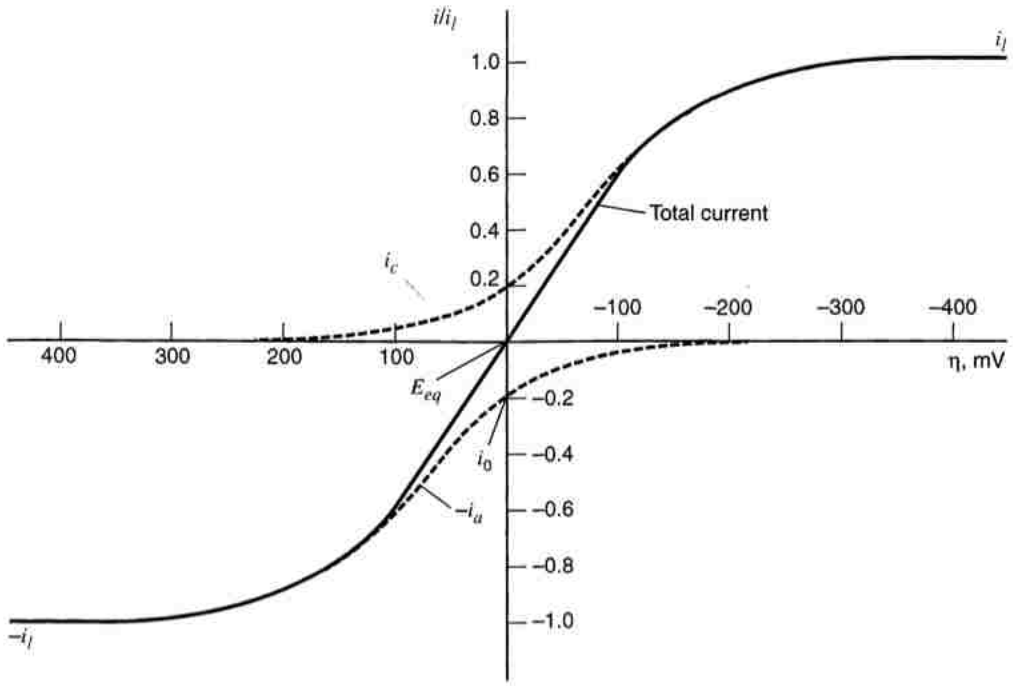

Figure 1.4: Current-overpotential curves[6]

1.2 - Fuel Cell

A fuel cell is a device that converts chemical energy directly to electricity. Combustion engines use the heat generated from burning a hydrocarbon to provide useful work. Nuclear, hydro, geothermal, and coal require energy conversion such as steam or mechanical agitation to operate turbines that generate electricity. Fuel cells are advantageous over these other sources of energy due various factors described by Stambouli et al[2]:

- Energy security: reduce oil consumption, cut oil imports, and increase the amount of the country's available electricity supply.
- Constant power production: generates power continuously unlike backup generators, diesel engines.
- Choice of fuel: allows fuel selection, hydrogen may be extracted from natural gas, propane, butane, methanol and diesel fuel. DAFCs allows for alcohols to be used directly in a fuel cell without reformation steps.
- Clean emissions: Waste emissions from hydrogen fuel cells or DAFCs are water or carbon dioxide.
- Quiet operations: quiet enough to be installed indoors, normal conversation possible near to fuel cell, and hearing protection is not required as for the combustion engines.
- High efficiency: PEM fuel cells are able to convert up to 50–70% of available fuel to electricity.

The fuel cell has two main parts, the anode and the cathode, which are sandwiched around an electrolyte. The fuel is fed to the anode where it is oxidized by a catalyst. The electrons are sent through an external circuit where useful work is performed. The protons or hydroxyl anions

travel through the electrolyte to the cathode or anode, respectively. The electrolyte serves multiple purposes, both to act as a barrier to the electrons from reaching the cathode without passing through the external circuit, to physically separate both the anode and cathode preventing electronic contact, and to conduct the charged ions between the cathode and anode. For a given chemical reaction, there is a barrier, or activation energy that must be overcome before the reaction progresses.

Catalysts are needed to allow the reactions that occur at the anode or cathode to proceed. A catalyst is a material that participates in the reaction to lower the energy barrier for the reaction to progress.

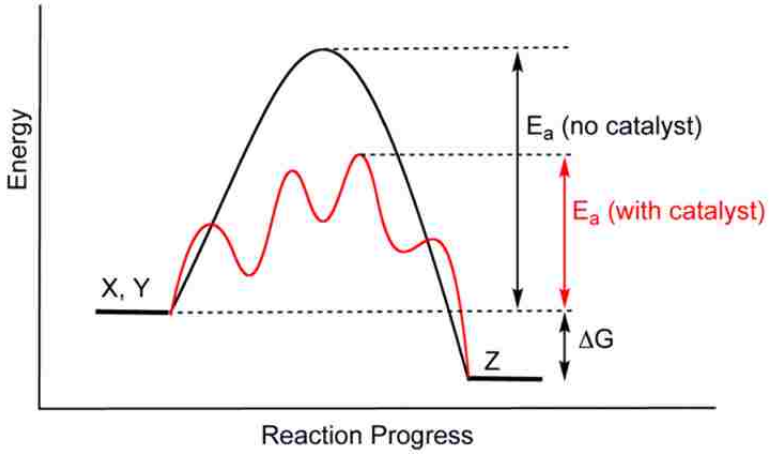

Figure 1.5: Role of catalysts in a reaction

The catalyst acts by increasing the rate of reaction, helping to form intermediate species, or by improving the selectivity towards a desired product, but the catalyst itself is not consumed during the reaction. It may however be inhibited by poisonous species from the reaction. Minimizing these inhibitory species is of great concern to fuel cell catalysis.

1.2.1 Polymer Electrolyte Membrane (PEM) Fuel Cell

A very common type of fuel cell is the Polymer Electrolyte Membrane Fuel Cell (PEM) that operates with a polymer membrane as the electrolyte.

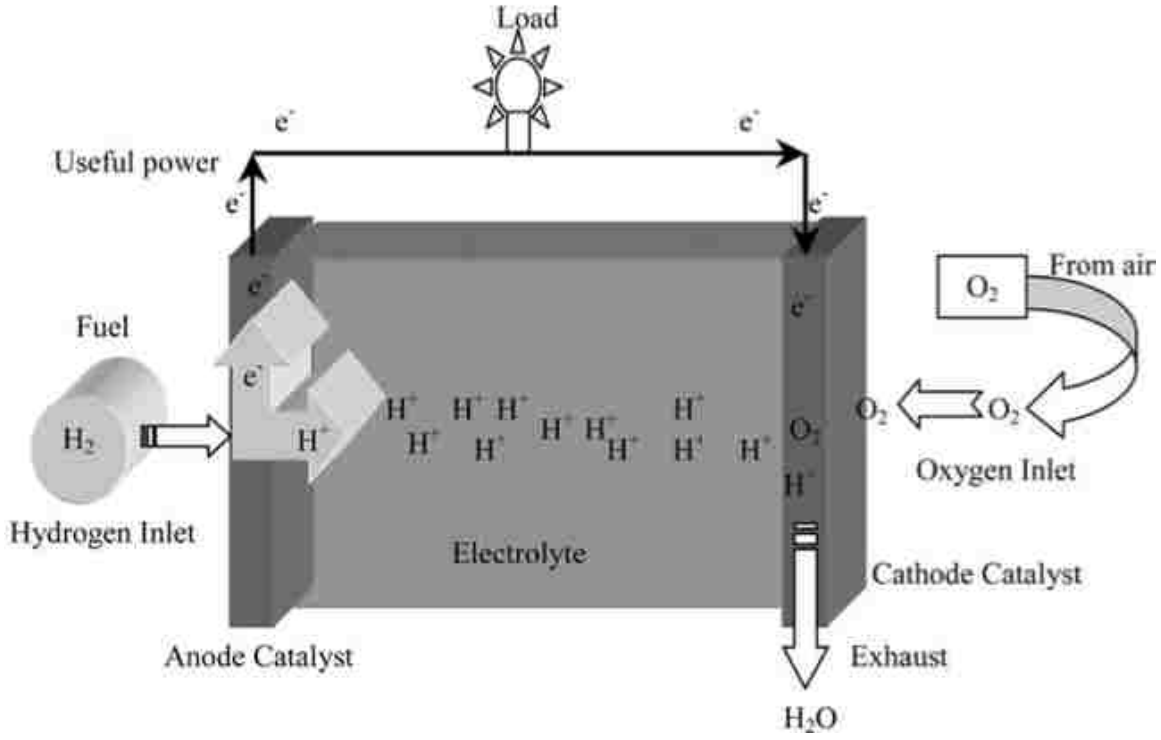

Figure 1.6: PEM fuel cell diagram[2]

Hydrogen fuel from a compressed source or reformed methanol is fed to the anode where it is oxidized over a platinum catalyst. Oxygen is fed to the cathode where it combines with the hydrogen from the anode and the electrons from the external circuit to create water, all over a platinum catalyst as well. The reaction at the anode and cathode, as well as the overall reaction is as follows:

Anode reaction $H_2 \rightarrow 2H^+ + 2e^-$ **23**

Cathode reaction $$\frac{1}{2}O_2 + 2H^+ + 2e^- \rightarrow H_2O$$ **24**

Overall $$H_2 + \frac{1}{2}O_2 \rightarrow 2H_2O$$ **25**

An electrolyte membrane made of Dupont Nafion 117 permits the transport of hydrogen ions while preventing electron conduction[7]. Nafion is a synthetic sulfonated tetrafluoroethylene based fluoropolymer-copolymer that functions as an ionomer due to perfluorovinyl ether groups terminated with sulfonate groups on a tetrafluoroethylene backbone. To function effectively, the Nafion must be hydrated or else it will dry out and lose its proton conductivity.

The cost of the platinum and other noble metals used in these fuel cells is a major factor hindering their widespread adoption as an energy source[8]. The platinum catalyst is sensitive to impurities such as carbon monoxide in the fuel feed. Many groups are researching ways to decrease the amount of platinum needed and to increase tolerance to monoxide and other poisonous species.

1.2.2 Alkaline Fuel Cell

An analog to the acid fuel cell is the alkaline fuel cell. These types of fuel cells were actually the first mature fuel cell technology that powered the Apollo and space shuttle programs, but were later abandoned as PEM fuel cells gained in popularity[9]. They operate at temperatures raging from 20 to 90 °C in a solution of 30 – 35% KOH[10]. The anode and cathode reactions are as follows:

Anode reaction	$H_2 + 2OH^- \rightarrow 2H_2O + 2e^-$	**26**
Cathode reaction	$O_2 + 2H_2O + 4e^- \rightarrow 4OH^-$	**27**
Overall	$H_2 + \frac{1}{2}O_2 \rightarrow 2H_2O$	**28**

There are specific advantages of using alkaline fuel cell technology over acid fuel cells. The major improvement is oxygen reduction kinetics at the cathode[11, 12]. These fuel cells have longer lifetimes, and do not require expensive noble metal catalysts to be used[13, 14]. Noble metal catalysts may be used, but less is needed to achieve a similar reaction rate. Unfortunately, the electrolyte is extremely sensitive to carbon dioxide, forming potassium carbonates that precipitates and blocks the electrodes.

$$2KOH + CO_2 \rightarrow K_2CO_3 + 2H_2O \quad \textbf{29}$$

The decrease in OH from this reaction lowers the conductivity of the electrolyte and decreases the oxygen transport at the cathode. Various groups are working to improve the membrane and performance of alkaline fuel cells[15-19].

1.2.3 Direct Alcohol Fuel Cells (DAFC)

Direct alcohol fuel cells are a promising fuel cell technology. Instead of using hydrogen as fuel, DAFCs feed a liquid alcohol, typically methanol or ethanol to the anode for direct oxidation. This eliminates the need for expensive, bulky reformers that strip hydrogen from methanol to feed to the fuel cell. Liquid alcohol fuels have high theoretical mass energy density, are easier to handle, and integrate in existing infrastructure easier than hydrogen fuel sources. Research into the feasibility of DAFCs have involved both acid and alkaline applications.

Fuels for direct-feed polymer-electrolyte fuel cells

Fuel	Fuel-cell reaction	Specific energy (Wh/g)	Energy density (Wh/cm^3)
Hydrogen	$H_2 + 0.5\,O_2 \rightarrow H_2O$	33.0	2.7*
Carbon	$C + O_2 \rightarrow CO_2$	9.1	19.2
Methane	$CH_4 + 2\,O_2 \rightarrow CO_2 + 2\,H_2O$	14.2	6.0*
Propane	$C_3H_8 + 5\,O_2 \rightarrow 3\,CO_2 + 4\,H_2O$	13.3	6.6*
Decane	$C_{10}H_{22} + 15.5\,O_2 \rightarrow 10\,CO_2 + 11\,H_2O$	12.9	9.4
Methanol	$CH_3OH + 1.5\,O_2 \rightarrow CO_2 + 2\,H_2O$	6.1	4.8
Ethanol	$C_2H_5OH + 3\,O_2 \rightarrow 2\,CO_2 + 3\,H_2O$	8.0	6.3
Ethylene glycol	$C_2O_2H_6 + 2.5\,O_2 \rightarrow 2\,CO_2 + 3\,H_2O$	5.3	5.9
Formaldehyde	$CH_2O + O_2 \rightarrow CO_2 + 2\,H_2O$	4.8	3.9*
Formic acid	$HCOOH + 0.5\,O_2 \rightarrow CO_2 + H_2O$	1.7	2.1
Oxalic acid	$C_2O_4H_2 + 0.5\,O_2 \rightarrow 2\,CO_2 + H_2O$	1.0	2.0
Ammonia	$NH_3 + 0.75\,O_2 \rightarrow 0.5\,N_2 + 1.5\,H_2O$	5.5	3.9*
Hydrazine	$N_2H_4 + O_2 \rightarrow N_2 + 2\,H_2O$	5.2	5.3

* Based on the density of liquefied gas

Figure 1.7: Fuels for direct-feed polymer-electrolyte fuel cells[20]

Of the fuels listed in Figure 1.7, methanol has been the most widely studied due to its relatively high energy density and ability for oxidation at temperatures below 100°C.

1.2.3.1 The Direct Methanol Fuel Cell (DMFC)

The Direct Methanol Fuel Cell (DMFC) is one of the most widely researched fuel cells in the literature, having been studied for the past three decades[21]. Methanol and other small organic molecules are more reactive in alkaline media; so early DAFCs used KOH or NaOH as the electrolyte material. Carbonate formation from complete oxidation as described above limited the performance of these fuel cells so work on DMFCs shifted to acid media where carbonate formation isn't a problem. With this switch came problems such as lower reactivity of methanol, the need for large quantities for precious metal catalysts, and corrosion of fuel cell materials from the acid electrolyte[19].

The reactions for a DMFC in acid electrolyte are as follows:

Anode reaction	$CH_3OH + H_2O \rightarrow CO_2 + 6H^+ + 6e^-$	**30**
Cathode reaction	$\frac{3}{2}O_2 + 6H^+ + 6e^- \rightarrow 3H_2O$	**31**
Overall	$CH_3OH + \frac{3}{2}O_2 \rightarrow 2H_2O + CO_2$	**32**

Early DMFCs suffered from very low performance compared to PEMFCs.

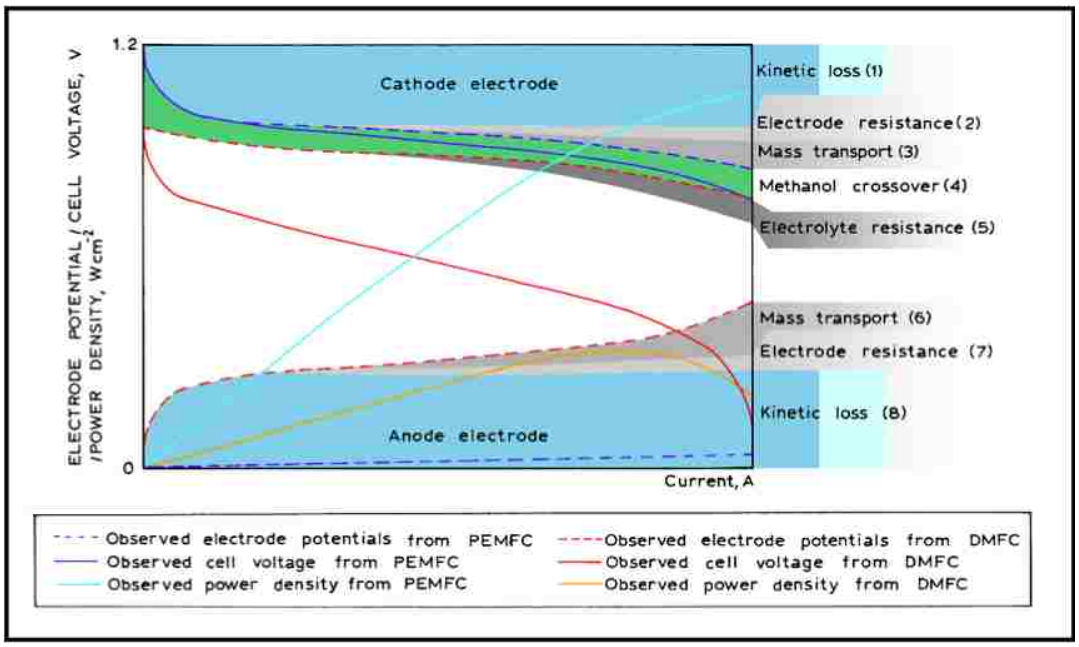

Figure 1.8: Performance losses in a DMFC with dilute MeOH at 80C vs. a PEMFC with pure hydrogen[5]

Using a liquid fuel introduced performance losses at the fuel cell as described by Hogarth et al. Both DMFCs and PEMFCs suffer from sluggish kinetics at the cathode, but there are additional losses at the anode for DMFCs. Compared to a hydrogen PEMFC, DMFCs suffer from higher kinetic losses, electrode resistance, mass transport limitations, and methanol crossover[22, 23]. Water and methanol are able to diffuse through the membrane material to travel from the anode and react at the cathode. Fuel crossover sabotages the performance of the DMFC due to a mixed potential effect at the cathode and flooding. Platinum catalysts used for oxidation of MeOH have strong affinity for CO that poisons the catalyst. A combination of these factors decreases the performance of the DMFC.

1.2.3.2 The Direct Ethanol Fuel Cell (DEFC)

Ethanol is a more attractive fuel for direct oxidation than methanol. Like methanol, it is easy to store and transport however it is less toxic, and ethanol can be produced in great quantities from renewable resources. Ethanol has a higher energy density (8.0 kWh/kg) compared to methanol (6.1 kWh/kg). The half reaction and overall reaction are as follows in an acid electrolyte:

Anode reaction	$\boldsymbol{C_2H_5OH + 3H_2O \rightarrow 2CO_2 + 12H^+ + 12e^-}$	**33**
Cathode reaction	$\boldsymbol{3O_2 + 12H^+ + 12e^- \rightarrow 6H_2O}$	**34**
Overall	$\boldsymbol{C_2H_5OH + 3O_2 \rightarrow 3H_2O + 2CO_2}$	**35**

One notable feature of ethanol is that for complete oxidation, scission of the C-C bond must occur. This is a relatively difficult problem to overcome, and is primarily achieved on platinum catalysts. CO byproducts of ethanol oxidation adsorb strongly to the platinum surface, effectively poisoning it as is the case with DMFCs. Platinum-ruthenium alloys are used in these catalysts to stabilize the reaction and bring hydroxyl groups closer to the reaction sites in order to promote a complete oxidation pathway versus an oxidation pathway that leads to CO.[24-26]

1.2.3.3 DAFCs with higher order fuels

Direct alcohol fuel cells based on fuels more complex than methanol and ethanol have great potential and are gaining interest. Fuels such as glycerol and ethylene glycol are attractive

because they are renewable from biomass, have high energy density, low vapor pressures, low cost, and easy storage and transportation needs. Fuel supply systems for liquid alcohol fuels are compatible or can be made compatible with minimal cost with existing distribution systems. Glycerol is especially of interest due to its production from biodiesel[27]. Global biodiesel production has increased from 530 million gallons in 2004 to 3 billion gallons in 2008[28]. Glycerol, a 10% by weight byproduct of biodiesel production via transesterification has essentially turned into a waste stream from being a once tightly supplied chemical.

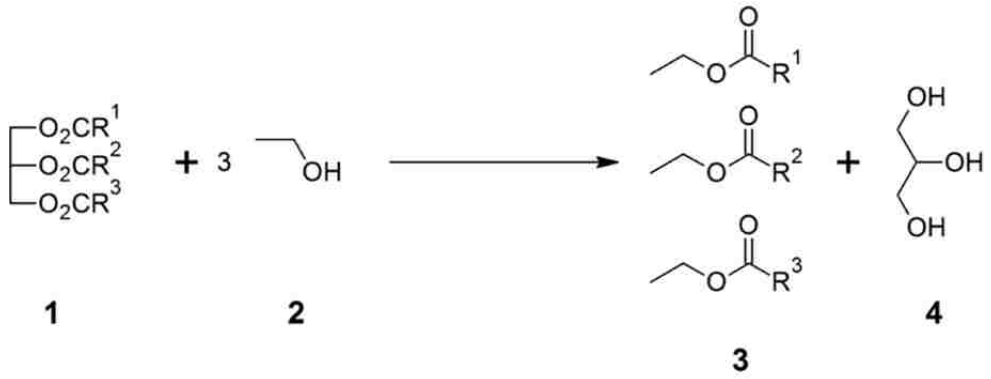

Figure 1.9: Transesterification reaction to form glycerol

Several major obstacles must be overcome before more complex fuels can be used in DAFCs. The amount of reaction intermediates increases as the fuel becomes more complex. Aliphatic alcohols are difficult to electrooxidize completely, with the main products of oxidation being aldehydes, ketones, acids, esters, and CO_2. Splitting of the C-C bond is a difficult task due to its low electron affinity and low ionization energy[29]. DAFCs also have much lower anode performance at room temperature due to poisoning by CO species compared to hydrogen PEMFCs[30] .

Oxidation of these fuels in acid media on a platinum-based catalyst is as follows[31]:

$$C_{x\geq 2}H_yO_z + (2x - z)H_2O \rightarrow xCO_2 + (4x + y - 2z)H^+ + (4x + y - 2z)e^- \quad 36$$

where oxidation of ethylene glycol and glycerol involves a 10 and 14 electron transfer, respectively. Anode kinetics are sluggish at low temperatures due to complex reaction steps for complete oxidation. For an efficient reaction, multi-electron transfer steps should occur simultaneously with adsorption, surface reactions, and desorption of reaction products. Unfortunately, poisoning species produced during electrooxidation can adsorb on platinum active sites causing obstruction of the catalyst and loss of performance.

Ethylene glycol oxidation over platinum and palladium catalysts proceeds through a 4 or 5 intermediate pathway to CO_2[32, 33]. This involves parallel reactions with 2 electron transfer steps.

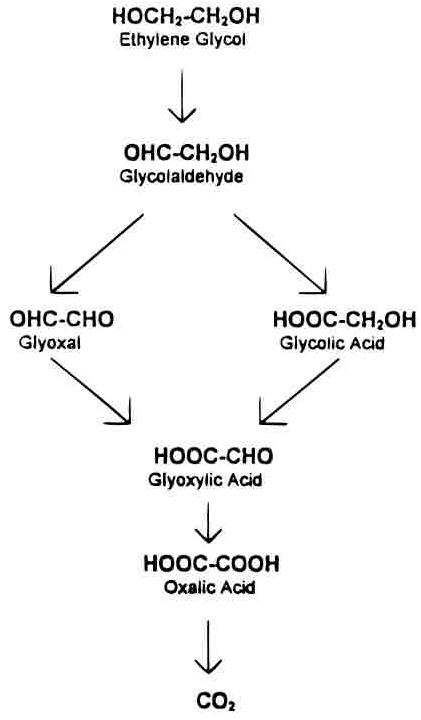

Figure 1.10: Ethylene glycol oxidation reaction pathway[33]

In acid media, the main products of oxidation are glycolic acid and CO2. In alkaline media the main oxidation products are glycolate, oxalate and CO_3^{2-}. Adsorbed CO intermediate species were present in both acid and alkaline media.

Glycerol oxidation is more complicated as it has 1 more C-C bond to break than ethylene glycol. The reaction pathway proceeds through multiple competing steps to oxalic or mesoxalic acid before being oxidized to CO_2[34, 35].

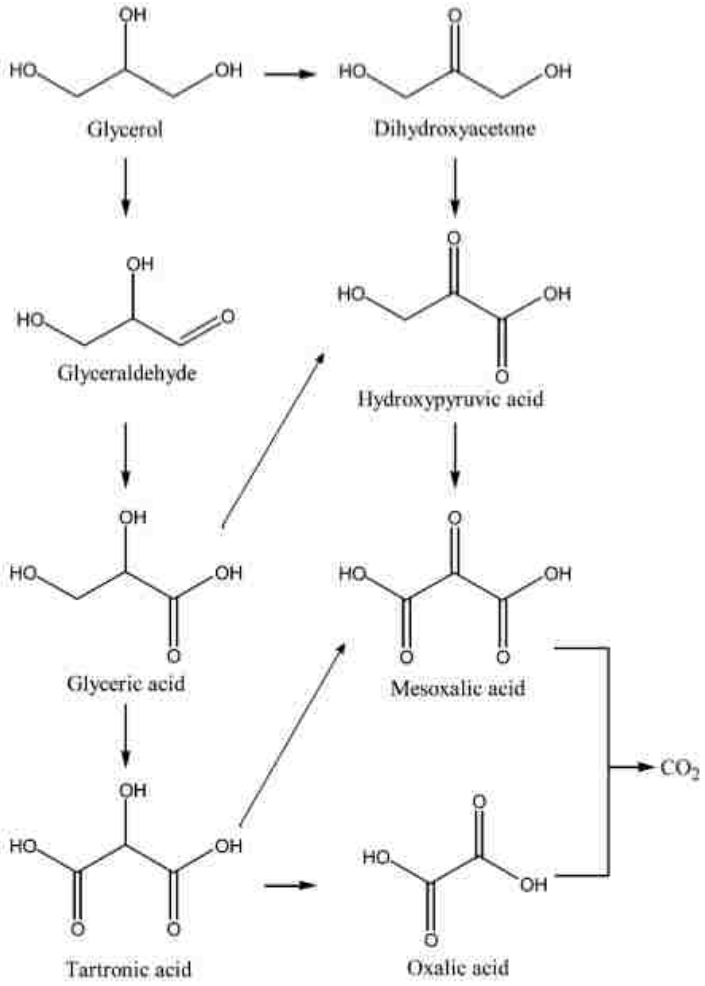

Figure 1.11: Glycerol oxidation pathway[36]

When designing a catalyst for oxidizing these fuels, the main goal is to generate the maximum amount of CO_2 while reducing or eliminating poisonous intermediates and being selective away from oxidation dead ends. A catalyst that does not produce adsorbed CO species would be ideal.

1.2.4 Catalysts for DAFCs

Platinum has very high stability and electrocatalytic activity in fuel cell applications for oxidation of hydrogen and small organic molecules. Polycrystalline and single crystal platinum has been used to oxidize methanol[37-43] and ethanol[44-47]. Unfortunately platinum is an expensive commodity, currently at $1810 USD per troy ounce as of August 2011, with a period average of $1454.60 for the past 5 years.

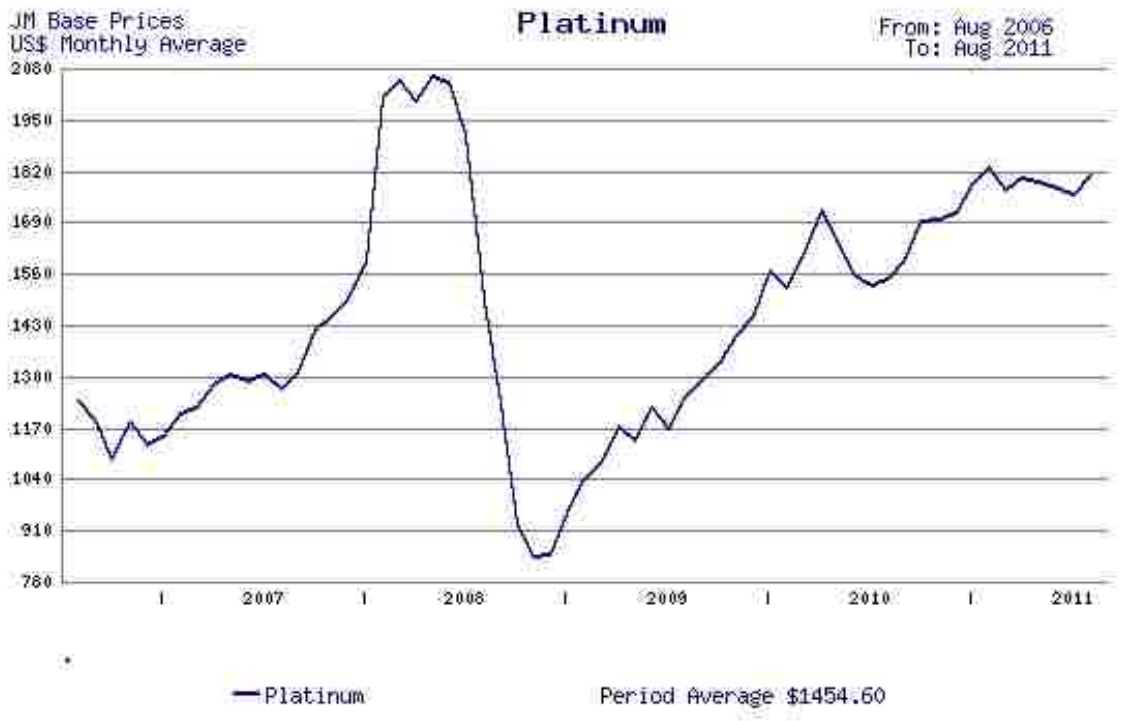

Figure 1.12: Historical price of platinum[48]

In order to decrease the amount of platinum used and improve performance, strategies such as alloying and templating are employed[49]. Alloying platinum with other metals can improve reaction kinetics for C-C bond scission. Cleavage of the C–C bond and promoting adsorbed CO species towards oxidation to CO_2 is favored in the presence of rhodium, ruthenium, tin or osmium alloyed with platinum on the electrode surface[5, 50-71]. The most commonly used catalyst is PtRu/C. The ruthenium participates in electronic modification that decreases the binding energy of CO on the platinum while binding OH to the ruthenium sites[24, 72]. This bifunctional mechanism also serves to adsorb hydroxyls at a lower potential that platinum can, and thus promotes fuel oxidation to CO_2 due to the proximity of oxygen species to adsorbed organic species on the platinum. Improved performance gains in the oxidation of methanol, ethanol, and other alcohol fuels mitigate the drawback of the high prices of the metals used to alloy with the platinum.

1.2.4.1 Templating

Templating the support of the catalyst can achieve increased utilization and lower cost, especially in the case of platinum based catalysts. Templating the support increases the surface area per gram of material, improving the mass activity of the catalyst due to more surface area being exposed to electrolyte and fuel[73-76]. Silica is commonly used as a templating material to make high surface area carbons. The silica acts as an agent that patterns the catalytic material or support, and is then sacrificed by calcination or etching leaving the templated structure behind. SBA-15, a hexagonally ordered mesoporous silica developed by the Stucky group is commonly used to synthesize ordered mesoporous carbons with high surface areas[77-80]. A templating procedure based on SBA-15 can yield carbon with surface areas of 1300 m^2/g[81]. Depositing

nanoscale platinum on the surface results in performance gains much higher than bulk platinum since a larger surface area of platinum is exposed to the fuel, which results in more active sites available for reaction and thus more current generated.

Unsupported structured catalysts can provide long-term stability because they do not suffer from carbon corrosion effects, while having high activity and/or high catalytic area, which is dependent on the synthesis method used. Historically, unsupported platinum was the first working electrocatalyst in low temperature fuel cells. Platinum black electrodes developed in the 1960s and with particle sizes approximately 5-50 nm and surface areas of 15 m^2/g became the primary electrocatalyst due to lower loadings, and decent durability. Over time coarsening of the platinum nanoparticles and degradation of the carbon support causes a loss of performance in fuel cells with supported catalysts. An unsupported platinum based catalyst could possibly provide longer lifetimes than a catalyst supported on traditional carbon because corrosion is eliminated[82]. A study by Liu et al. comparing the performance of a supported and unsupported PtRu electrocatalyst showed that the unsupported catalyst required 4x the loading amount for comparable performance[83]. Unsupported catalysts though do allow for very thin catalytic layers to be used with high loadings, which decreases ohmic drop and allows for better transport of fuel though the catalyst layer[84, 85]. In order to be comparable to supported electrocatalysts, synthesis methods that increase the mass activity by reducing nanoparticle size, increasing the surface area, and improving the specific activity need to be developed and utilized.

1.2.4.2 Spray pyrolysis

Spray pyrolysis is a rapid, consistent method of creating templated materials, with the ability for scale up. Bulk templating techniques are inefficient because the templating does not permeate through the entirety of the sample resulting in poor homogeneity. With spray pyrolysis, impregnation of the template with the catalytic precursors does not need to be repeated multiple times as with bulk templating methods, as the precursors are mixed intimately with the templating silica in a precursor solution[86]. Synthesis procedures for electrocatalysts can be tailored in many different ways. Compositions of the final catalysts are simply determined by the precursor solution. The pyrolysis temperature can control alloying and phase segregation of multi-metal catalysts. The degree of oxidation can be tailored by varying the pyrolysis temperature and also the composition of the carrier gas. The atomizer used in generating the aerosol can influence particle sizes and distributions and the spray pyrolysis process is compatible with surfactants that are used to template materials. The most beneficial aspect of spray pyrolysis is the ability to scale up synthesis of catalysts from a bench top scale producing a few grams to an industrial process capable of producing kilogram quantities or more.

1.2.5 Biological fuel cells

Another class of fuel cells utilizes oxidoreductase enzyme and bacteria as the catalyst driving fuel oxidation and oxygen reduction reactions. Biofuel cells that use enzymes derived from bacterial sources are a viable alternative to PEM fuel cells for hydrocarbon oxidation. They operate at near neutral pHs with temperatures ranging between 20 and 37 °C in order to preserve the enzyme's secondary and tertiary structure. Examples include glucose oxidase from

Aspergillus niger, alcohol dehydrogenase from *Saccharomyces cerevisiae* and aldehyde dehydrogenase from *Saccharomyces cerevisiae* as anode catalysts, and bilirubin oxidase from *Myrothecium verrucaria* and laccase from *Trametes versicolor* for cathode catalysts. Expensive and complex PEMs required to separate the anodic and cathodic compartments in a traditional fuel cell are not needed because the enzymes used are selective towards their fuel. Unfortunately, incomplete fuel oxidation, short lifetimes due to enzyme stability, reduced performance due to electron transfer kinetics and problems with the stability or thermodynamics of redox mediators plague these systems[87].

Enzyme stability is a major engineering hurdle for improved lifetime of biofuel cells. Typically, enzymes are active for only a few hours to a few days, but their lifetimes can be extended by immobilization in hydrogels or binding to the electrode surface[88]. Immobilization strategies focus on providing a microenvironment that improves or maintains activity and lifetimes. Moore et al. have developed a Nafion binder modified with quaternary ammonium bromides that is capable of stabilizing immobilized enzymes within the polymer by providing a protective outer shell and an ideal chemical environment that resists a decrease in pH within the pore structure[89]. Lau et al. have developed a multi-dimensional chitosan matrix featuring mesopores for enzyme immobilization, and highly interconnected macropores that balance the need between smaller pores that provide large active surface areas for enhanced enzyme loading, and larger pores that provide spacious pore channels for reduced drag on the mass transport of liquid phase fuels[90]. Balancing mass transport with microenvironment stability is a key challenge to developing immobilization strategies that optimize performance and enzyme lifetime.

Electron transfer kinetics are also a major research focus for enzymatic fuel cells. The enzyme has two options of transferring electrons from the enzyme to the surface of the electrode; mediated and direct electron transfer.

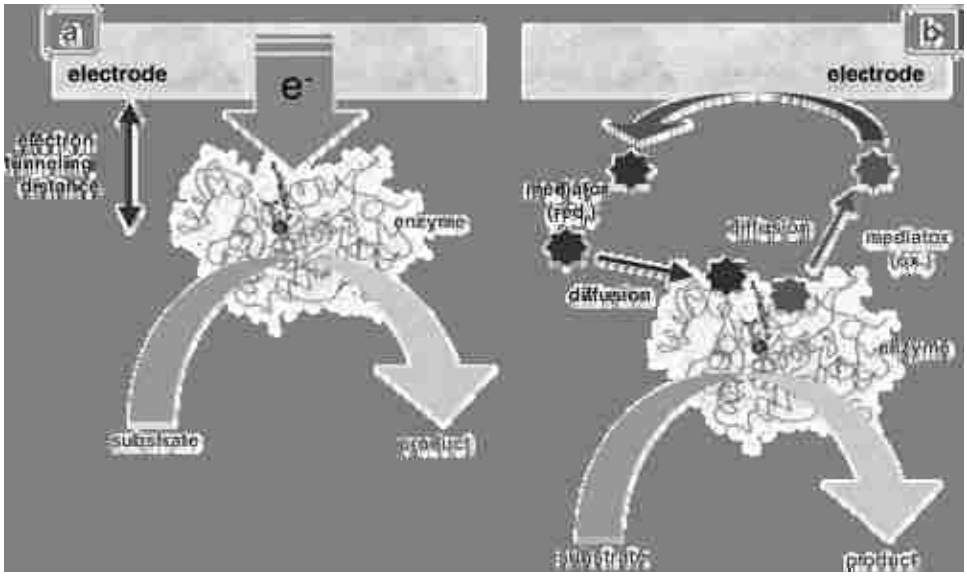

Figure 1.13: Enzyme electron transfer mechanisms. (a) Direct electron transfer (tunneling) mechanism from electrode to enzyme active site. (b) Electron transfer via redox mediator

The method of electron transfer depends on the enzyme itself. Enzymes incapable of transferring electrons themselves utilize low molecular weight active redox compounds or polymers such as hydroquinone or osmium compounds to mediate transfer of electrons between enzyme and electrode. Some mediators such as polyazines can be electropolymerized on the electrode surface[91]. There are over 300 dehydrogenase enzymes that are dependent on the nicotinamide adenine dinucleotide cofactor for electron transport. Once the enzyme oxidizes its substrate, it passes the electron to the NAD^+ molecule, converting it to NADH. The NADH must then be regenerated back to NAD^+ in order for the enzyme to continue catalysis. Oxidation of NADH at glassy carbon or platinum electrodes is an irreversible process that requires large overpotential

that can exceed 1 V[92, 93]. Enzyme electron transfer that use mediators are collectively termed Mediated Electron Transfer (MET). Mediators are usually chosen with redox centers close to the potential of the enzyme itself to minimize overpotential. Adding a mediator decreases the potential difference between cathode and anode, which in turn decreases the maximum energy that can be extracted from the cell. Direct Electron Transfer (DET)-capable enzymes eliminate this complication.

Enzymes that do not require mediators are capable of Direct Electron Transfer (DET), which is a method in which electrons released by the active site of the enzyme are passed directly to the electrode surface. This is in contrast to a mediated system where redox couples (e.g. quinines, osmium compounds, ferrocyanide) or polymers serve to shuttle electrons between the electrode surface and active site of the enzyme. The enzyme's active site is capable of being able to convert a chemical signal directly to an electrical one through charge transfer of the redox species and transfer of charge to another molecule or electrode surface. Use of these types of enzymes eliminates the complexity of the entire fuel cell package by removing the need for additional components such as redox mediators. However, DET is still dependent on enzyme proximity and orientation to the electrode surface. In order to address this issue immobilization techniques have been developed to use carbon nanotubes to decrease the electron transfer path from active site to electrode surface.

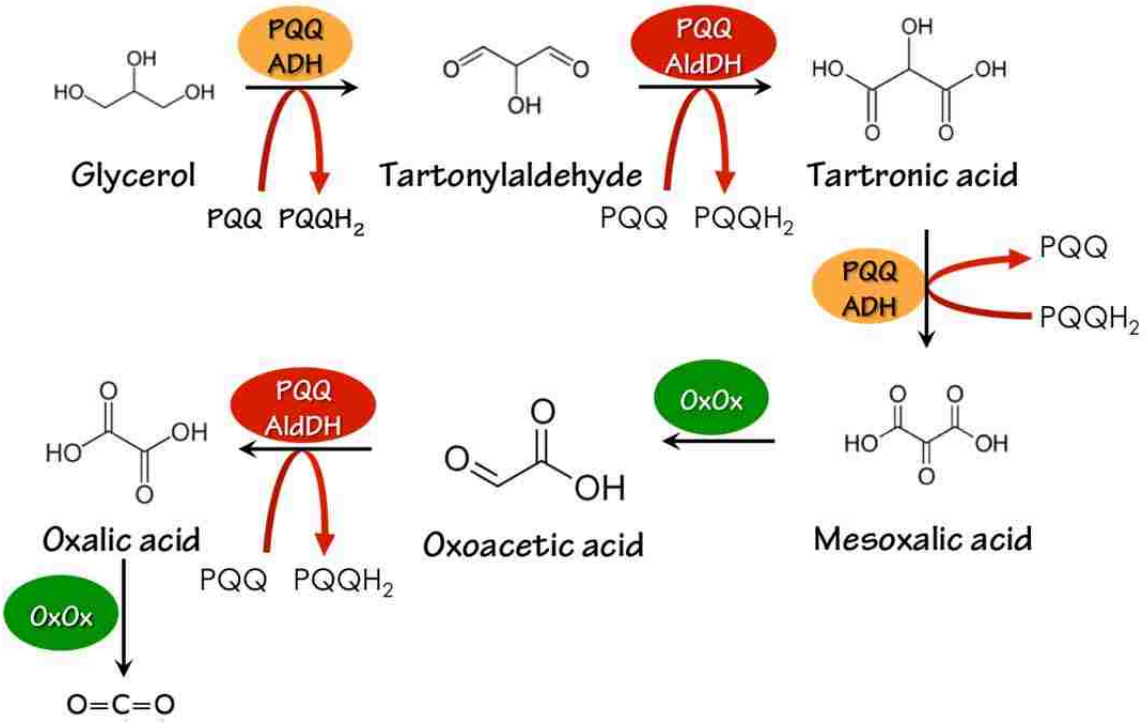

Figure 1.14: Reaction pathway of complete oxidation of glycerol in a biofuel cell. Image adapted from reference[94].

The current state of the art for glycerol oxidation rests with the Minteer group at the University of Utah (formerly at Saint Louis University), who has led in the selection, isolation and testing of an alcohol and aldehyde dehydrogenase PQQ-dependent enzymes[94-96] and is shown in Figure 1.14. These enzymes were chosen due to their ability to perform DET to the electrode surface. The current state of the art with the PQQ enzymes for glycerol oxidation is capable of electrochemically oxidizing glycerol to oxalic acid. A final catalyst is needed to complete the oxidation to carbon dioxide.

1.2.5.1 Anode Design

PQQ enzymes used as electrochemical catalysts have been well characterized in the literature[97-100]. Much of the research has been focused on enzyme extraction and purification from bacteria, immobilization on electrode materials, and fuel cell performance.

In order for the enzymes to be used effectively in fuel cells, they need to be immobilized in such a way as to have the active site of the enzyme accessible to the electrode surfaces. Carbonaceous materials such as Toray Paper or Reticulated Vitreous Carbon (RVC) [101] have fibers that are a few microns in diameter which is a 100 orders of magnitude of difference compared to the size of an enzyme. Graphite and other carbonaceous materials have been used for many years in fuel cells, batteries and other electrochemical applications. Graphitic carbon nanotubes in a mixture with the enzymes and an immobilization agent such as chitosan can bridge the size gap between the enzyme and electrode because their electrical properties promote electron transfer reactions [102-104].

Carbon nanotubes mixed with an enzyme immobilization agent and deposited on the electrode complement the electrode due to their ballistic electron transfer properties, ability to increase the surface area of the electrode, and nanoscale size features which are on the order of the enzymes themselves. Since the efficiency of a fuel cell ultimately depends on the rate of electron transfer, carbon nanotubes can raise efficiency by increasing the rate of transfer of electrons and surface area. Another option is to grow the nanotubes directly on the surface of the electrode using metal seeds as catalyst for Chemical Vapor Deposition (CVD) [98, 105, 106]. CVD is an advantageous method to grow carbon nanotubes due to the process's relatively low operating temperature (compared to arc discharge[107, 108] or laser ablation[109]), direct growth on the substrate and also the control over the size of the nanotubes via the size of the catalyst used for growth. Catalyst

particles are deposited on the electrode from a solution of cobalt and nickel acetates, and boric acid in water. The electrode is then dried and placed in a furnace with nitrogen and a carbon source gas stream. In this technique, MWNTs are produced when a hydrocarbon feedstock (e.g. acetylene, ethylene) dissociates onto the transition metal catalyst at temperatures around 700°C. An immobilizing agent such as chitosan or Tetrabutylammonium bromide modified Nafion (TBAB Nafion)[110] is still needed to fix the enzymes in place while still retaining activity and stability. TBAB Nafion is a modified Nafion mixture that helps to stabilize and increase the activity of enzymes by providing a protective outer shell and ideal chemical environment that resists pH changes within the pore structure. While both Toray paper and RVC support the growth of carbon nanotubes, RVC is more conducive for the construction of a flow through cell due to its reticulated nature that gives large pore sizes supporting flow of a liquid fuel.

1.2.5.1.1 Chitosan as an immobilization matrix

With the distance between the active site of the enzyme and the electrode surface bridged with carbon nanotubes, an immobilization strategy is still needed to ensure that the enzyme maintains its activity but will not wash out of a flow through cell. Recently, chitosan has been investigated as a material that can immobilize enzymes while creating a multi-dimensional pore structure needed for fuel transport in flow through cells. The thermal induced phase separation technique produces controllable bimodal pore structures that can support enzyme function while providing large active surface areas.

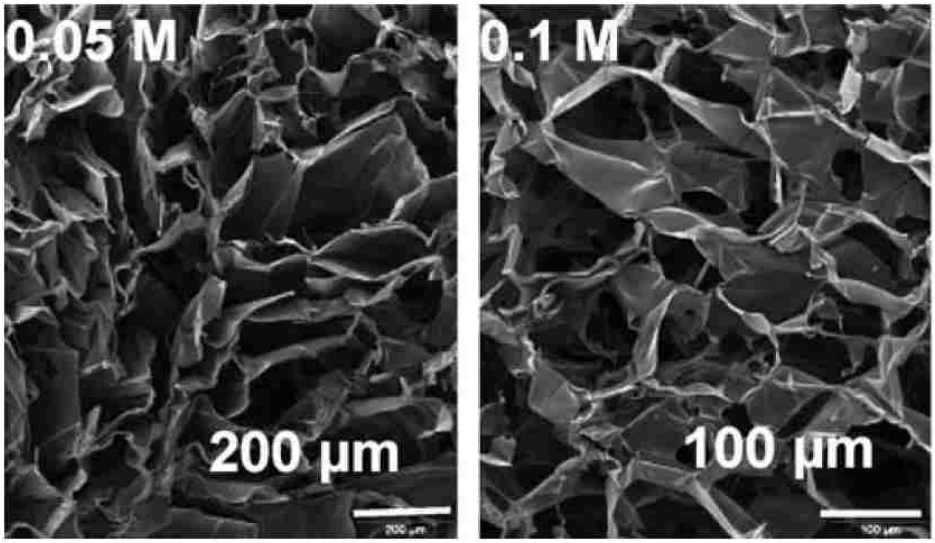

Figure 1.15: SEM images of 1wt% chitosan scaffolds frozen for 1 hour at -20C at 0.05M (left) and 0.1M (right) acetic acid concentrations. Image reproduced from reference [102].

Macropores on the order of 30µm provide channels for fluid transport and amphiphilic mesopores 10-12 nanometers in size line the walls provide zones for enzyme entrapment and stability[111]. Carbon nanotubes can be incorporated into the macroporous scaffold to provide more area for the enzymes to be immobilized on, giving a larger surface area per unit electrode volume and enhancement of the conductivity of chitosan. Chitosan can also provide another area of control by hydrophobic modification[112].

Ultimately the major engineering focus of enzyme based biofuel cells centers on the interface between the enzyme and electrode. This catalysis interface is required to provide microenvironments that maximize long-term stability, minimize electron transfer resistance, and augment the electron transfer ability of the enzyme catalysts. The catalysis interface must meet these requirements for each enzyme system that will be used, be it an enzymatic cascade, an artificial metabolon structure, or a hybrid interface that combines inorganic metal catalysts with enzymes.

1.2.6 Oxidation of higher order fuels

The wide application of direct alcohol fuel cells (DAFCs) for portable power applications depends on high performance with readily available fuels. Methanol and ethanol are valid candidates with energy density comparable to or higher than hydrogen and facile distribution requirements, but methanol is toxic, and ethanol is difficult to completely oxidize. Fuels such as ethylene glycol and glycerol are being considered because they have high energy density, are compatible with current liquid fuel distribution infrastructure, and are less toxic than methanol (MeOH LD_{50} =0.4mg/kg, EG LD_{50}=0.786 mg/kg). Higher order alcohols and polyols such as sugars would be ideal fuels because they are cheaper, more biorenewable and safer than other aforementioned fuels.

The difficulty in realizing these fuels as viable sources of energy stems from the fact that complete oxidation is a non-trivial task, mainly due to the difficulty of C-C bond splitting at low potentials. In addition, poisonous species from byproducts of these complex fuels oxidative pathways can poison and block the catalysts surface, thus decreasing performance. Enzyme catalysts are better able to start the oxidation of these complex molecules, but they are unable to extract the maximum energy unless they are grouped in cascades, metabolon structures, or other artificial complexes that mimic living systems that allows for deep oxidation of fuels.

Anode designs to be able to utilize these fuels must take into account the factors that have been described. A hybrid anode that is composed of an inorganic metal catalyst and an enzyme catalytic scheme has the potential of solving these issues. The enzyme portion of the anode will begin the oxidation process of these higher order fuels, while the inorganic catalyst will complete the oxidation and cleave the C-C bond to form CO_2. This approach is chosen to combine the benefits of the reduction in the fuel complexity through oxidation by enzymes, and efficient

catalysis of simple organic molecules by metal catalysts. This hybrid system will promote cooperation between these dissimilar catalysts in order to complete deep or complete oxidation of complex fuels including ethylene glycol, glycerol, and ultimately glucose.

Chapter 2 - Problem Statement and Objectives

Higher order alcohol based fuel cells can potentially provide greater energy than hydrogen PEM fuel cells or DAFCs that use methanol or ethanol for fuel. The benefits of using fuels such as glycerol and ethylene glycol can only be realized if oxidation proceeds completely to CO_2 and reaction byproducts are minimized. Platinum based electrocatalysts are so far currently the most ideal for performing these reactions due to the synergistic effects of ruthenium and tin atoms alongside platinum promoting oxidation of fuels to CO_2. The primary objective of this work is to identify and develop catalysts that are capable of oxidizing organic fuels such as ethylene glycol and glycerol based on performance metrics gleaned from studies performed on catalysts used to oxidize methanol and ethanol. Binary and ternary platinum-based catalysts will be evaluated for their activity towards oxidation of these higher order fuels. The quality of the catalyst as determined by CO_2 evolution will be evaluated by *in situ* Fourier Transform Spectroscopy. After synthesizing, characterizing and establishing that these catalysts are capable of oxidation of these fuels, a hybrid anode will be constructed that combines the efficient oxidation properties of metal catalysts with the enzymes that are able to oxidize reaction intermediates for improved anode performance.

- **Objective 1:** Synthesize, characterize and evaluate nanostructured templated electrocatalysts using spray pyrolysis. Identify optimum synthesis techniques based on the catalyst precursors used.

Spray pyrolysis will be used rapidly synthesize binary and ternary platinum based catalyst compositions for the oxidation of higher order fuels. Silica will be used in the precursor solution to provide a template for the final catalyst structure. Synthesized catalysts will be characterized

by physically and electrochemically. TGA will be used to determine optimal reaction and calcination conditions for synthesis catalysts. BET will be used for surface area measurements. XRD will be used to determine crystal structure of the catalytic material. SEM and TEM will be used to observe catalyst morphology and to determine if the tinplating of the catalyst was successful. EDS will be used to verify final catalyst compositions. These catalysts will be evaluated electrochemically by cyclic voltammetry to determine oxidative performance, and by using polarization curves to determine catalyst electrochemical stability.

- **Objective 2:** Identify catalysts capable of complete oxidation of oxalic acid and analogous fuels in neutral media.

Due to the inability of oxalate oxidase to electrochemically oxidize oxalic acid, and substitute catalyst must be identified. Platinum based catalysts will be evaluated because there is a wealth of literature that discusses complete oxidation of similar fuels in alkaline and acid media. These catalysts will be evaluated with cyclic voltammetry to test sensitivity to the fuels.

- **Objective 3:** Construct and align an *in situ* Infrared Reflection Absorbance Spectroscopy (IRRAS) apparatus capable of detecting CO_2 and organic product formation *in situ* on the electrode surface and in solution.

An *in situ* Infrared Reflection Absorption Spectroscopy apparatus will be constructed and aligned based on similar previously reported IRRAS setups in the literature.

- **Objective 4:** Qualitatively determine the degree of fuel oxidation and evaluate synthesized catalysts ability of C-C bond scission by monitoring CO_2 formation using IRRAS.

An *in situ* Infrared Reflection Absorption Spectroscopy will be used to evaluate oxidation products of glycerol and ethylene glycol oxidation occurring on synthesized catalysts. Reaction product analysis results will be compared to published data in the literature to determine the quality of catalysts synthesized. The degree of oxidation will be qualitatively determined by the presence of CO_2 and other reaction products. Reaction kinetics of each catalyst will be evaluated by IRRAS to link product formation to potential formed.

- **Objective 5:** Elucidate reaction pathway of small organic molecule oxidation.

Synthesized catalysts will be evaluated in alkaline media for complete oxidation of ethylene glycol and glycerol. CO_2 formation will be determined by IRRAS.

- **Objective 6:** Using insight gained from oxidation of small organic molecules in neutral media, incorporate a biological enzyme catalyst for increased fuel flexibility

Synthesized platinum-based catalysts will be incorporated with an enzymatic catalyst for co-oxidation of fuels. The combination of these two inherently different catalysts will allow for a higher conversion of fuel. Immobilization techniques that permit the enzyme and inorganic catalyst to operate will be developed.

- **Objective 7:** Verify CO_2 evolution from enzymatic cascades that are claimed to fully oxidize fuel

Using the IRRAS system, enzyme cascades will be evaluated to determine if CO_2 is evolved from enzymatic cascades.

Chapter 3 - Experimental Methods

3.1 - Spray Pyrolysis

Spray pyrolysis is an aerosol synthesis method capable of creating tunable mesoporous particles that can be used as anode electrodes[113-116]. An aqueous solution of silica template and metal precursors is ultrasonically atomized. An air stream or inert carrier gas is used to transport the aerosol droplets through a furnace where controlled temperature conversion and pyrolysis can occur. The particles are then collected on filter paper and then post-processed. Depending on the desired final catalyst, post-processing procedures can range from simple reduction in hydrogen-nitrogen gas streams to complex multi-step oxidation-reduction treatments.

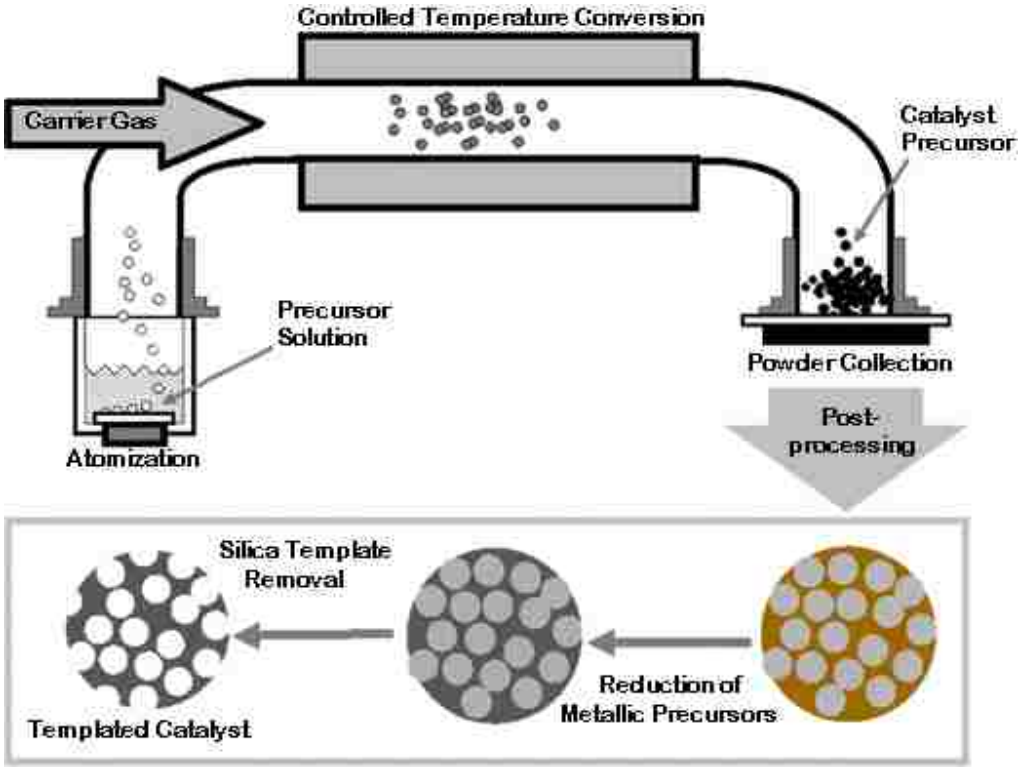

Figure 3.1: Spray Pyrolysis schematic[68]

After the particles have been thermo-reduced, the silica template is etched away. This is achieved via etching by HF, or a concentrated base, usually 7M KOH. Etching the silica template away can take as little as a few hours using HF to a couple of days using KOH, depending on the silica template used, the concentration of the etchant, agitation of the solution of etchant with catalyst, and applied temperature.

3.2 - Structural and Compositional Analysis

3.2.1 Brunauer-Emmet-Teller (BET) method surface area analysis

The synthesis of mesoporous materials via the spray pyrolysis method offers various advantages, particularly in terms of morphology as described previously. In order to establish that successful synthesis of a catalytic material has been performed, one must determine the surface area of said catalyst. A useful technique is the BET method, which employs adsorption isotherms of gas molecules on a sample of interest to determine the surface area. A sample is prepared by heating while flowing gas (He) over the sample to remove impurities such as water. The treated samples are then cooled with liquid nitrogen, evacuated of air, and analyzed by measuring the volume of gas (usually N_2) that adsorbs at specific pressures. At the saturation pressure, a monolayer of gas forms on the surface of the sample. Approximating the space at which each adsorbed gas molecule occupies the surface, a total sample area per mass unit can be calculated from porosimetry based on inert gas adsorption isotherms, usually reported in m^2/g.

3.2.2 Thermogravimetric Analysis (TGA)

TGA is a technique that determines change in mass of a sample when heated using a controllable temperature profile. Samples can be heated in air or specific compositions of gases can be flown over the sample at specified flow rates. The mass of the sample is constantly measured verses a reference sample in order to determine mass loss at a specific temperature. This technique is used in order to determine calcination temperatures of synthesized catalysts. Once a stable mass is reached during the heating program, one can assume that the precursor material has been successfully thermally decomposed, and only the pure metal remains. This technique is also useful to determine when a sample undergoes oxidation/reduction, or loses water by monitoring the heat flux and changes in mass. To provide proper accuracy, a sample weight of at least 10mg is needed, and a heating rate must be chosen properly to allow diffusion through the entire sample.

3.2.3 Scanning and Transmission Electron Microscopy (SEM & TEM)

SEM is a powerful technique that provides information on the nanoscale morphology of the catalyst. An electron beam is generated by a thermionic emission from a tungsten filament cathode electron gun at accelerating voltages from 2-30keV. The resulting electron beam is focused by magnetic condenser lenses as it travels down the column to a final lens where it is deflected in both x and y directions so that a raster scan is performed over the sample surface. The electrons interact with the sample where they lose energy by repeated collisions and absorption within the interaction volume whose depth is controlled by the accelerating voltage of the electron beam. The interaction is also controlled by the composition of the sample. These

interactions case elastic scattering of the electrons, inelastic scattering via secondary electrons, and electromagnetic radiation emission that can be detected by various detectors. The beam current that is absorbed by the specimen is used to create images of the sample. Magnification is controlled by the current supplied to the scanning coils, or voltage supplied to the x and y deflector plates.

TEM detects electrons from a beam accelerated at 100keV – 300keV that pass through the sample. The image that is generated is a projection of a cross section where the beam is focused. This technique can be used to determine morphology, lattice parameters, and elemental composition. TEMs can image specimens at resolution higher than SEMs. The TEM is limited to sample thickness; a sample must be thin enough for the beam to be able to pass through.

In both microscope methods, samples to be analyzed are placed in the microscope chamber, which is then pumped to high vacuum. In order to prevent attenuation and scattering of the electron beam, samples must be completely dry and have minimal outgassing[117].

3.2.4 Energy-dispersive X-ray Spectroscopy (EDS)

The electron microscope not only provides qualitative information about morphology and structure from the sample, but also X-rays generated from the electron beam hitting the sample gives qualitative information about a sample's composition. EDS spectroscopy is possible when a high-energy electron ejects an unexcited ground state electron from an atom in the sample. A higher energy electron from the same atom then fills the resulting hole. The energy difference from the electron movement is sometimes released as an x-ray. The energy and amount of x-rays emitted from the sample can be correlated to the atom's structure. This information is collected

by a detector and converted to valuable information on sample analysis. This technique is applicable to atoms with atomic number higher than 4.

3.2.5 X-ray Diffraction

X-ray diffraction is a technique that reveals information about the crystal structure of a catalytic material. This technique involves an x-ray beam that impinges on a sample at controlled angles of incidence. The material under investigation diffracts the incoming x-rays and causes interference as they exit the crystal sample. The diffraction pattern is used to determine the chemical composition, crystallographic structure, and physical properties of the sample as a function of incident and scattered x-rays' angle, polarization, and energy.

3.3 - Electrochemical Studies

All electrochemical experiments were done with a three-electrode half-cell setup consisting of a working gold or glassy carbon working electrode with catalyst deposited, a platinum counter electrode, and a reference electrode. The counter electrode balances the reaction occurring at the working electrode by passing current, and must be higher surface area than the working electrode, so as not to limit the reaction. The reference electrode is used as a stable standard with which the potential of the working electrode is measured against. No current passes through the reference electrode, and the counter electrode is chosen so as to not influence the working electrode of interest.

3.3.1 Cyclic Voltammetry

Cyclic voltammetry is the primary initial electrochemical characterization technique used to determine the behavior of oxidation-reduction reactions that occur on the electrocatalyst. A potentiostat applies a potential that varies with time. The potential follows a triangular waveform that varies as a function of the potential range as well as the rate of change of the potential.

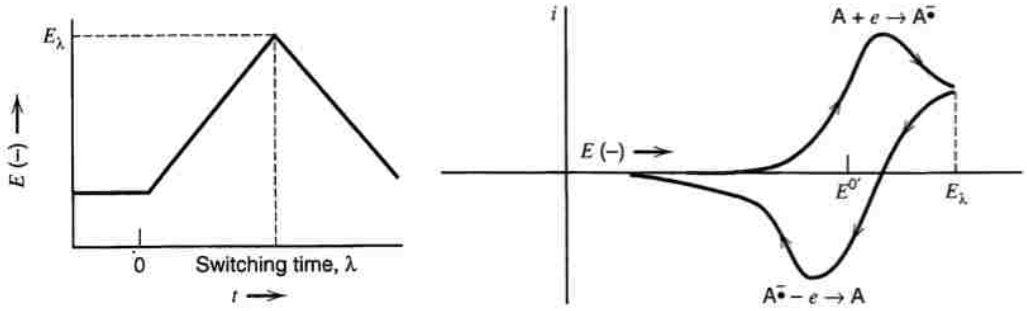

Figure 3.2: Cyclic Voltammetry sweep(left). Resulting cyclic voltammogram (right)

3.3.2 Steady State Polarization Curves

Polarization curves are a useful tool for evaluating an electrocatalyst's performance. The open circuit potential of the electrode of interest is obtained, and the electrode is subsequently step-polarized for an amount of time until a maximum current is reached. Evaluating the steady state current of the system (versus a dynamic current given by cyclic voltammetry) elucidates complex behavior of the system, such as kinetic, ohmic, and mass transfer resistances. Polarization curves can be constructed for the anode, cathode, and full cell. A power curve can be obtained from the polarization curve my multiplying the current by the potential.

3.3.3 In-Situ Infrared Reflection Absorption Spectroscopy (IRRAS)

Oxidation of organic molecules produces intermediate products during the time course of the electrochemical reaction whose identification is useful to determine kinetic parameters of the reaction. IRRAS is a technique that exploits the interaction of near infrared radiation from 800 nm to 2500 nm with chemical bonds for species identification. When light in that wavelength region interacts with certain molecules, the chemical bonds that constitute functional groups absorb this radiation and use that energy to vibrate. These vibrations are grouped into categories called normal modes. The total number of normal modes for a molecule depends on if the molecule is linear or nonlinear. Linear molecules have 3N-5 while nonlinear molecules have 3N-6 modes, where N is the number of atoms in the molecule. For example, a linear 3-atom molecule such as CO_2 has 4 normal modes, whereas a nonlinear molecule such as H_2O has 3 normal modes. CO_2 has a symmetric stretch, an asymmetric stretch, and two bending modes, and water as a symmetric and asymmetric stretch along with one bending mode. Not all of these modes are infrared active though, because not every vibration is infrared active. Absorption occurs with molecules that have a dipole moment, or a charge asymmetry due to the different electronegativities of between atoms sharing a chemical bond. The dipole moment can be induced or permanent, and is described in equation 37, where μ is the magnitude of the dipole moment, q is the charge, and r is the distance.

$$\boldsymbol{\mu = qr} \qquad \textbf{37}$$

The peak position, intensity and width of an IR active species are intrinsic properties that depend on the molecules themselves. The wavenumber at which an IR species absorbs is determined by the force constant and reduces mass of the species. If we assume that in a heterogeneous diatomic species with masses M1 and M2 connected with a chemical bond, the reduced mass of the molecule is defined by μ.

$$\mu = \frac{M_1 M_2}{M_1 + M_2} \quad (38)$$

Combining this with Hooke's Law and Newton's second law:

$$F = -kx \quad (39)$$

$$F = ma \quad (40)$$

where F is the force, k is the spring constant, x is the distance between two atoms, m is mass and a is acceleration, we end up with

$$W = \frac{1}{2\pi c}(k/\mu)^{1/2} \quad (41)$$

where W is the wavenumber in cm^{-1}, c is the speed of light in m/s, k is the force constant in N/cm and μ is the reduced mass in Kg. The wavenumber thus depends solely on the chemical bond force constant and reduced mass.

The intensity of absorption peak is described by Beer's law described in equation 6, which correlates the absorbance to the absorptivity of a species ε, the path length l, and the concentration of the species, c.

$$\boldsymbol{A = \varepsilon l c} \qquad \textbf{42}$$

The chemical environment determines the width of an absorption peak. Hydrogen bonding influences the force constants and therefore the wavenumbers at which species absorbs. The more chemical environments a species has, the more slightly different wavenumbers of IR radiation it will absorb.

To obtain IR spectra, an infrared source generates an IR beam that passes through a beamsplitter, usually made of a salt such as KBr. On one side of the beamsplitter is a stationary mirror, and on the other side is a moving mirror. The beam travels to both of these mirrors, and then combines back at the beamsplitter and travels to the sample. The moving mirror causes the combined IR light to vary in intensity with respect to time, causing regions of constructive interference and destructive interference. After passing through a sample of interest, the IR radiation is collected with a detector. The signal is converted from an analog signal to a digital signal, where it is then Fourier Transformed and analyzed.

An external module was installed on a commercial FTIR to allow an infrared beam to interrogate the electrolyte and working electrode as an experiment is being performed. The apparatus consists of a bottomless Teflon cell with ports on the side that allows for insertion of a counter electrode, a reference electrode and a purge gas. A dilute amount of catalyst is deposited on the working electrode, which is the pressed against an IR window to form a thin layer of electrolyte.

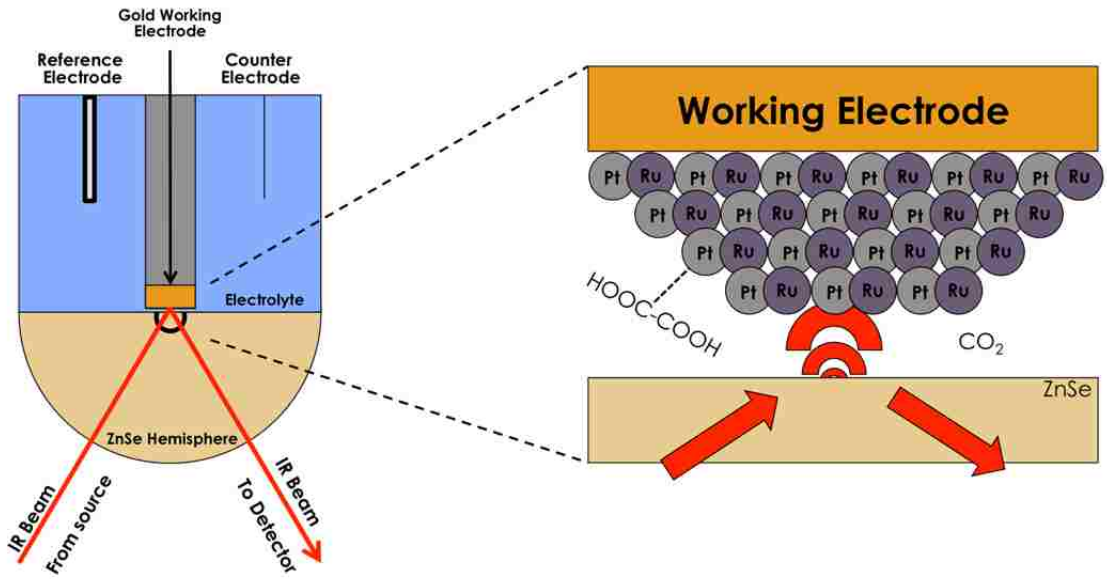

Figure 3.3: IRRAS working electrode schematic[118]

The incoming IR radiation from the FTIR is reflected with a flat mirror, focused using a curved mirror, reflects off a gold mirror and then passes through the ZnSe IR window. The IR beam travels through electrolyte and catalyst, reflects off of the working electrode, and then passes again through the catalyst and electrolyte through the IR window then reflects off of a gold mirror, is focused again using a BaF_2 lens and then enters the detector.

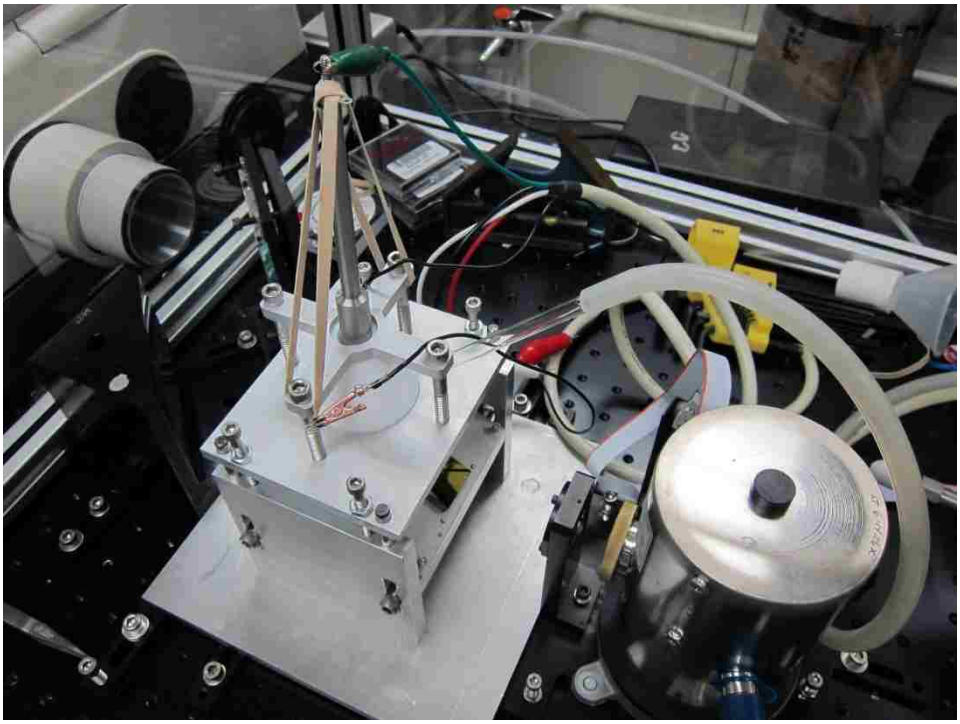

Figure 3.4: IRRAS experimental setup

The FTIR must be time correlated to the cyclic voltammogram being recorded to obtain meaningful data. One scan in the FTIR at a resolution of 8cm^{-1} occurs very quickly, but the signal to noise ratio (SNR) is very low. The SNR improvement is proportional to the square root of the number of scans taken and averaged together to give a final spectrum.

$$\boldsymbol{SNR \propto (N)^{1/2}} \qquad \textbf{43}$$

Therefore taking 100 scans results in a 10 factor improvement in signal to noise over a single scan. For a given experiment, 128 scans at 8cm^{-1} resolution is suitable to provide a sufficient number of scans in a reasonable time period.

Chapter 4 - Electrochemical and *in situ* IR characterization of PtRu catalysts for complete oxidation of ethylene glycol and glycerol

4.1 - Introduction

Primary alcohols such as methanol and ethanol have been well explored in the literature as anode fuels in fuel cells. The liquid fuels used in direct alcohol fuel cells (DAFCs) have higher volumetric energy density than gaseous fuels such as hydrogen, with methanol being the most well-known and studied alcohol due to its chemical simplicity [30]. Due to higher energy density, low toxicity, and easy integration to existing infrastructure, electrochemical oxidation of polyols are gaining interest.

Various groups interested in sensors for oxalic acid detection, and the reaction mechanism to CO_2 have studied oxidation of oxalic acid, glycerol, and ethylene glycol using various catalysts in both acidic and alkaline electrolytes [52, 60, 119-123]. Binary platinum based catalysts benefit from the addition of ruthenium or tin modifiers to improve catalytic activity and decrease adsorbed oxidation intermediates during oxidation of alcoholic fuels intermediates [24, 59, 64, 124]. CO_2 generation from fuel oxidation indicates that all available electrons have been harvested, and oxidation is complete. *In situ* Infrared Reflection Adsorption Spectroscopy (IRRAS) is commonly used to monitor oxidation products and verify CO_2 production in solution and on the surface of the electrode [125].

Biological fuel cells use enzymes derived from bacteria, fungi, or other sources for catalysis at room temperature and near-neutral pHs. Utilizing a single enzyme or an enzyme cascade immobilized on an electrode, fuel can be oxidized completely [94]. Combining a traditional metal-

based catalyst operating at 'mild' operating conditions of near neutral pH and room temperature with an enzyme-based biofuel cell allows for a complimentary relationship that can drive oxidation of fuels further than either catalyst alone.

We present a nanostructured PtRu catalyst produced by spray pyrolysis, an aerosol synthesis technique extensively used to create mesoporous silica [113]. The catalyst is capable of oxidizing oxalic acid, ethylene glycol, and glycerol to CO_2 at neutral pH and room temperature. We compare our synthesized nanostructured catalysts to commercial E-Tek HP precious metal PtRu catalysts. We also present a pH study to determine the efficiency of catalysis in biologically relevant buffer solutions with pHs ranging from pH 5 – 8.

4.2 - Materials and Methods

Nanostructured PtRu catalyst synthesis has been reported previously [68], and was used to create nanostructured $Pt_{50}Ru_{50}$ and $Pt_{30}Ru_{70}$ unsupported catalysts. Surface areas were measured by the N_2-BET method using a Micrometrics 2360 Gemini Analyzer. Scanning Electron Microscopy (SEM) and EDS analysis was performed using a Hitachi S-5200 Nano SEM with an accelerating voltage of 10 keV. Transmission electron microscopy (TEM) was performed on a JEOL 2010 instrument with an accelerating voltage of 200keV.

Electrochemical studies were performed via cyclic voltammetry using a glassy carbon electrode (5 mm diameter) with a potential sweep from -900 mV to 900 mV vs. Ag/AgCl reference electrode in a conventional three electrode cell with a platinum mesh as a counter electrode at a rate of 10 mV/s for 4 cycles. In order to prepare the working electrode, 17 mg of catalyst was dispersed ultrasonically in 1 ml of 5 wt.% Nafion solution. A 3 µl aliquot of this mixture was

then transferred to a polished glassy carbon disk electrode, which corresponds to a loading of 0.05 mg of catalyst on the working electrode, and allowed to air dry for 30 minutes. The electrochemical measurements were performed at room temperature in nitrogen purged buffer solutions ranging from pH 5 – 8. 30 mM fuel concentrations were used in solutions at a scan rate of 10 mV/s for 4 cycles.

In situ Infrared Reflection Adsorption Spectroscopy (IRRAS) experiments using a setup described previously [126]. The reference spectrum was collected at -600 mV vs. Ag/AgCl in 1.5 mL of 0.1 M respective fuel (oxalic acid, glycerol, or ethylene glycol) and 0.1 M potassium phosphate buffer solution at pH 7, using linear sweep voltammetry with a scan rate of 1 mV/s from -600 mV to +600 mV vs. Ag/AgCl.

4.3 - Results and discussion

The BET surface area of the synthesized nanostructured PtRu catalysts was approximately 32 m^2/g for the $Pt_{50}Ru_{50}$, and 30 m^2/g for the $Pt_{30}Ru_{70}$ sample. This is in contrast to commercially available E-Tek HP Precious metal Catalyst 40% PtRu on Vulcan XC-72 1:1 and 60% PtRu on Vulcan XC-72 1:1 which have surface areas of 107 m^2/g and 112 m^2/g total surface area, respectively.

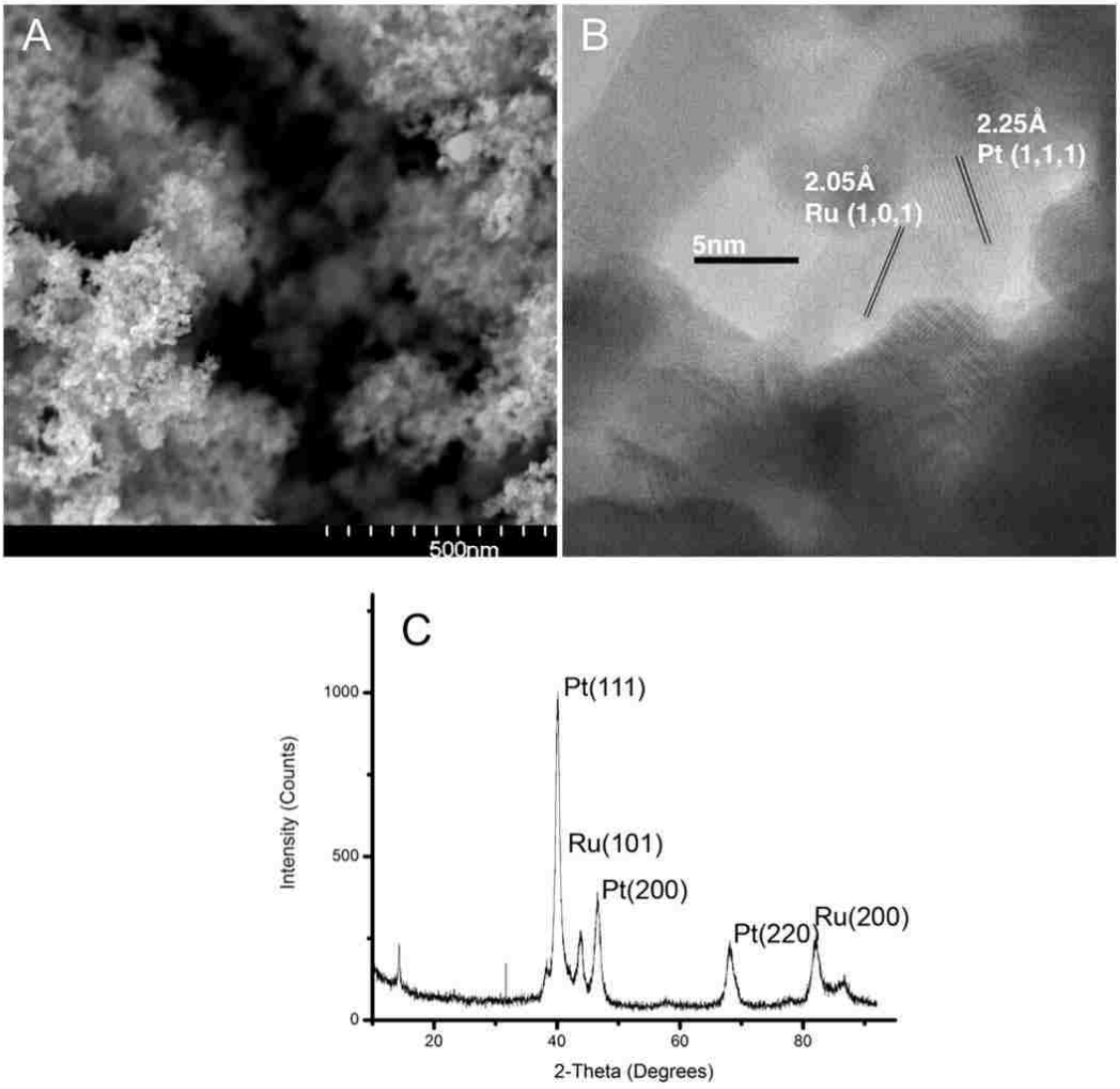

Figure 4.1: SEM (A), and TEM (B) micrograph of $Pt_{30}Ru_{70}$ sample with XRD pattern (C). The SEM image shows the nanostructured "sponge-like" morphology of the catalyst samples. TEM micrograph shows existence of Pt (111) and Ru (101) faces, correlating to the XRD results. Grain sizes range from 5-15nm

SEM (Figure 4.1) micrographs show the "sponge-like" nanostructured metal catalyst. EDS analysis of Pt-M and Ru-L lines confirms the presence of $Pt_{30}Ru_{70}$ and $Pt_{50}Ru_{50}$ (data not shown).

TEM observation of the catalyst shows the existence of the [111] platinum and [101] ruthenium faces, correlating to the XRD results.

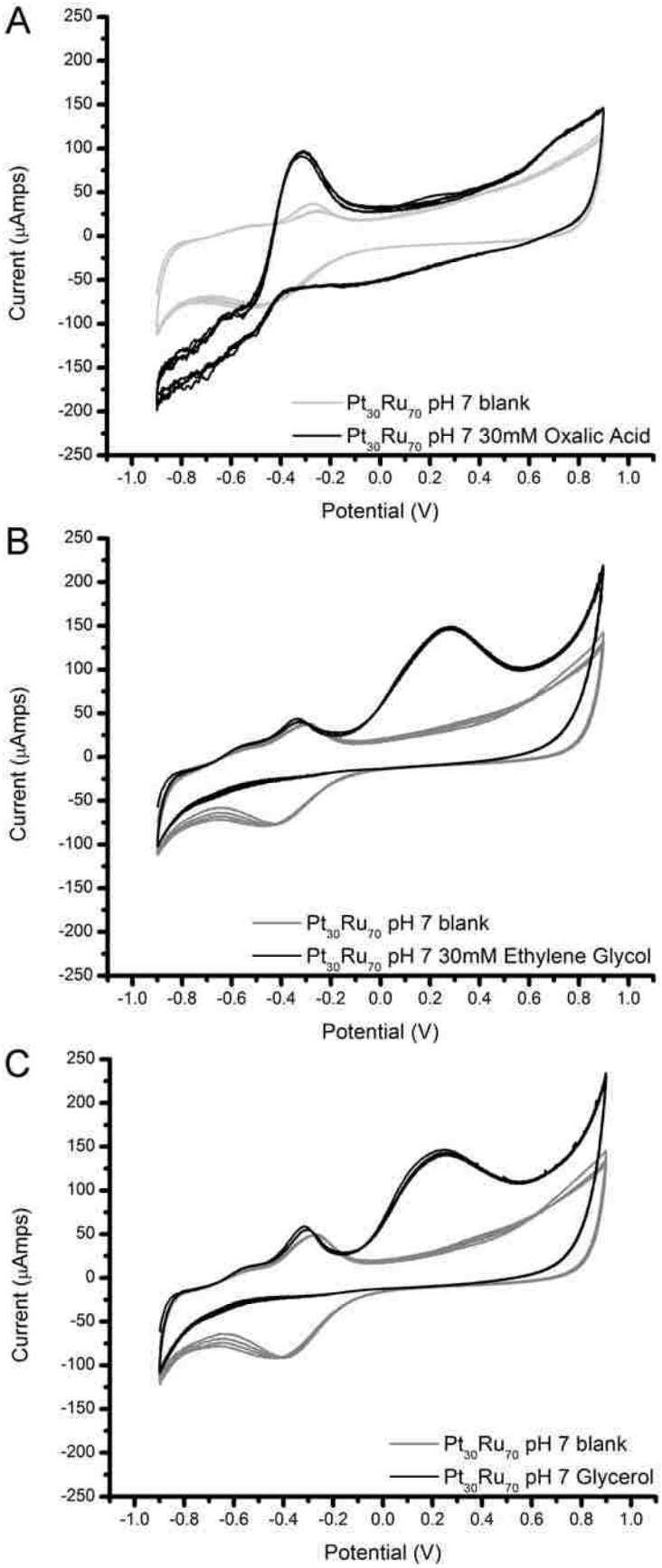
A
Current (μAmps)
Potential (V)
Pt30Ru70 pH 7 blank
Pt30Ru70 pH 7 30mM Oxalic Acid
B
Current (μAmps)
Potential (V)
Pt30Ru70 pH 7 blank
Pt30Ru70 pH 7 30mM Ethylene Glycol
C
Current (μAmps)
Potential (V)
Pt30Ru70 pH 7 blank
Pt30Ru70 pH 7 Glycerol

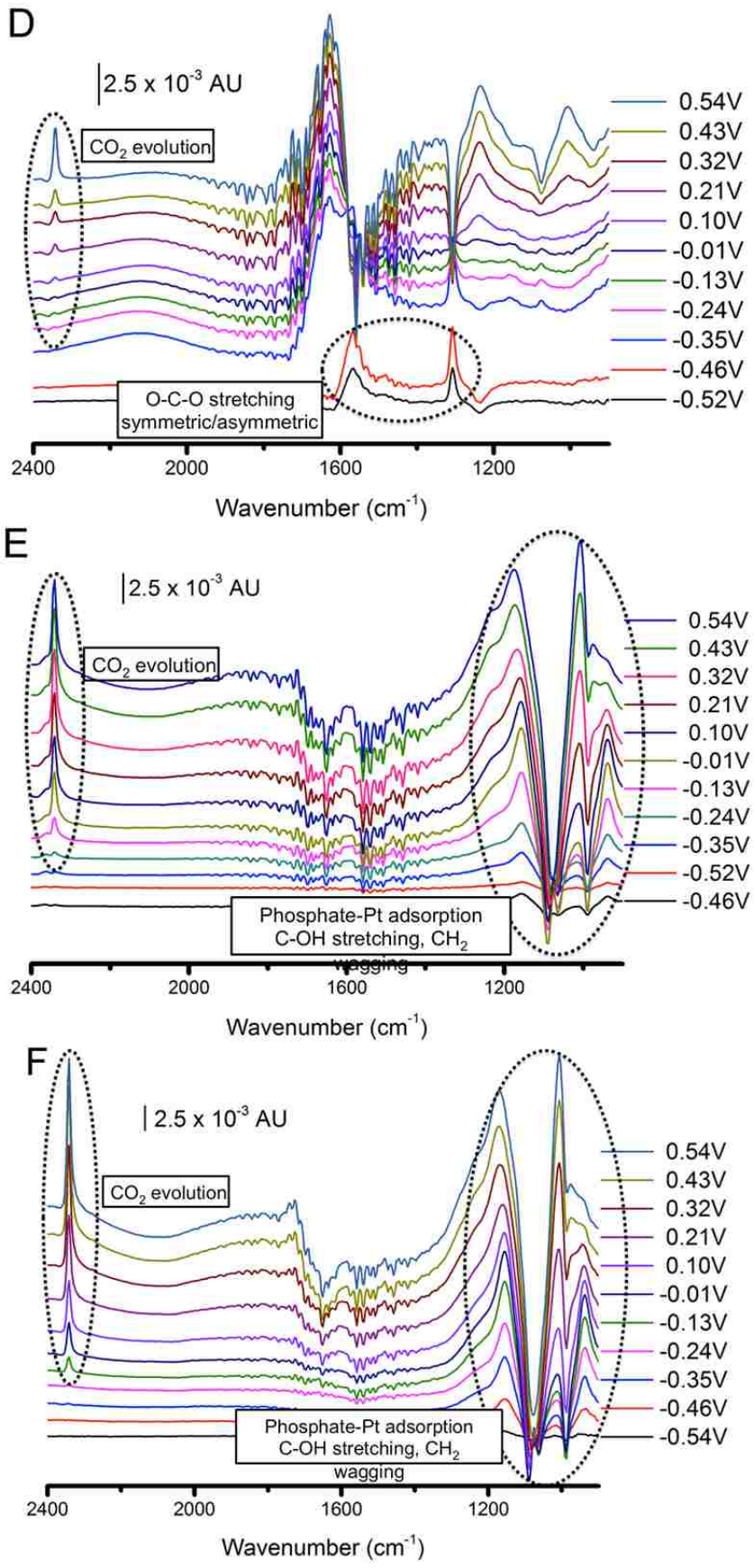
D
2.5 x 10-3 AU
CO2 evolution
O-C-O stretching
symmetric/asymmetric
0.54V
0.43V
0.32V
0.21V
0.10V
-0.01V
-0.13V
-0.24V
-0.35V
-0.46V
-0.52V
2400
2000
1600
1200
Wavenumber (cm-1)
E
2.5 x 10-3 AU
CO2 evolution
Phosphate-Pt adsorption
C-OH stretching, CH2
wagging
0.54V
0.43V
0.32V
0.21V
0.10V
-0.01V
-0.13V
-0.24V
-0.35V
-0.52V
-0.46V
2400
2000
1600
1200
Wavenumber (cm-1)
F
2.5 x 10-3 AU
CO2 evolution
Phosphate-Pt adsorption
C-OH stretching, CH2
wagging
0.54V
0.43V
0.32V
0.21V
0.10V
-0.01V
-0.13V
-0.24V
-0.35V
-0.46V
-0.54V
2400
2000
1600
1200
Wavenumber (cm-1)

Figure 4.2: Cyclic voltammetry of $Pt_{30}Ru_{70}$ in pH 7 media. Light grey scan corresponds to no fuel, while dark grey scan includes 30mM each of oxalic acid (A), ethylene glycol (B), and glycerol (C). In-Situ IRRAS spectra recorded during oxalic acid (D), ethylene glycol (E), and glycerol (F) oxidation on $Pt_{30}Ru_{70}$ nanostructured catalysts. Scans were performed at 10 mV/s in 100mM PBS electrolyte pH 7 with 100mM fuel. All potentials are vs. Ag/AgCl reference electrode.

The electrochemical oxidation of oxalic acid, ethylene glycol and glycerol was tested for all four PtRu catalysts in a neutral pH range (pH 5 to 8). Figure 4.2 (A-C) represent the cyclic voltammogram for $Pt_{30}Ru_{70}$ (for clarity only that catalyst is shown). The blank PtRu catalyst shows a stable and reversible couple of redox peaks at -500 mV and -300 mV, which is specific to formation of Pt-oxides in phosphate buffer.

The oxidation of oxalic acid exhibits a single peak at approximately -350 mV whereas ethylene glycol and glycerol result in a dual oxidation at -300 mV and 300 mV or -300 mV and 250 mV, respectively. Parallel to the electrochemical scan we employed *in situ* FTIR spectroscopy to monitor the formation of oxidation products (Figure 4.2, D-F). The oxidation peak at -350 mV for oxalic acid corresponds to the decreasing bands at 1308 cm^{-1} and 1571 cm^{-1}, both specific wavenumbers for the symmetric and asymmetric oxalate O-C-O stretching vibration mode [127]. The oxalic acid FTIR spectra shows a large peak centered at 1626 cm^{-1} and 1723 cm^{-1} due to δ(H-O-H) mode of water and ν(C=O) carboxylic stretching of adsorbed oxalate species that can be interpreted as the major contribution to the -350 mV oxidation peak. Finally, the CO_2 formation starts at -240 mV, with the appearance of a small perturbation at 2343 cm^{-1}. This absorbance peak grows in intensity as the electrode becomes more positively polarized, reaching a maximum at the end of the sweep.

The oxidation of ethylene glycol and glycerol in neutral media exhibits striking interference peaks due to the absorbance of phosphates to the platinum catalyst from 939 cm^{-1} to 1190 cm^{-1} [128, 129]. Phosphate is a polyprotic molecule that has multiple dissociation constants, resulting in both the H_2A^- and HA^{2-} species present at pH 7. The peak at 1157 cm^{-1} correlates to the asymmetrical PO_2 stretch, the peak at 1078 cm^{-1} correlates to the PO_3 degenerate stretch and the PO_2 symmetrical stretch of $H_2PO_4^-$, and the peak at 939 cm^{-1} correlates to the $P(OH)_2$ asymmetrical stretch of $H_2PO_4^-$. The IR spectrum for oxalic acid oxidation shows none of these phosphate peaks, suggesting stronger adsorption of oxalate anions to the catalyst surface compared to phosphate species. The intensity of the phosphate peaks in the ethylene glycol and glycerol spectra are much stronger than that of a blank spectrum (data not shown) with just the buffer. Therefore it is safe to assume that contributions from C-O stretching at 1006 cm^{-1}, the C-OH stretching at 1078 cm^{-1}, and the CH_2 wagging at 1153 cm^{-1} adds to the intensity of the peaks. For ethylene glycol at -460 mV there is the appearance of a shoulder at 1227 cm^{-1} that corresponds to CH_2 twisting of an adsorbed species. Glycerol has a peak at 320 mV forming at 1730 cm^{-1} corresponding to C=O stretching of C-COOH in solution. The CO_2 band at 2343 cm^{-1} for both ethylene glycol and glycerol appears at -240 mV, and continues to grow in intensity until the end of the scan. Both fuels, ethylene glycol and glycerol, are known to form various organic acid intermediates (e.g. glyoxylic acid, glycolic acid, tartronic acid, formic acid, oxalic acid, mesoxalic acid) that most likely all contribute to the CO_2 formation. There is no evidence of bridge bonded (~1840 cm^{-1}) or linear bonded (~2030 cm^{-1}) CO monoxide adsorption or formation for any of the fuels.

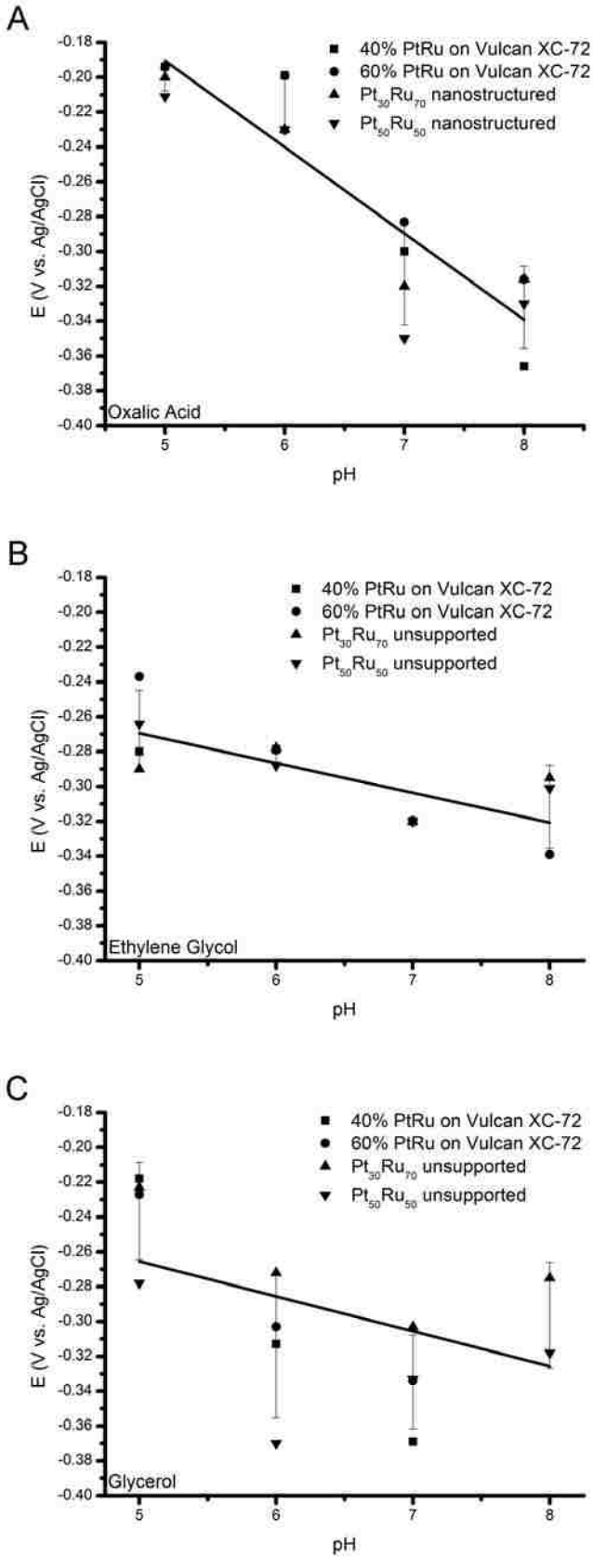
A
40% PtRu on Vulcan XC-72
60% PtRu on Vulcan XC-72
Pt30Ru70 nanostructured
Pt50Ru50 nanostructured
E (V vs. Ag/AgCl)
pH
Oxalic Acid
B
40% PtRu on Vulcan XC-72
60% PtRu on Vulcan XC-72
Pt30Ru70 unsupported
Pt50Ru50 unsupported
E (V vs. Ag/AgCl)
pH
Ethylene Glycol
C
40% PtRu on Vulcan XC-72
60% PtRu on Vulcan XC-72
Pt30Ru70 unsupported
Pt50Ru50 unsupported
E (V vs. Ag/AgCl)
pH
Glycerol

Figure 4.3: Peak potential vs. pH for oxalic acid (A), ethylene glycol (B), and glycerol (C).

For all tested catalysts and fuels the majority of CO_2 production starts at a potential of app. -240 mV, which matches the oxidation peak at -300 mV.

To determine the pH effect on the catalytic production of CO_2, that corresponding peak potential was plotted against the pH in Figure 4.3 (A-C). For all tested catalysts and fuels peak potential reveals a general negative shift with increasing pH from 5 to 7. The $Pt_{30}Ru_{70}$ catalyst shows a general trend towards more negative potentials from pH 5 – 7, but the trend does not continue at pH 8. One we would expect a 59 mV/pH dependence for a one proton one electron transfer or a 28mV/pH for a two proton two electron transfer due to the Nernst equation [4], however the results indicate that anion adsorption is not accompanied by simultaneous proton and electron transfer. A species change from [HA] to $[A^-]$ or $[A^{2-}]$ due to pH is not expected at the pH conditions of the experiments. Oxalic acid has two dissociation constants; with pKa1 equal to 1.38 and pKa2 equal to 4.28. At pH 7 and 8, the molecule is completely dissociated from the $[H_2A]$ form of oxalic acid to the $[A^{2-}]$ species, unlike ethylene glycol and glycerol with pKa values of 14.22 and 14.15, respectively that do not dissociate at neutral and basic pH.

4.4 - Conclusions

Platinum based catalysts have been synthesized using a spray pyrolysis procedure with varying atomic compositions. A ruthenium rich and platinum rich PtRu were compared to supported E-Tek PtRu on Vulcan XC-72 at a pH range from 5 – 8 for the oxidation of ethylene glycol and glycerol. The oxidation of oxalic acid, ethylene glycol and glycerol has been compared with synthesized PtRu nanostructured catalysts and commercial E-Tek PtRu blacks from pH 5 - 8.

The nanostructured catalysts were evaluated by SEM and exhibited a sponge-like morphology that helped to increase the metal utilization despite its low surface area. *In situ* FTIR spectroscopy was used to probe the reaction to determine if complete oxidation occurred by monitoring the production of CO_2. While there is a wealth of literature that discusses oxidation of ethylene glycol and glycerol in acid and alkaline media [52, 60, 119-123], to the best of our knowledge our work is the first that shows oxidation using binary catalysts in neutral media with complete oxidation to CO_2. The peak currents did not trend at 60 mV/pH unit as would be expected from the Nernst equation, suggesting that adsorption of fuel to the surface of the electrode is not an electron-transfer step. Oxidation of all three fuels leads to formation of CO_2 at approximately -240 mV, growing in intensity as the scan reaches more positive potentials with no CO poisoning species. Since this catalyst can operate in a pH range suitable for biological enzymes, we suggest that a "hybrid" enzymatic-metallic biofuel cell could be built to oxidize more complex fuels.

Chapter 5 - Preliminary Comparison of Pt-Based Binary and Ternary Templated Catalysts for the Electrooxidation of Ethylene Glycol and Glycerol in Alkaline Media

5.1 - Introduction

Continuing with the work presented in Chapter 5, we decided to tests our catalysts in alkaline media. Alkaline media presents many unique advantages over acid media for electrochemical reactions including improvements in the oxidation and reduction kinetics [15, 16, 70, 130-135]. Tin and ruthenium have been described in the literature as beneficial modifiers for biomass oxidation using platinum catalysts by helping to improve catalytic activity and decrease adsorbed oxidation intermediates [24, 55, 57, 59, 61, 64, 69, 124, 136, 137]. Most reports discuss a bifunctional mechanism where the added metal provides oxygen species to aid in the removal of adsorbed CO and other incomplete oxidation products in acid and alkaline media. Coupling the benefits of an alkaline environment with the stability and reactivity improvements gained by using binary and ternary catalysts presents a system in which the degree of fuel oxidation is maximized and catalyst poisoning is minimized.

We have synthesized, characterized, and electrochemically evaluated binary PtRu, and PtSn catalysts, along with a ternary PtRuSn catalyst. We utilized a spray pyrolysis approach that allows us to synthesize a templated catalyst by etching away a monodisperse silica support [68, 69, 113]. This results in an "open frame" catalyst possessing improved transport and kinetic properties. Electrochemical characterization by cyclic voltammetry and steady state polarization revealed the performance improvements gained by alloying platinum with ruthenium and tin.

5.2 - Experimental

5.2.1 Electrocatalyst synthesis via spray pyrolysis

Synthesis of templated binary and ternary platinum alloys was achieved using spray pyrolysis (Figure 3.1). A precursor solution of tetraamineplatinum (II) hydroxide, hexaammineruthenium (III) chloride, tin (II) chloride hydrate [Sigma-Aldrich Co.], and 20 nm monodisperse Ludox® TM50 colloidal silica [Sigma-Aldrich Co.] in 30 mL of DI water was used. Concentrated HCl was added drop-wise while stirring until the solution became clear. The dissolved precursor solution was atomized and dried in a furnace at 125°C using N_2 as the carrier gas. A standard humidifier was modified in order to expose the ultrasonic membrane. The catalyst precursor solution was then positioned on top of the membrane in order to generate the vapor.

Dried particles were collected on a filter, and alloys were formed by reduction of the oxide powders under 5% H_2 in N_2 at 300°C for 2 hours. The silica template was then etched using a 7 M KOH solution for 72 hours. Afterwards, the solution was centrifuged and washed three times with DI water to remove the KOH. The collected catalyst was then dried in an oven at 80°C.

Surface areas were measured by the N_2-BET method using a Micrometrics 2360 Gemini Analyzer. Scanning Electron Microscopy (SEM) was performed using a Hitachi S-5200 Nano SEM with an accelerating voltage of 10 keV. Transmission electron microscopy (TEM) was performed using a JEOL 2010 instrument with an accelerating voltage of 200 keV. Catalyst compositions and BET surface area are described in Table 5.1. Polarization curves were constructed by averaging the last 10 percent of points (90 points) during each 15-minute step in potentiostatic mode with step increments of 25 mV.

Table 5.1: Pt binary and ternary catalyst compositions

Catalyst Name	Composition (EDS)	Weight percent of silica	BET surface area (m^2/g)
PtRu	47:53	20	30
PtSn	90:10	20	44
PtRuSn	86:7:7	20	16

5.3 - Characterization

Following reduction, morphology, purity, and composition of the synthesized powders were determined using Scanning Electron Microscopy (SEM), Transmission Electron Microscopy (TEM), and Energy Dispersion Spectroscopy (EDS). SEM and TEM provided information on the morphology of the bulk and individual particles of the catalysts while EDS allowed us to determine the composition of the samples and compare them to the starting solution.

5.4 - Electrochemical evaluation

A 5 µL aliquot of a 2.95 mg/mL catalyst ink composed of 5 wt% Nafion, DI:IPA 4:1 and respective catalyst was deposited on polished glassy carbon electrodes for a final catalyst loading of 15 µg. The electrodes were allowed to air dry for 30 minutes under a gentle stream of nitrogen.

Electrochemical experiments were conducted in 1 M KOH at room temperature, at a scan rate of 10 mV/s from -0.4 to 0.8 V vs. SHE. When required, glycerol and ethylene glycol were added to

the electrolyte to make 100 mM solutions. A platinum mesh and a Hg/HgO electrode [XR-440 Radiometer Analytical SAS] were used as counter and reference electrodes, respectively. Before each experiment, the electrolyte solution was deoxygenated by bubbling N_2 gas for at least 15 minutes.

5.5 - Results and Discussion

5.5.1 Characterization of electrocatalysts

A major feature of the spray pyrolysis procedure used to synthesize the templated catalysts is the benefit of each particle having the same composition as the precursor solution. SEM micrographs show a porous "sponge-like" catalyst (Figure 5.1), as expected from the templating procedure. The removal of the silica nanoparticles leaves pores in the catalytic structure that increases catalyst utilization, even though the surface area is lower than catalysts supported on high surface area materials such as carbon. TEM observation of the lattice fringes of PtRu binary catalyst shows the existence of platinum 1,1,1 and ruthenium 1,0,1 faces. Grain sizes of the particles were 5 – 15 nm.

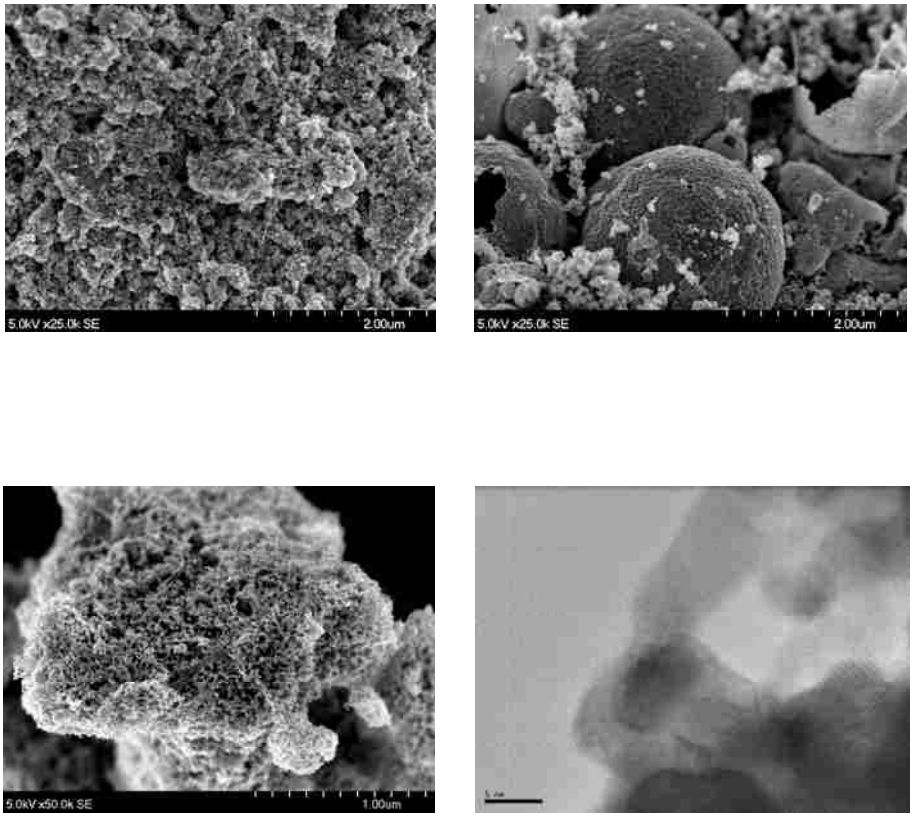

Figure 5.1 - SEM micrographs of PtSn (top left), PtRuSn (top right), and PtRu (bottom left). TEM Micrograph of PtRu (bottom right).

The PtSn and PtRu catalyst samples are amorphous in nature. The PtRuSn catalyst has a slightly more defined morphology, presenting as scattered spherical catalyst particles amongst amorphous particles. The differences in morphology can be attributed to the synthesis procedure [115, 116]. As the aerosolized particle-containing droplets travel through the furnace, the solvent is evaporated, resulting in morphologically spherical final particles.

The synthesized binary and ternary catalysts were tested as electrocatalysts for the anodic oxidation of ethylene glycol and glycerol. Cyclic voltammetry was used to evaluate the performance of the electrocatalysts for the oxidation of each fuel. The data is normalized to the BET surface area (Table 5.1) of the catalysts in order to determine metal utilization. The ternary

PtRuSn catalyst showed enhanced oxidation behavior for both ethylene glycol oxidation and glycerol oxidation (Figure 5.2). The onset potential for the PtRuSn catalyst is also shifted slightly towards more negative potentials as compared to the binary catalysts (see Figure 5.2 and Table 5.2). The potential window might need to be widened because the onset of the reaction for the ternary catalyst could possibly be even more negative than the chosen potential window allows.

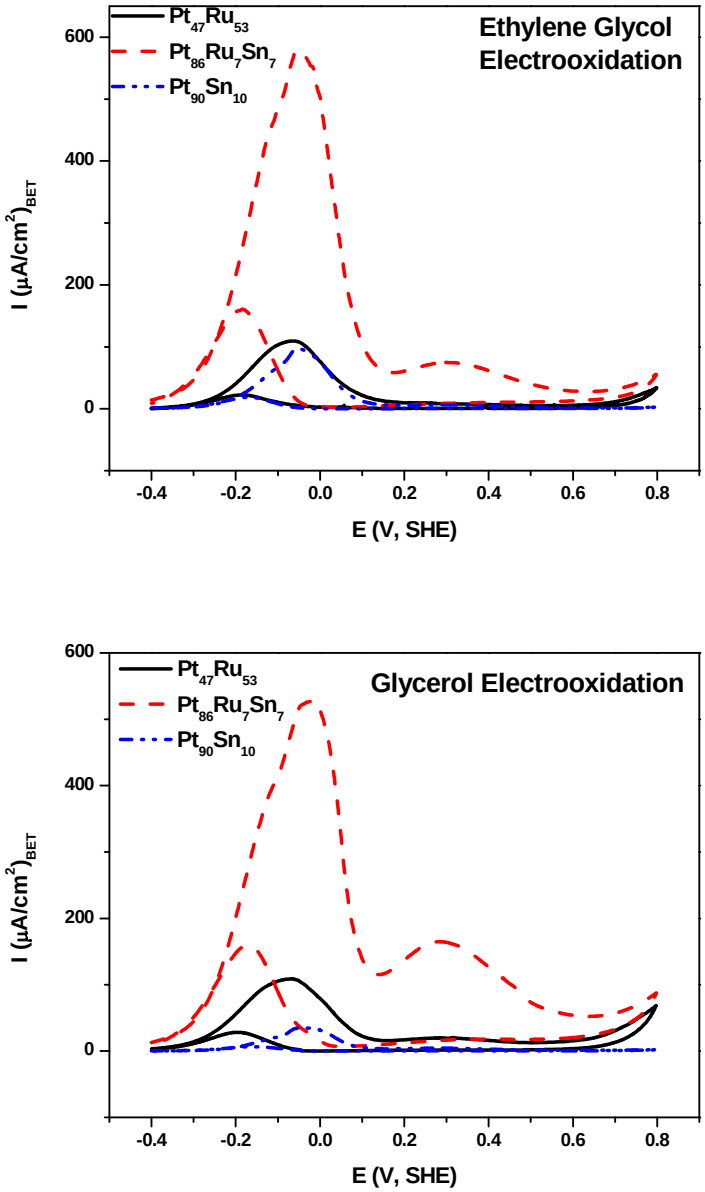

Figure 5.2: Cyclic voltammograms of PtRu, PtRuSn, and PtSn catalysts vs. ethylene glycol (top) and glycerol (bottom). 10 mV/s in 1 M KOH electrolyte with 100 mM ethylene glycol and glycerol, respectively. The current density was calculated with respect to the BET surface area.

Amongst the binary Pt-based catalysts, the PtRu catalyst had higher currents and lower onset potential than the PtSn catalyst. The shapes of the CV curves display the characteristic electrooxidation reactions of alcohols, with two oxidative peaks at approximately -50 mV and +300 mV. The singular anodic peak in the negative sweep represents oxidation of incompletely oxidized carbonaceous intermediates on the surface of the catalysts left over from the positive sweep [31, 138]. Accumulation of these adsorbed products blocks the catalyst during subsequent cycles.

A summary of the catalyst performance is given in Table 5.2. The catalysts were evaluated in terms of their onset potential, the peak potential and current density, and the ratio of forward anodic peak to reverse peak current. The PtRuSn catalyst had the highest peak currents at similar onset potentials and peak potentials compared to the binary catalysts. All three catalysts have high I_f/I_r ratios due to the beneficial effect of alloying metals that provide oxygen species at low potential, and also signaling that accumulation of oxidation residues during the catalytic processes is less than that of similar catalysts reported in acidic media [139].

Table 5.2: Comparison of catalyst performance vs. ethylene glycol (EG) and glycerol (Gly) oxidation

Catalyst	**E_{onset} (V)**	**E_f (V)**	**I_f ($\mu A/cm^2$)**	**I_f/I_r**
$Pt_{47}Ru_{53}$	-0.29 (EG)	-0.07 (EG)	112 (EG)	4.48 (EG)
	-0.29 (Gly)	-0.07 (Gly)	111 (Gly)	3.37 (Gly)
$Pt_{86}Ru_7Sn_7$	-0.37 (EG)	-0.06 (EG)	579 (EG)	3.55 (EG)
	-0.38 (Gly)	-0.02 (Gly)	528 (Gly)	3.31 (Gly)
$Pt_{90}Sn_{10}$	-0.20 (EG)	-0.55 (EG)	101 (EG)	4.42 (EG)
	-0.23 (Gly)	-0.02 (Gly)	34 (Gly)	4.73 (Gly)

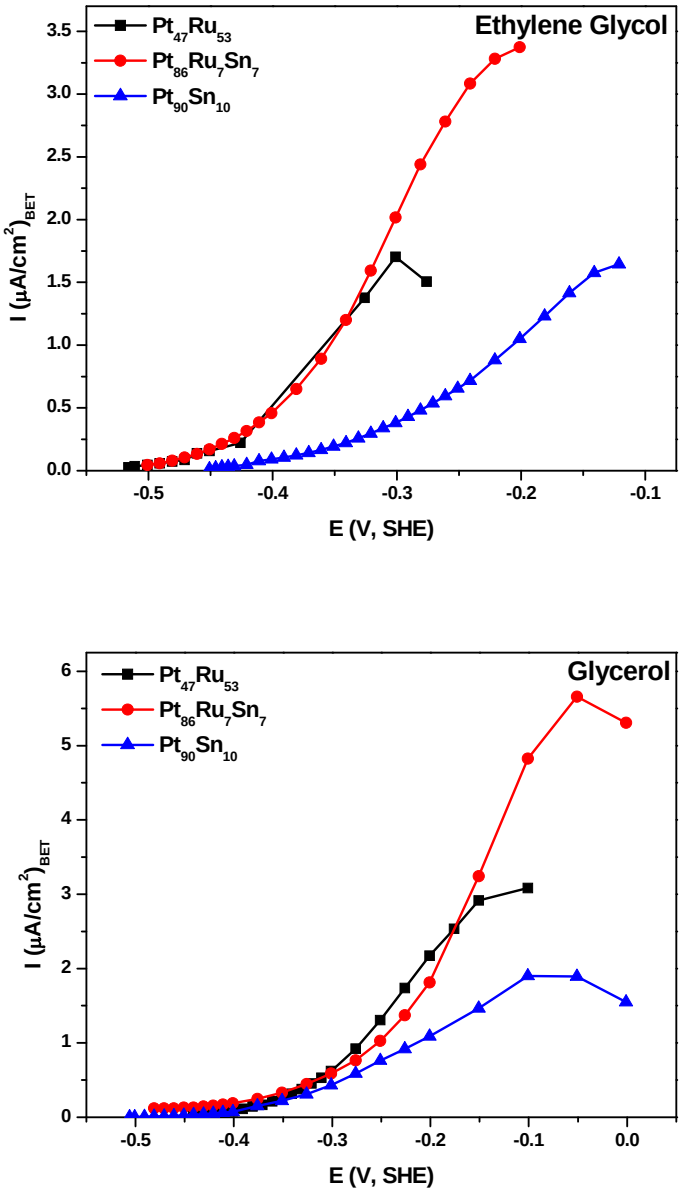

Figure 5.3: Steady-state polarization curves of PtRu, PtRuSn, and PtSn catalysts vs. ethylene glycol (top) and glycerol (bottom). 1 M KOH electrolyte with 100 mM ethylene glycol and glycerol, respectively. The current density was calculated with respect to the BET surface area.

Steady-state polarization curves of ethylene glycol and glycerol oxidation on the catalyst were obtained under potentiostatic conditions (Figure 5.3). The open circuit potential for the catalysts is near -0.5 V (vs. SHE). Maximum currents for the PtRuSn catalysts were higher than the binary catalysts for both ethylene glycol and glycerol, followed by the PtRu catalyst and then the PtSn catalyst.

5.6 - Conclusions

We have reported the synthesis and characterization of binary and ternary template catalysts synthesized by spray pyrolysis. The use of spray pyrolysis was chosen due to its ease of creating templated catalysts with desired composition. Characterization of the catalysts was performed using SEM, TEM, and EDS to determine morphology, purity and composition. EDS analysis confirmed the composition of the as-created catalysts. The catalysts had an open frame sponge like morphology caused by template removal via etching of the silica catalyst. Cyclic voltammetry showed that the ternary PtRuSn catalyst performed better than both binary PtRu and PtSn catalysts. The ternary catalyst had better metal utilization despite its lower surface area. The ratio of forward peak current to reverse peak current was high, indicating that accumulation of oxidation products is not as significant as it is for reactions using similar catalysts in acid media. We plan on including different catalyst compositions in order to fully determine the effect of Sn and Ru modifiers to the Pt catalyst. We also plan on performing IRRAS to determine oxidation products of these reactions. This work demonstrates the complimentary effect of Ru and Sn modifiers in a ternary PtRuSn catalyst to achieve higher catalyst performance for the electrooxidation of ethylene glycol and glycerol.

Chapter 6 - Electrooxidation of Ethylene Glycol and Glycerol by Platinum-Based Binary and Ternary Nano-structured Catalysts

6.1 - Introduction

Due to the success of the work in the previous chapter, we created several different compositions of PtRu, PtSn, and PtRuSn catalysts and compared then to nano-structured Pt catalysts for oxidation of ethylene glycol and glycerol. Ethylene glycol and glycerol have attracted interest in recent years as fuels for direct alcohol fuel cells (DAFCs). These fuels are advantageous compared to methanol due to their low toxicity, renewability from biomass, cost, and high energy density. Various groups have studied the reaction kinetics and feasibility of DAFCs based on these fuels in acid and alkaline media. Using an alcohol reduction catalyst synthesis process, Neto et al. showed that electrooxidation of ethylene glycol starts at lower potentials and current values increase with increasing ruthenium content, with similar effects with a PtSn/C catalyst [60]. Overall they discovered that PtSn/C electrocatalysts are better for ethylene glycol oxidation than PtRu/C catalysts due to oxidation at lower potentials and higher current values. Livshits, Peled and coworkers demonstrated the feasibility of a direct ethylene glycol fuel cell (DEGFC) by building a 10-cell stack with good performance in acid media with a nanoporous proton conducting membrane [140-143]. Chetty and Scott noted superior performance by a PtRuW ternary electrocatalyst compared to PtRu binary, and PtRuNi and PtRuPd ternary alloys [144]. While many of the reports concerning the feasibility of these fuel cells have dealt mostly with acid electrolytes, alkaline media presents many unique advantages for electrochemical reactions such as improvements in reaction kinetics at the anode and cathode, and has thus been gaining interest in the literature [15, 16, 70, 130-135].

Oxidation of these fuels in alkaline media is advantageous not only due to the improved kinetics of the reaction, and higher conversions [26, 35]. The general reaction for oxidation of ethylene glycol and glycerol can be described by Equation 44.

$$\boldsymbol{C_{x\geq 2}H_yO_z + (2x - z)H_2O \rightarrow xCO_2 + (4x + y - 2z)H^+ + (4x + y - 2z)e^-} \qquad 44$$

Complete oxidation of ethylene glycol is a 10 electron reaction while that of glycerol is a 14 electron reaction. Harvesting the maximum number of electrons is of utmost importance to utilize the fuel fully. Unfortunately, the complex oxidation reactions generate intermediates that can adsorb to and block the active sites of the catalyst, decreasing performance. Tin and ruthenium have been described in the literature as beneficial modifiers of platinum catalysts for biomass oxidation by helping to improve catalytic activity and decrease adsorbed oxidation intermediates [24, 55, 57, 59, 61, 64, 69, 124, 136, 137]. Most reports discuss a bifunctional mechanism where the added metal provides oxygen species to aid in the removal of adsorbed CO and other incomplete oxidation products in acid and alkaline media. Coupling the benefits of an alkaline environment with the stability and reactivity improvements gained by using binary and possibly ternary catalysts presents a system in which the degree of fuel oxidation is maximized and catalyst poisoning is minimized.

We have synthesized, characterized, and electrochemically evaluated binary $Pt_{84}Ru_{16}$, and $Pt_{96}Sn_4$ catalysts, along with a ternary $Pt_{88}Ru_6Sn_6$ catalyst. The catalysts were synthesized using a spray pyrolysis approach that allows us to produce a nano-structured catalyst by etching away the monodisperse silica template [68, 69, 113]. This results in an "open frame" catalyst possessing improved transport and kinetic properties. Electrochemical characterization by cyclic

voltammetry and steady state polarization revealed the performance improvements gained by alloying platinum with ruthenium and tin. We use infrared reflection absorption spectroscopy (IRRAS) to gain insight into the reaction kinetics on the surface and monitor oxidation products.

6.2 - Experimental

6.2.1 Preparation of binary and ternary electrocatalysts via spray pyrolysis

Synthesis of templated nanostructured binary and ternary Pt alloys and a templated nanostructured Pt catalyst was achieved using spray pyrolysis. This procedure has been described previously, but we have performed the catalyst synthesis with modifications to the precursor material and reduction temperature [68, 69]. Calculated amounts of platinum (IV) chloride, ruthenium (III) chloride hydrate, and/or tin (II) chloride hydrate [Sigma-Aldrich Co.], with 20 nm monodisperse Ludox® TM50 colloidal silica [Sigma-Aldrich Co.] were mixed as a precursor solution in 30 mL of de-ionized water. Concentrated hydrochloric acid was added drop-wise while stirring until the precursors dissolved. The dissolved precursor solution was atomized and dried through a furnace at 125°C using N_2 as the carrier gas. A standard humidifier was modified in order to expose the ultrasonic membrane. The catalyst precursor solution was then positioned on top of the membrane in order to generate the aerosol. All catalysts were made as 20 weight percent catalyst on silica template.

Pyrolyzed particles were collected on 0.2 μm filter paper, and alloys were formed by reduction of the oxide powders under 5% H_2 in N_2 at 500°C for 2 hours with a ramp rate of 1°C/min and at a total gas flow rate of 100 mL/min. The silica template was then etched in a 7 M KOH solution for 72 hours. Afterwards, the solution was filtered and washed 3 x with DI water to remove the KOH. The collected catalyst was then dried in an oven at 80°C.

6.2.2 Physical characterization

Following reduction and etching the silica template from the catalysts, morphology, purity, and composition of the synthesized powders were determined using Scanning Electron Microscopy (SEM), Transmission Electron Microscopy (TEM), and Energy Dispersion Spectroscopy (EDS). SEM and TEM provided information on the morphology of the bulk and individual particles of the catalysts while EDS was used to determine the composition of the samples and compare to the starting solution.

Surface areas were measured by the N_2-BET method using a Micrometrics 2360 Gemini Analyzer. Scanning Electron Microscopy (SEM) was performed using a Hitachi S-5200 Nano SEM with an accelerating voltage of 10 keV. Transmission electron microscopy (TEM) was performed using a JEOL 2010 instrument with an accelerating voltage of 200 keV. Powdered samples were analyzed by X-ray diffraction (XRD) using a Scintag Pad V diffractometer (Bragg-Brentano geometry) with DataScan 4 software (from MDI, Inc.) for system automation and data collection. Cu KR radiation (40 kV, 35 mA) was used with a Bicron Scintillation detector (with a pyrolitic graphite curved crystal monochromator). Data were analyzed with Match! 1.11 Software (Crystal Impact) using the ICDD (International Center for Diffraction Data) PDF4 data- base (rev. 2009) for phase identification. Various catalyst compositions were synthesized and screened based on reports of similar catalysts in the literature. The best performing catalysts in each group are presented.

6.2.3 Electrochemical and in situ infrared characterization

A 5 μL aliquot of a 3 mg/mL catalyst ink composed of 5 wt.% Nafion, and de-ionized water with isopropyl alcohol in a 4:1 ratio was deposited on polished glassy carbon electrodes with a 5 mm outer diameter for a final catalyst loading of 15 μg, or 0.076 mg/cm^2. The electrodes were allowed to air dry for 30 minutes.

Cyclic voltammetry was conducted in 1.0 M KOH at room temperature. When required, glycerol and ethylene glycol were added to the electrolyte to make 0.1 M solutions. A Pt mesh and Hg/HgO electrode [XR-440 Radiometer Analytical SAS] were used as counter and reference electrodes, respectively. Before each experiment, the electrolyte solution was deoxygenated by bubbling N_2 gas for at least 15 minutes. Polarization curves were constructed by averaging the last 10 percent of points (90 points) during each 15-minute step in potentiostatic mode with step increments of 25 mV. All potentials in this discussion are referred to the reversible hydrogen electrode (RHE) scale.

In situ Infrared Reflection Adsorption Spectroscopy (IRRAS) experiments were performed at room temperature with a Nicolet 6700 FT-IR spectrometer equipped with a Mercury Cadmium Telluride (MCT) detector cooled with liquid nitrogen. Experimental setup is described previously [53, 126]. For each spectra, 128 interferograms were added together to each spectrum at a resolution of 8 cm^{-1} with unpolarized light. Absorbance units of the spectra are defined as $A=-\log(R/R_0)$, where R and R_0 represent reflected IR intensities corresponding to the sample and reference single beam spectrum, respectively. Thus, a positive peak in the resulting spectrum indicates a production of species, while a negative peak indicates consumption or decrease in

concentration of a species compared to the reference spectrum. The reference spectrum was collected at 0.140 V (RHE) vs. an Ag/AgCl reference electrode in 1.5 mL of 0.1 M respective fuel (ethylene glycol or glycerol) and 0.1 M KOH, using linear sweep voltammetry with a scan rate of 1 mV/s from 0.140 V to 1.18 V (RHE). A thin layer of ink was pipetted onto a polished glassy carbon electrode with a diameter of 5 mm. A ZnSe hemisphere was used as the IR window, and the working electrode was pressed against the window, creating a thin solution layer with a thickness of a few micrometers. The incident angle of the IR radiation passing through the ZnSe window was 36° [145]. Argon was used to purge the electrolyte while dry air was used to purge the spectrometer and chamber, reducing the spectral interference from CO_2 and water vapor.

6.3 - Results and discussion

6.3.1 Characterization of electrocatalysts

Spray pyrolysis of templated catalysts is a powerful synthesis tool due to the degree of control granted over the final catalyst composition due to each individual aerosol droplet having the same composition as the precursor solution. SEM micrographs show the droplet and porous "sponge-like" morphology (Figure 6.1 a, b), as expected from the templating procedure. The removal of the silica nanoparticles leaves pores in the catalytic structure that increases catalyst utilization, even though the surface area is lower than catalysts supported on high surface area materials such as carbon. Catalyst compositions and BET surface area are described in Table 6.1.

Table 6.1: Pt based nanostructured catalyst compositions and surface areas

Catalyst Name	Expected Composition	Composition (± 2)	BET surface area (m^2/g)
$Pt_{(nanostructured)}$	100	100	
$Pt_{84}Ru_{16}$	85:15	84:16	27
$Pt_{96}Sn_4$	95:5	96:4	27
$Pt_{88}Ru_6Sn_6$	90:5:5	88:6:6	33

TEM micrographs show the void spaces in the pores of the catalyst as well as the individual grains of the catalytic particles (Figure 6.1 c, d, d insert). Grain sizes of the particles were 5 – 15 nm.

Catalyst morphology, particle size and distribution are dependent on synthesis procedures. The spray pyrolysis procedure can be performed with an atomizer, producing particles with a narrower size distribution than those produced here with a modified humidifier serving as the aerosol generator [115, 116].

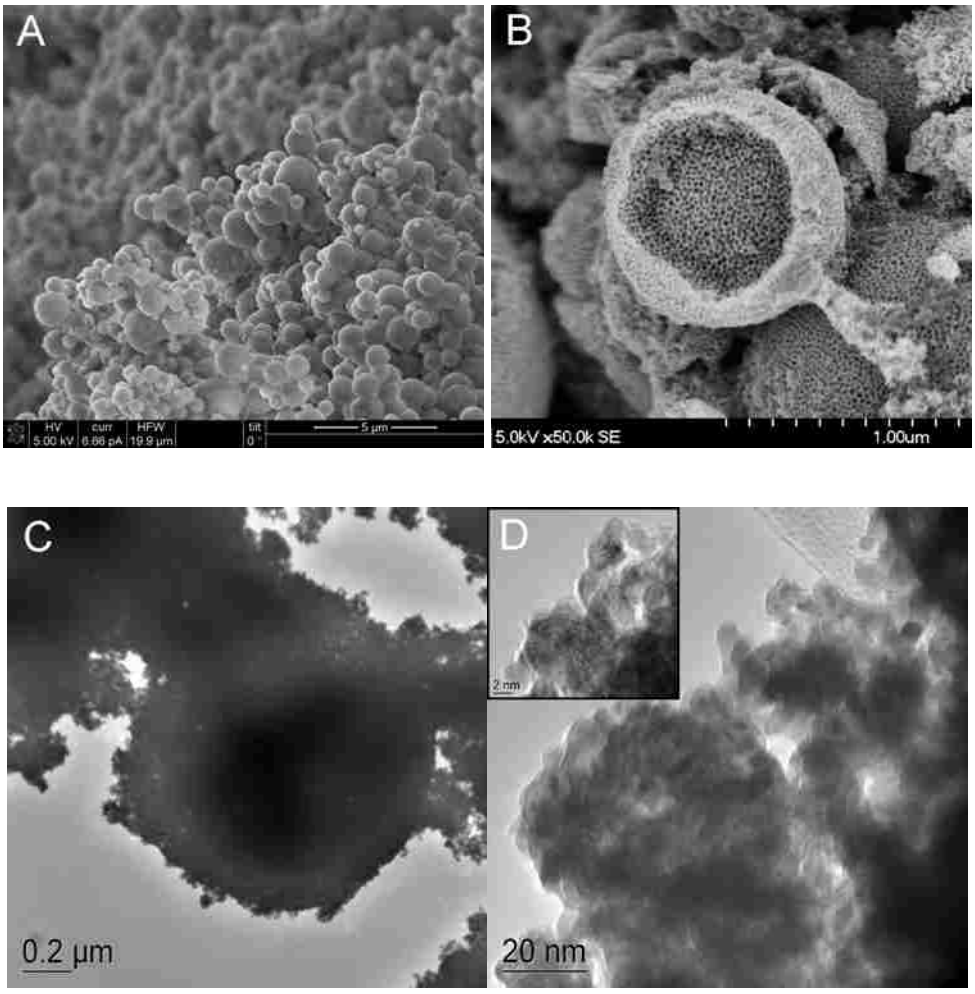

Figure 6.1: SEM and TEM micrographs of $Pt_{88}Ru_6Sn_6$ catalyst. Images of the unetched (A) and etched (B) catalyst show the droplet-like morphology of each individual catalyst particle. The templated morphology extends through the interior of the particle as shown in the SEM (B) and TEM (C, D) micrographs. The high resolution image (D, insert) shows lattice fringes from the Pt, Ru, and Sn catalyst.

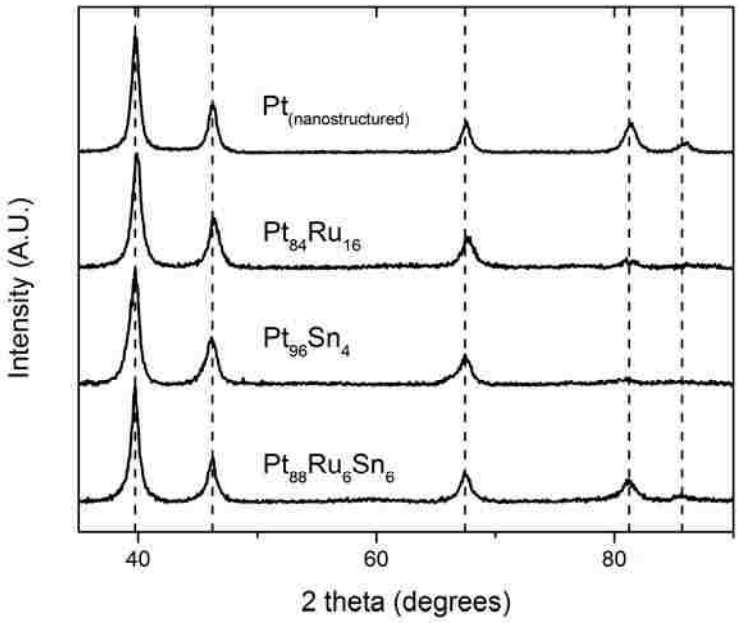

Figure 6.2. XRD diffraction patterns of synthesized nanostructured Pt and Pt based catalysts over the scan range of 2-90° (35 – 90° shown for clarity). The dashed lines represent the typical diffraction angles of the *fcc* phase of Pt.

XRD patterns of the synthesized Pt, PtRu, PtSn, and PtRuSn catalysts are shown in Figure 6.2. Phase planes of the platinum appear at the corresponding angles from (111), (200), (220), (311), and (222) phases. There were no diffraction peaks associated with separated ruthenium, tin or their oxide species detected from the XRD measurements. The peaks are shifted slightly compared to one another possibly due to incorporation or ruthenium or tin into the platinum crystal lattice. The nanostructured Pt catalyst is also slightly shifted from the dashed lines, but this could be due to the instrument itself because no impurities were detected by EDS during SEM or TEM analysis.

6.3.2 Electrochemical studies of binary and ternary catalysts for ethylene glycol and glycerol oxidation

The synthesized binary and ternary catalysts were tested as electrocatalysts for the anodic oxidation of ethylene glycol and were compared to a synthesized spray pyrolyzed nanostructured platinum catalyst. Cyclic voltammetry was used to evaluate the performance of the electrocatalysts for the oxidation of each fuel. The catalysts were cycled through the potential range multiple times until a steady state value was reached (cycle 4 for all catalysts presented here). The performance of each catalyst is presented in Figure 6.3.

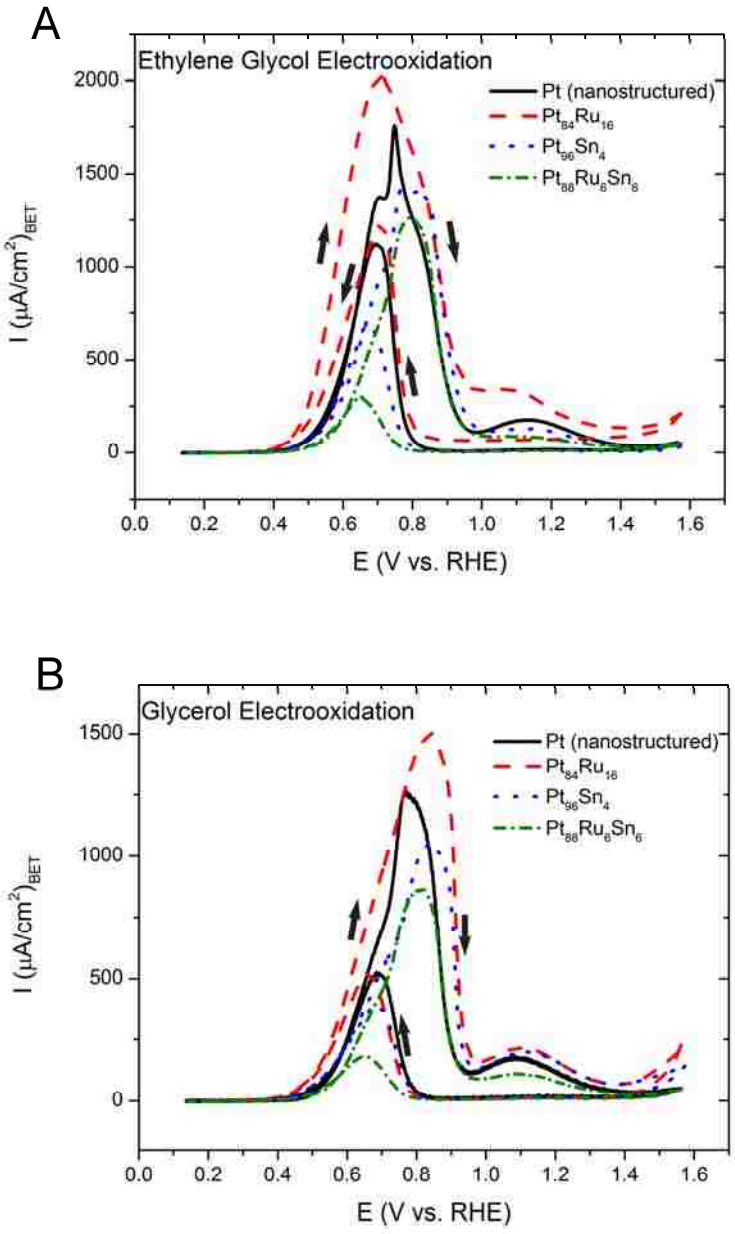

Figure 6.3. Cyclic voltammograms of Pt, $Pt_{84}Ru_{16}$, $Pt_{96}Sn_4$, and $Pt_{88}Ru_6Sn_6$ catalysts vs. ethylene glycol (A) and glycerol (B). Each catalyst was cycled until a steady state was reached at 10 mV/s in 1.0 M KOH electrolyte with 0.1 M ethylene glycol and glycerol, respectively. The current density was calculated with respect to the BET surface area.

The voltammograms exhibit expected behavior previously described regarding oxidation of these fuels in alkaline media [146, 147]. There are two oxidation peaks in the forward scan direction and one in the reverse direction. The singular anodic peak in the negative sweep represents oxidation of incompletely oxidized carbonaceous intermediates on the surface of the catalysts left over from the positive sweep [31, 138]. Accumulation of these adsorbed products block active sites on the catalyst, decreasing performance. Roquet et al. speculated that since the first oxidation wave of glycerol occurs in the platinum oxidation region, glycerol oxidation requires the presence of adsorbed hydroxyls on the surface [34]. They also speculated that because the forward and reverse sweep oxidative curves are not aligned, there is a limiting rate of glycerol adsorption on the reduced platinum surface. Since the profiles for ethylene glycol and glycerol oxidation are similar, we believe that this explanation is suitable for oxidation of both fuels.

The recorded current is normalized to the BET surface area (Table 6.1) of the catalysts in order to determine metal utilization. In terms of maximum peak current, the binary $Pt_{84}Ru_{16}$ catalyst showed enhanced oxidation behavior for both ethylene glycol oxidation and glycerol oxidation (Figure 6.3), followed by the nanostructured platinum. The $Pt_{96}Sn_4$ had higher oxidative currents than the $Pt_{88}Ru_6Sn_6$ catalyst, but both performed worse than the $Pt_{84}Ru_{16}$ and nanostructured Pt catalysts. When oxidizing ethylene glycol, the nanostructured Pt catalyst exhibits 3 distinct features. There is a shoulder at 0.704 V, the peak at 0.747 V, and a softer shoulder at 0.826 V. Possible shoulders for the binary and the broad oxidative peaks that they exhibit obscure ternary catalysts. Although glycerol has more electrons to transfer during complete oxidation, more maximum current is achieved while oxidizing ethylene glycol compared to glycerol due to a less complex oxidative pathway.

Table 6.2: Comparison of catalyst performance for ethylene glycol and glycerol electrooxidation

Ethylene Glycol						
Catalyst	**Eonset (V)**	**E_F (V)**	**I_F (μA/cm$^2_{BET}$)**	**E_R (V)**	**I_R (μA/cm$^2_{BET}$)**	**I_F/I_R**
Pt (nanostructured)	0.36	0.76	1718.52	0.69	1117.47	1.54
$Pt_{84}Ru_{16}$	0.29	0.72	2109.55	0.69	1271.58	1.66
$Pt_{96}Sn_4$	0.35	0.78	1408.29	0.67	691.21	2.04
$Pt_{88}Ru_6Sn_6$	0.38	0.80	1260.27	0.64	295.05	4.27
Glycerol						
Catalyst	**Eonset (V)**	**E_F (V)**	**I_F (μA/cm$^2_{BET}$)**	**E_R (V)**	**I_R (μA/cm$^2_{BET}$)**	**I_F/I_R**
Pt (nanostructured)	0.40	0.79	1245.21	0.68	514.86	2.42
$Pt_{84}Ru_{16}$	0.33	0.85	1568.50	0.65	542.41	2.89
$Pt_{96}Sn_4$	0.34	0.85	1044.91	0.67	378.80	2.76
$Pt_{88}Ru_6Sn_6$	0.36	0.82	862.79	0.64	183.30	4.71

E_{onset}: Onset potential (vs. RHE)

E_F, I_F: Peak potential and current density, respectively, of main oxidation peak at 10mV/s (vs. RHE)

E_R, I_R: Peak potential and current density, respectively, of reverse oxidation peak at 10mV/s (vs. RHE)

I_F/I_R: Ratio of forward main and reverse oxidation peak current density

A summary of the catalyst performance is given in Table 6.2. The catalysts were evaluated in terms of their onset potential, the peak potentials, current densities, and the ratio of forward anodic peak to reverse peak current. The trend of the onset potential for ethylene glycol oxidation was $Pt_{84}Ru_{16}$ < $Pt_{96}Sn_4$ < nanostructured Pt <$Pt_{88}Ru_6Sn_6$ while for glycerol oxidation the trend was $Pt_{84}Ru_{16}$ < $Pt_{96}Sn_4$ < $Pt_{88}Ru_6Sn_6$ < nanostructured Pt. For both fuels the binary catalysts had the lowest onset potentials.

The binary PtRu catalyst had the lowest oxidative peak potential, and the highest current for both ethylene glycol and glycerol oxidation. For both fuels, the ternary PtRuSn electrocatalyst performed poorly compared to the binary and nanostructured Pt catalyst. From these results it seems that alloying platinum specifically with both ruthenium and tin simultaneously as a ternary catalyst is not beneficial in terms of achieving the maximum current compared to binary PtRu

and PtSn catalysts, in contrast to the results obtained in Chapter 5. The binary and ternary electrocatalysts have higher I_F/I_R ratios than the nanostructured Pt catalyst, signaling that accumulation of oxidation residues during the catalytic processes is less than on the pure Pt catalyst and similar catalysts reported in acidic media [139]. The ternary catalyst had the highest I_F/I_R ratio, suggesting that the effects of the modifier tin and ruthenium atoms help to prevent buildup of oxidation products on the platinum active sites, even though its oxidative performance lacked that of binary and nanostructured Pt catalysts.

Steady-state polarization curves of ethylene glycol and glycerol oxidation on the catalyst were obtained under potentiostatic conditions (Figure 6.4). Maximum currents for the PtRu catalyst were higher than the PtRu and PtRuSn catalysts for both ethylene glycol and glycerol oxidation. For ethylene glycol electrooxidation, the maximum current achieved by the PtRu catalyst was twice that of the PtSn, 3.2 times that of the nanostructured platinum catalyst and 6 times that of the ternary PtRuSn catalyst following a trend of PtRu>PtSn>Pt>PtRuSn. Similar performance was seen with glycerol. The maximum current for the PtRu electrocatalyst was 1.2 times higher than the PtSn, 1.77 times that of the platinum, and 3.7 times higher than the PtRuSn. At potentials lower than 0.51 V, the Pt catalyst has a higher current than the binary PtSn catalyst, but at higher potentials the PtSn catalyst outperforms the Pt catalyst. The trend for catalyst performance during glycerol oxidation trends as PtRu>PtSn>Pt>PtRuSn at potentials higher than 0.51 V.

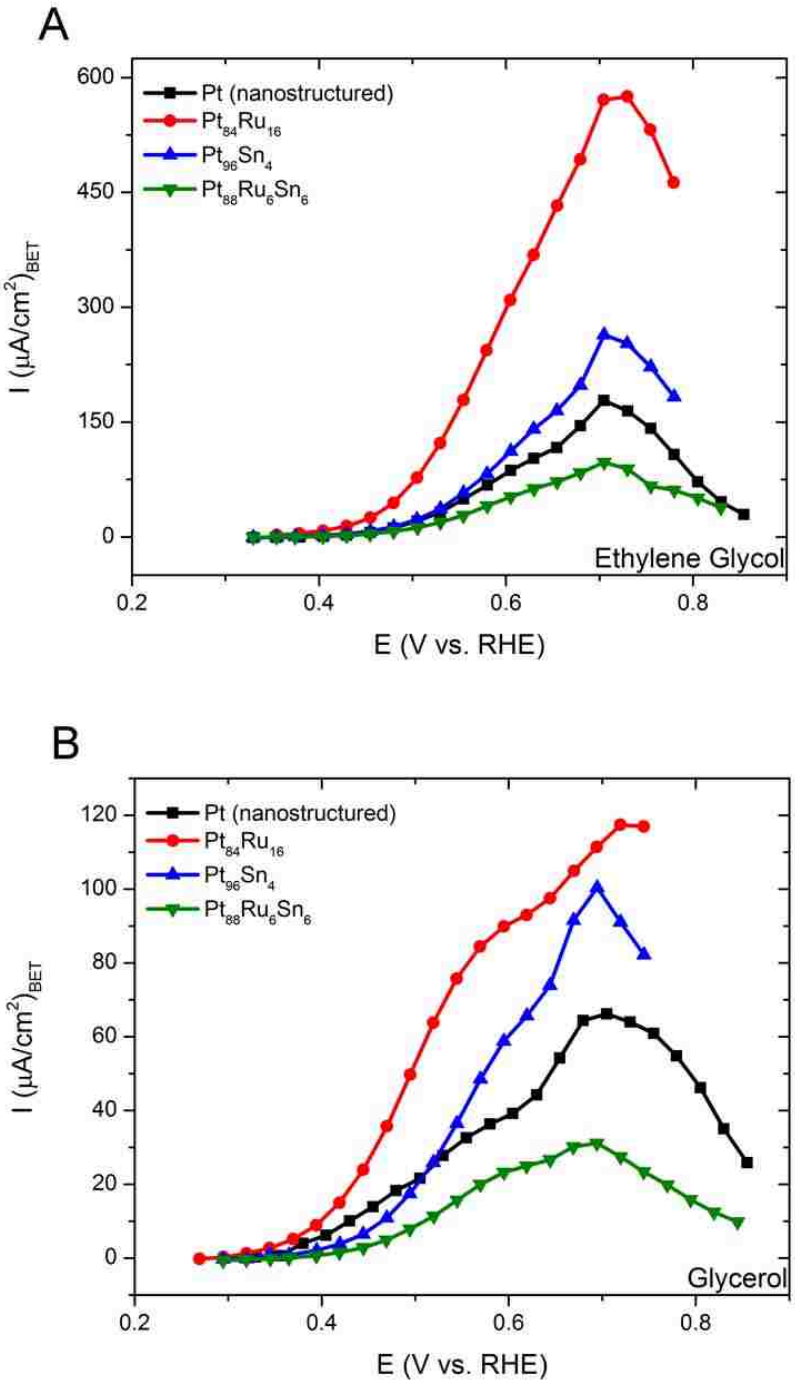

Figure 6.4. Steady-state polarization curves of $Pt_{84}Ru_{16}$, $Pt_{88}Ru_6Sn_6$, and $Pt_{96}Sn_4$ catalysts vs. ethylene glycol (top) and glycerol (bottom). 1.0 M KOH electrolyte with 0.1 M ethylene glycol and glycerol, respectively. The current density was calculated with respect to the BET surface area.

6.3.3 IRRAS characterization of ethylene glycol and glycerol oxidation

The oxidation pathway of ethylene glycol has been described previously [32, 33]. This reaction scheme consists of a complex parallel 2-electron steps oxidation mechanism first from ethylene glycol to glycoaldehyde. The molecule is then oxidized to either glyoxal or glycolic acid, then to glycoxylic acid followed by oxalic acid and then finally CO_2. It is worth noting that oxalic acid is in the [A^{2-}] deprotonated state due to its relatively low pKa values of 1.38 and 4.28.

Infrared spectroscopy was used to elucidate the ethylene glycol electrooxidation reaction mechanism on the binary and ternary catalysts. Each spectrum was recorded in 0.1 M potassium hydroxide solution with 0.1 M of ethylene glycol or glycerol. Some major band frequencies are summarized in Table 6.3 for ethylene glycol and glycerol oxidation. Glycolaldehyde is not present in the table due to dimerization in neutral media that is further complicated in alkaline solution [148].

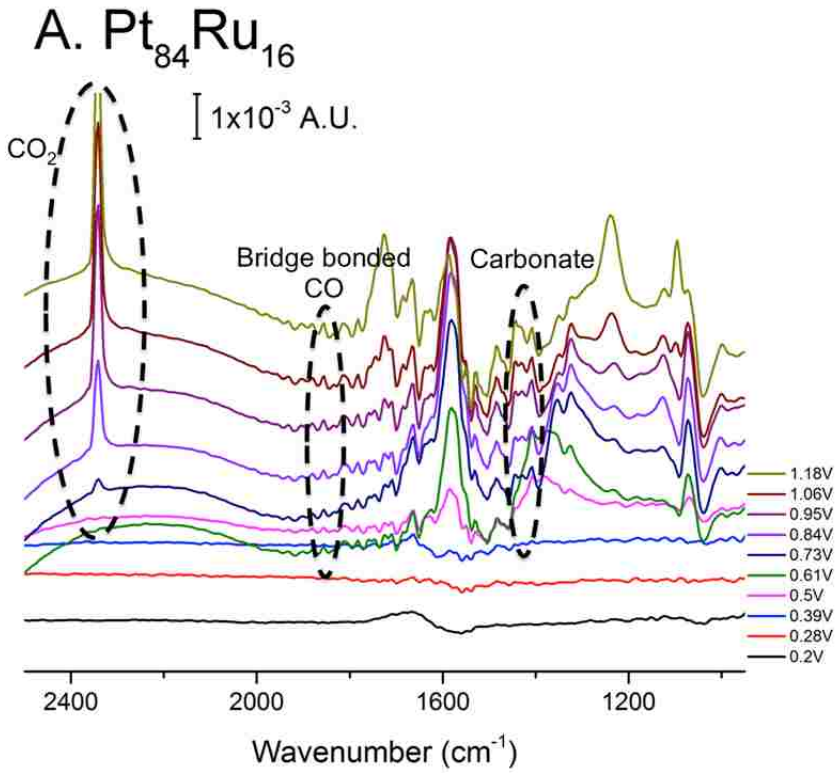
A. $Pt_{84}Ru_{16}$
1x10^{-3} A.U.
CO_2
Bridge bonded CO
Carbonate
1.18V
1.06V
0.95V
0.84V
0.73V
0.61V
0.5V
0.39V
0.28V
0.2V
2400
2000
1600
1200
Wavenumber (cm^{-1})

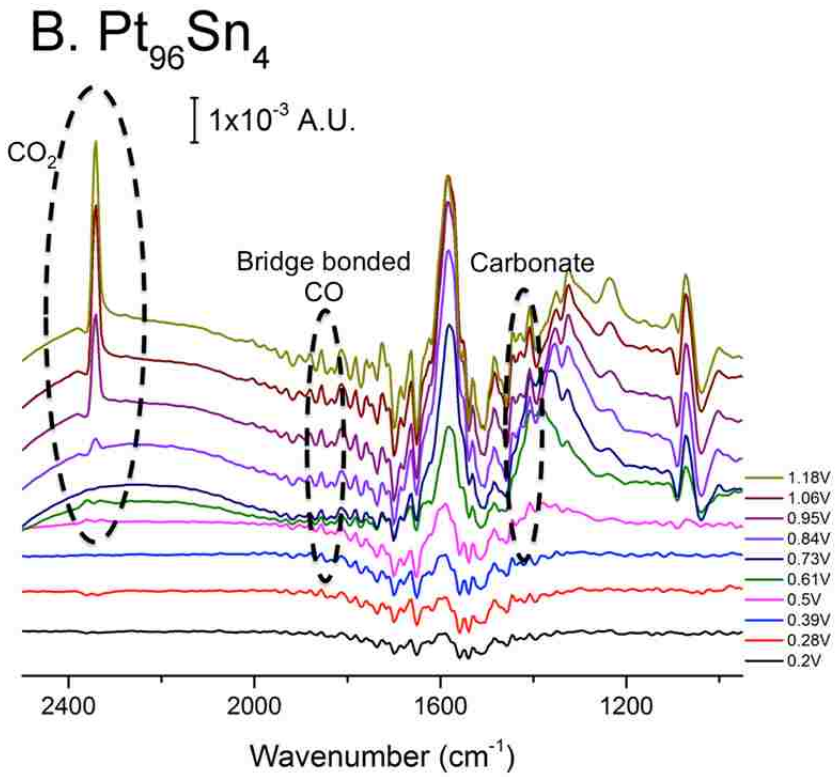
B. $Pt_{96}Sn_4$
1x10^{-3} A.U.
CO_2
Bridge bonded CO
Carbonate
1.18V
1.06V
0.95V
0.84V
0.73V
0.61V
0.5V
0.39V
0.28V
0.2V
2400
2000
1600
1200
Wavenumber (cm^{-1})

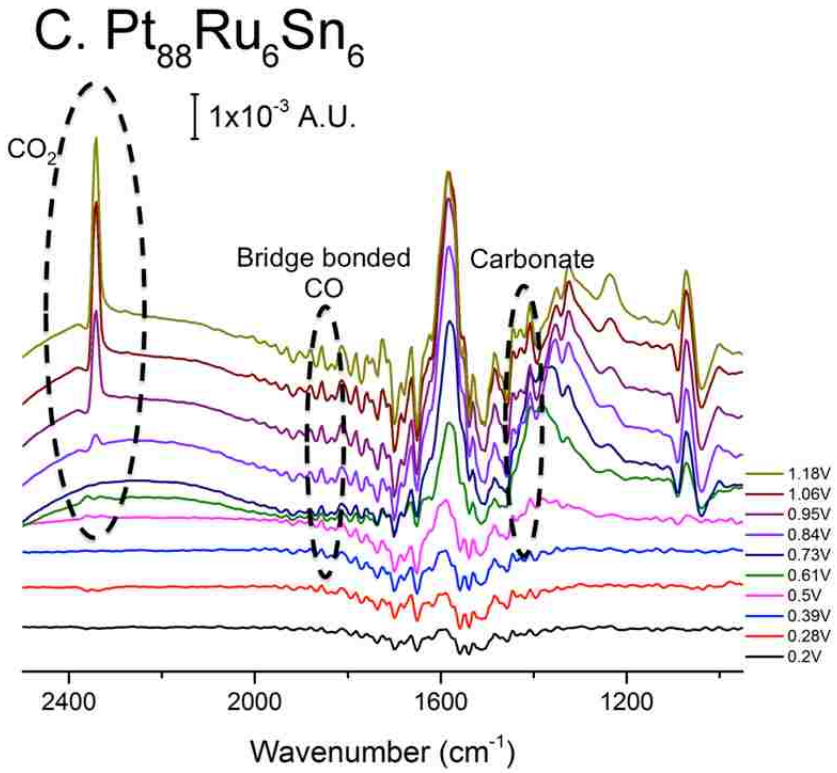
C. Pt88Ru6Sn6
1x10-3 A.U.
CO2
Bridge bonded CO
Carbonate
1.18V
1.06V
0.95V
0.84V
0.73V
0.61V
0.5V
0.39V
0.28V
0.2V
2400
2000
1600
1200
Wavenumber (cm-1)

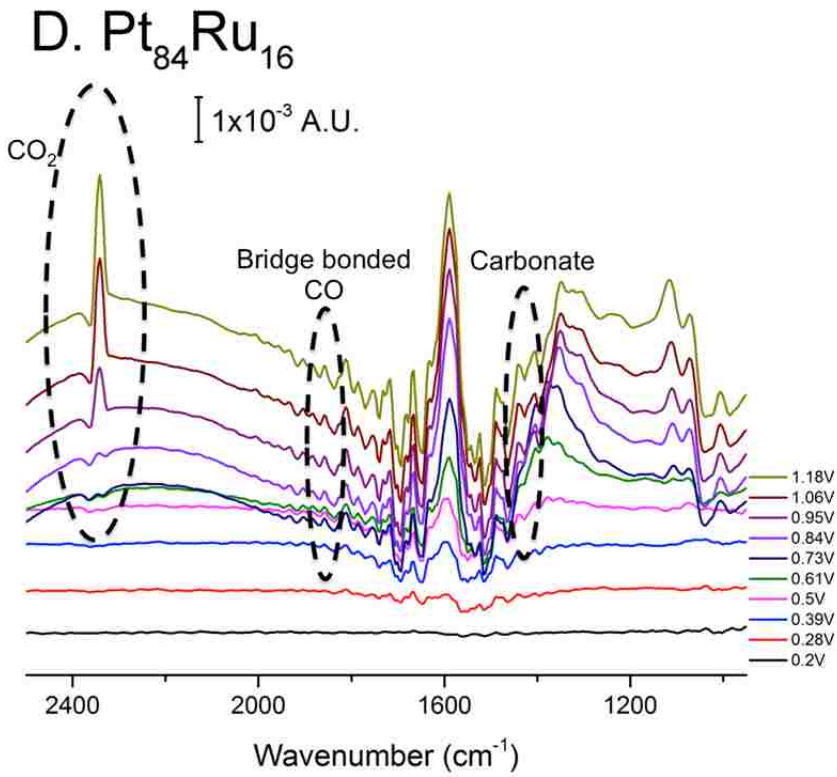
D. Pt84Ru16
1x10-3 A.U.
CO2
Bridge bonded CO
Carbonate
1.18V
1.06V
0.95V
0.84V
0.73V
0.61V
0.5V
0.39V
0.28V
0.2V
2400
2000
1600
1200
Wavenumber (cm-1)

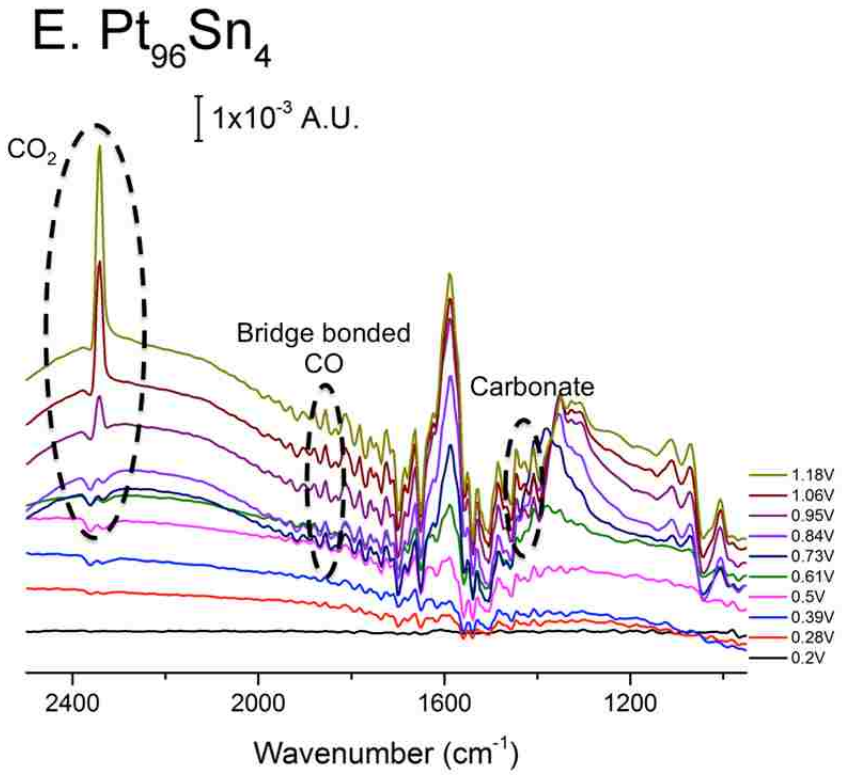
E. $Pt_{96}Sn_4$
1x10^{-3} A.U.
CO_2
Bridge bonded CO
Carbonate
1.18V
1.06V
0.95V
0.84V
0.73V
0.61V
0.5V
0.39V
0.28V
0.2V
2400
2000
1600
1200
Wavenumber (cm^{-1})

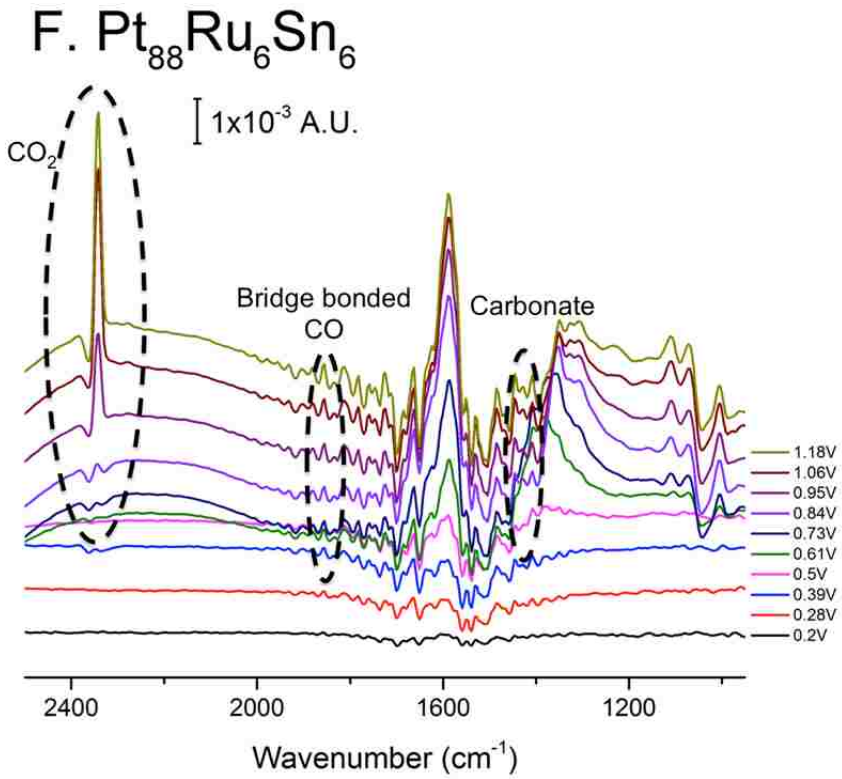
F. $Pt_{88}Ru_6Sn_6$
1x10^{-3} A.U.
CO_2
Bridge bonded CO
Carbonate
1.18V
1.06V
0.95V
0.84V
0.73V
0.61V
0.5V
0.39V
0.28V
0.2V
2400
2000
1600
1200
Wavenumber (cm^{-1})

Figure 6.5: IRRAS spectra of ethylene glycol (A-C) and glycerol (D-F) oxidation on binary and ternary Pt-based catalysts. 1 mV/s scan rate in 0.1 M KOH and 0.1 M fuel.

Table 6.3: Infrared frequencies observed by *in situ* FTIR spectroscopy of oxidation products formed during EG and Gly electrooxidation

Wavenumber (cm^{-1})	Assignment
1004	Alcohol CH_2-OH stretch [149]
1071	Aldehyde stretch (glyoxal, glycolate, glyceraldehyde) [32, 147-149]
1094	Alcohol stretching [149]
1111	CH-OH stretch [149]
1236	C-O stretch of glycolate [150]
1303	Symmetric $^{-}OOC\text{-}COO^{-}$, glyceraldehyde [32, 151]
1320	Symmetric COO^{-} stretch of glycolate, oxalate [148, 150]
1353	Adsorbed carbonylate [150]
~1405	Carbonate CO_3^{2-} [32, 150]
1445, 1548, 1630	Carboxylate groups [152]
1574	Asymmetric $^{-}OOC\text{-}COO^{-}$ [32]
~1589	H-O-H deformation of adsorbed water, asymmetric COO^{-} stretch of glyoxal, glycolate, glyoxylate [148]
~1665	Carbonyl and carboxyl stretches [152]
1723	Carboxyl stretching [152]
2343	CO_2 asymmetric stretch

The oxidation pathway and kinetics as shown via infrared spectra for ethylene glycol oxidation are very similar for the binary and ternary catalysts. The peaks for alcohol stretching at 1000 cm^{-1}, aldehyde stretching at 1070 cm^{-1} indicative of glyoxal and glycolate species, symmetric COO^{-} stretching at 1320 cm^{-1}, and asymmetric $^{-}OOC\text{-}COO^{-}$ stretching at 1574 cm^{-1} indicate the presence of glyoxal and glycolate at 0.5 V for the PtRu catalyst, and 0.61 for the PtSn and PtRuSn catalyst. Asymmetric COO^{-} stretching along with water deformation results in a very strong peak at 1589 cm^{-1}. Carbonate formation at 1405 cm^{-1} begins between 0.4 and 0.5 V, and increases up to 0.6 V where it seems to remain steady or decrease as Demarconnay et al. observed [150]. A small peak due to bridge bonded CO species at 1856 and 1813 cm^{-1} with the

much smaller corresponding linear CO peak at 2000 cm^{-1} appears at 0.28 V for the PtSn and PtRuSn catalysts, and at 0.61 V for the PtRu catalyst [72, 153]. These peaks grow slightly in intensity as the electrode becomes more polarized. As the reaction progresses, CO_2 begins to form at 0.73 V for the PtRu catalyst [150], and 0.84 V for the PtSn and PtRuSn catalysts. Production of a carboxylic acid evident by absorbance bands at 1723 cm^{-1} 1236 cm^{-1} and 1095 cm^{-1} is enhanced on the $Pt_{84}Ru_{16}$ catalyst at high (1.18 V) potentials compared to the PtSn and PtRuSn catalyst.

The electrooxidation pathway of glycerol has been described recently in alkaline media. Kwon et al. used high performance liquid chromatography coupled with online electrochemical mass spectroscopy to elucidate the complex oxidation reaction scheme on gold and platinum catalysts [35]. They found high concentrations of glyceraldehyde to be the first oxidation product at 0.4 V, followed by glyceric acid. Dihydroxyacetone, hydroxypyruvic acid, glycolic acid, formic acid, oxalic acid, and tartronic acid were detected at low concentrations.

The oxidation reaction pathway of glycerol on the binary and ternary Pt based catalysts was similar amongst the catalysts. Absorbance bands at 1070 cm^{-1} corresponding to aldehydes appear at 0.61 V and grow in intensity as the potential increases. As with ethylene glycol, a strong peak at 1589 cm^{-1} results from the water stretching and carboxylic acids that absorb at the same wavelength. A small peak due to bridge bonded CO species at 1856 and 1813 cm^{-1} with the even smaller corresponding linear CO peak at 2000 cm^{-1} appears at 0.28 V and grows slightly in intensity as the electrode becomes more polarized. CO_2 formation begins at 0.84 V for all three catalysts.

6.4 - Conclusions

We have reported the synthesis and characterization of binary and ternary templated catalysts synthesized by spray pyrolysis. The use of spray pyrolysis was chosen due to its ease of creating templated catalysts with desired composition. Characterization of the catalysts was performed using SEM, TEM, and EDS to determine morphology, purity and composition. EDS analysis confirmed the composition of the as-created catalysts. The catalysts had an open frame sponge like morphology caused by template removal via etching of the silica catalyst. Cyclic voltammetry and steady state polarization showed that the binary $Pt_{84}Ru_{16}$ had both higher oxidative currents and better catalytic stability versus nanostructured platinum, binary PtSn, and ternary PtRuSn catalysts. The ratio of forward peak current to reverse peak current was high, indicating that accumulation of oxidation products on the catalyst surface is not as significant as it is for reactions using similar catalysts in acid media. The addition of both ruthenium and tin modifiers to platinum catalysts is not beneficial for maximum current generation, as seen in the cyclic voltammetry and steady state polarization experiments, but adsorption of reaction intermediates that can block the electrode and decrease performance is lower on the ternary catalysts than the binary PtRu, PtSn and nanostructured Pt catalyst. Both the binary and ternary electrocatalysts are capable of complete oxidation of both ethylene glycol and glycerol via the presence of CO_2 as shown by *in situ* IRRAS. This work demonstrates the complimentary effect of Ru and Sn modifiers in a binary platinum based catalyst to achieve higher catalyst performance for the electrooxidation of ethylene glycol and glycerol.

Chapter 7 - Complete oxidation of methanol using a protein engineered enzymatic cascade

**Akinbayowa Falase contributed to the infrared chracaterization of this work.*

7.1 - Introduction

The need for alternative sources of energy has led to exploration of nontraditional fuel sources, unique inorganic and biological catalysts, and substitute power generating devices. Enzymes derived from bacteria and other sources have been widely reported in the literature as potential catalysts for fuel cells. These enzymatic fuel cells are fast becoming an important research focus due to the ubiquity of the catalysts, the availability of the fuel, and the simplicity of the design compared to the conventional Proton Exchange Membrane (PEM). Hydrogen or readily available liquid hydrocarbon fuels such as sugars (e.g. glucose) and alcohols (e.g. methanol) are used to power these PEM fuel cells, depending on the type of cell. Traditional precious metal catalysts are unable to completely harvest the electrons from the fuel, leaving partially oxidized byproducts that foul the catalyst. In biological organisms, groups of enzymes are used in a cascade to oxidize complex fuels completely to CO_2, which is respired away. We present an enzymatic cascade that oxidizes methanol to carbon dioxide. The enzymes used in the cascade are genetically modified to include hydrogel domains that allow for self-assembly of the cascade[154-158]. We used in situ Fourier Transform Infrared Spectroscopy to determine the reaction kinetics of the enzymatic biofuel cell, the extent of reaction and to verify complete oxidation via CO_2 generation.

7.2 - Results

Three NAD(H)-dependent dehydrogenase enzymes from different sources were modified for self-assembly. The first enzyme was a tetrameric alcohol dehydrogenase (ADH) from *Bacillus stearothermophilus* which is able to oxidize methanol to formaldehyde[159]. The second enzyme was a tetrameric human aldehyde dehydrogenase (ALDH2), which can oxidize formaldehyde to formate[160, 161]. The final enzyme, a dimeric formate dehydrogenase (FDH1) from *Saccharomyces cerevisiae*, is able to oxidize formate to CO_2[162]. When combined these enzymes produce a synthetic metabolic pathway capable of the complete oxidation of methanol[163-165]. A schematic diagram of this reaction is as shown in Figure 7.1. An alpha-helical leucine zipper domain (H) and randomly structured soluble peptide domain (S) were genetically appended to the N-termini of each of the three dehydrogenase genes. The three new bifunctional enzyme constructs (HSADH, HSALDH2, and HSFDH1) were overexpressed in E. coli and purified. HSADH and HSFDH1 were readily expressed and purified, while the HSALDH2 enzyme required the addition of the maltose binding protein (MBP) to enable functional expression. An intein domain was added between the MBP and HSALDH2 such that it spontaneously cleaved after expression within the cells and thus the HSALDH2 protein could be purified as though no fusion protein had been included in the construct[166-169].

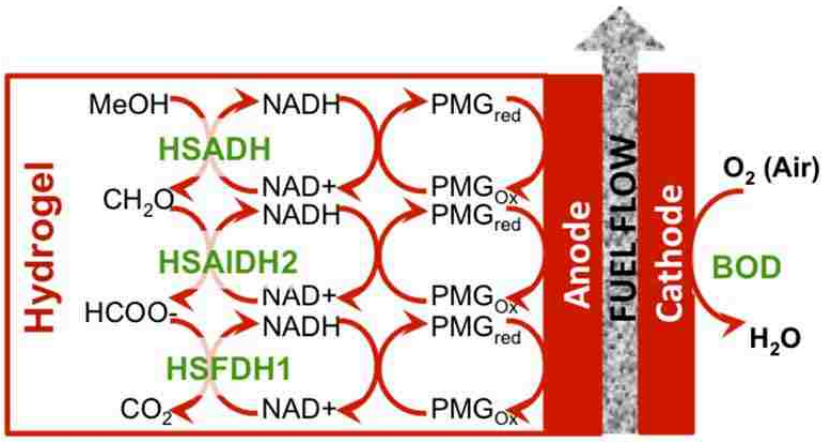

Figure 7.1: Protein engineered hydrogel enzyme cascade. The cascade consists of a tetrameric alcohol dehydrogenase, a tetrameric aldehyde dehydrogenase, and a dimeric formate dehydrogenase that catalyzes the oxidation of methanol, formaldehyde, and formate, respectively. The anode is paired with a bilirubin oxidase enzyme at the cathode.

In order to test the performance of the enzyme cascade, an anode with the enzymes was paired against a Ag/AgCl reference electrode and with a bilirubin oxidase cathode and polarization curves were constructed. With only methanol fuel, the anode had an open circuit potential of -0.02 V, and reached 0.03 V at 65 μA/cm^2 (Figure 7.2). Upon addition of formaldehyde the open circuit potential of the anode dropped to -0.07 V, and the anode reached 0.03 V at 72 μA/cm^2. The final addition of formate to the cell dropped the open circuit even more to -0.08V, with an increase to 0.03V at 100 μA/cm^2. When paired with the bilirubin oxidase cathode, the full cell had performed similarly. Instead of starting with methanol and adding the subsequent fuels to the cell, each curve was generated using only the specified fuel. The full cell's open circuit potential with only methanol as fuel was 0.04 V, and dropped to 0.1 V at 20 μA/cm^2. A higher open circuit potential at 0.45 V and 0.48 V for formaldehyde and formate respectively was achieved, but the potential dropped quickly with increasing current. When all three fuels are present, the fuel cell

had the highest open circuit potential at 0.55V, and held a high potential to 0.3 V at a current density of 82 μA/cm^2.

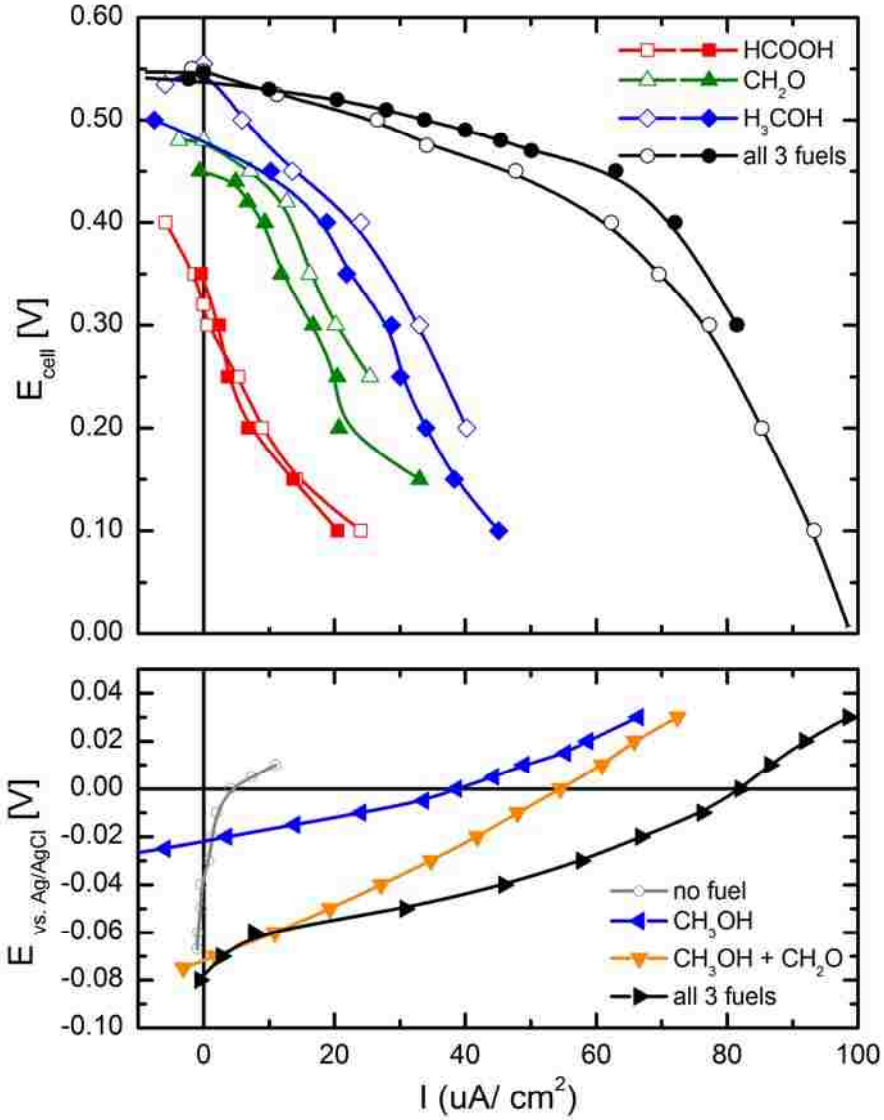

Figure 7.2: Polarization curve of enzyme cascade anode vs. bilirubin oxidase (top), and enzyme cascade anode vs. Ag/AgCl reference electrode (bottom). pH 7.5 PBS, 100mM potassium phosphate buffer and 100mM respective fuel.

Power curves were constructed using the full cell. A maximum of 2.5 μW/cm^2 at 25 μA/cm^2 was achieved with only methanol as the fuel. Slightly better performance was achieved with formaldehyde and also with formate. The maximum cell performance of 28 μW/cm^2 at 72 μA/cm^2 occurred with all three fuels present.

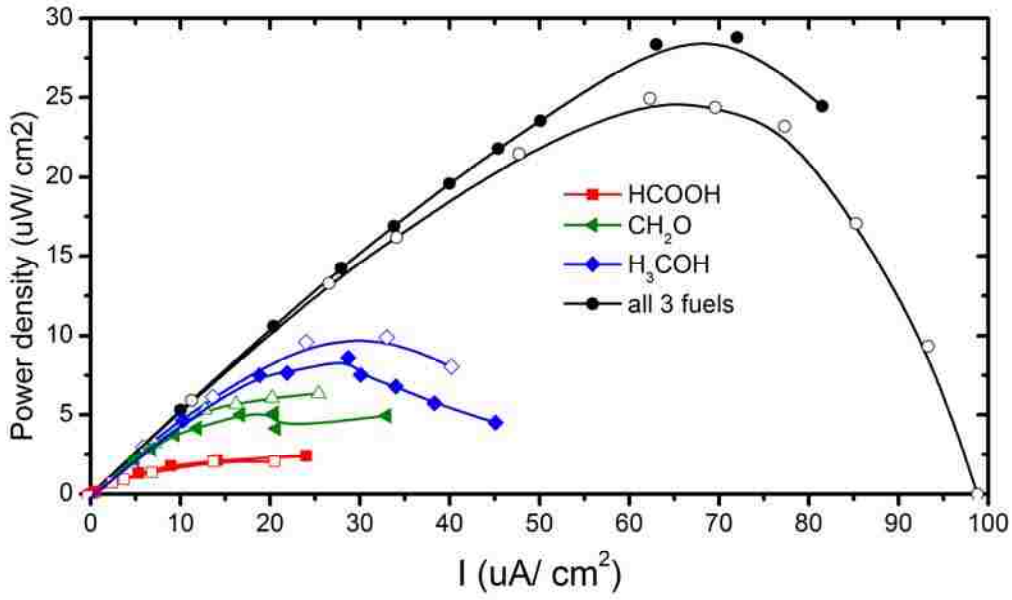

Figure 7.3: Full biofuel cell polarization curves of enzymatic hydrogel cascade anode paired with bilirubin oxidase cathode. pH 7.5 PBS, 100mM KCl, 100mM each fuel. Maximum power is achieved with addition of all three fuels.

To determine the extent of reaction by generation of CO_2, the enzyme cascade was evaluated by *in situ* infrared spectroscopy. The electrode with the enzyme cascade was held at a 0.05 V vs. Ag/AgCl throughout the entirety of the experiment. Aliquots of 0.1 M methanol, formaldehyde, and formic acid respectively were added to the cell sequentially. The fuels were allowed to

diffuse into the pressed space between the electrode and IR window for at least an hour. Each subsequent fuel was added once the current reached a steady state value (Figure 7.4).

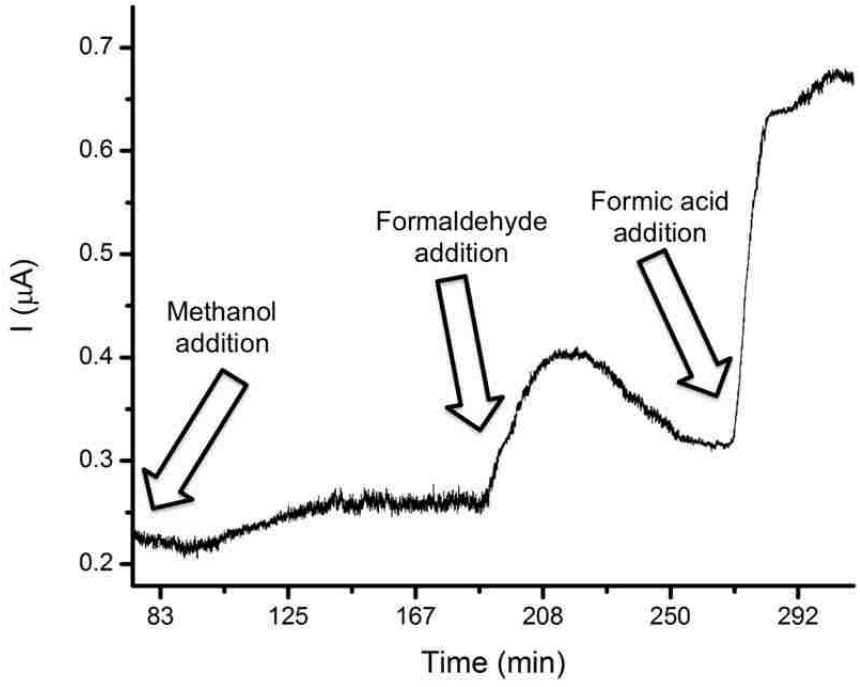

Figure 7.4: Chronoamperommetry (E = +50mV) plot during addition of fuels in the infrared cell. pH 7.5 PBS with Ag/AgCl reference electrode and Pt wire counter electrode. The external module was purged with air cleaned of water vapor and CO_2.

The chronoamperommetry results matched the polarization data recorded earlier. Upon addition of methanol, there is a small current response. When formaldehyde is added, the current response is larger, but the maximum current increase occurs when formic acid is added so the cell has all three fuels present. When methanol and formaldehyde was added to the cell, there was very little change in the level of CO_2 detected (Figure 7.5).

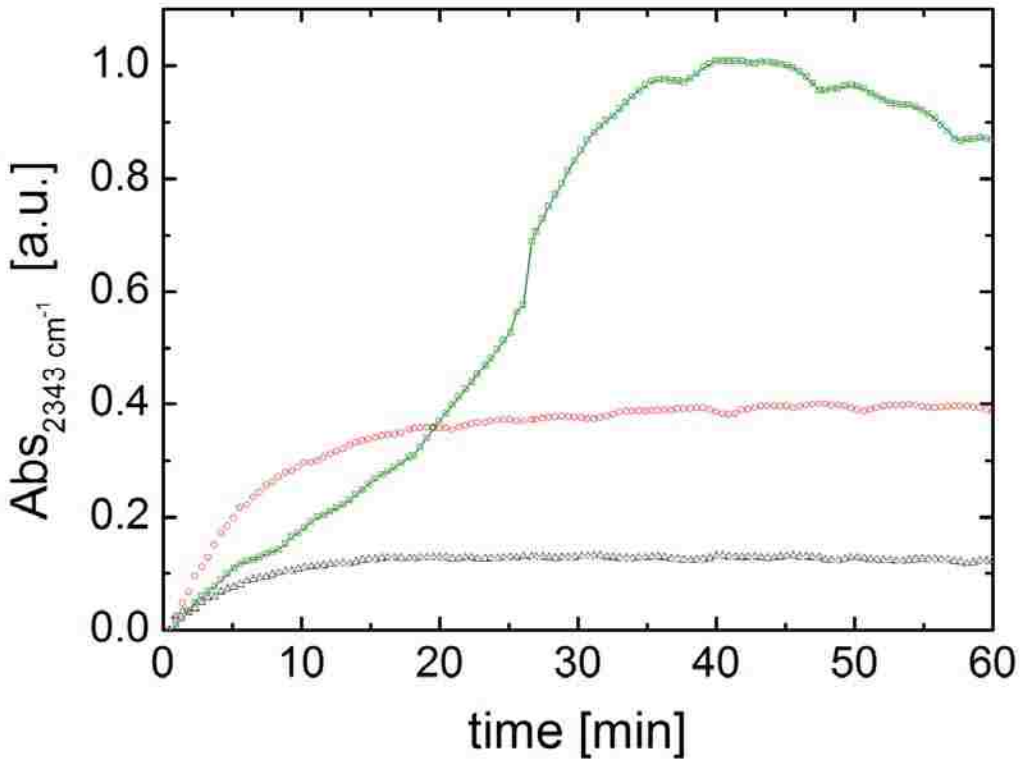
1.0
0.8
0.6
0.4
0.2
0.0
Abs2343 cm-1 [a.u.]
0
10
20
30
40
50
60
time [min]

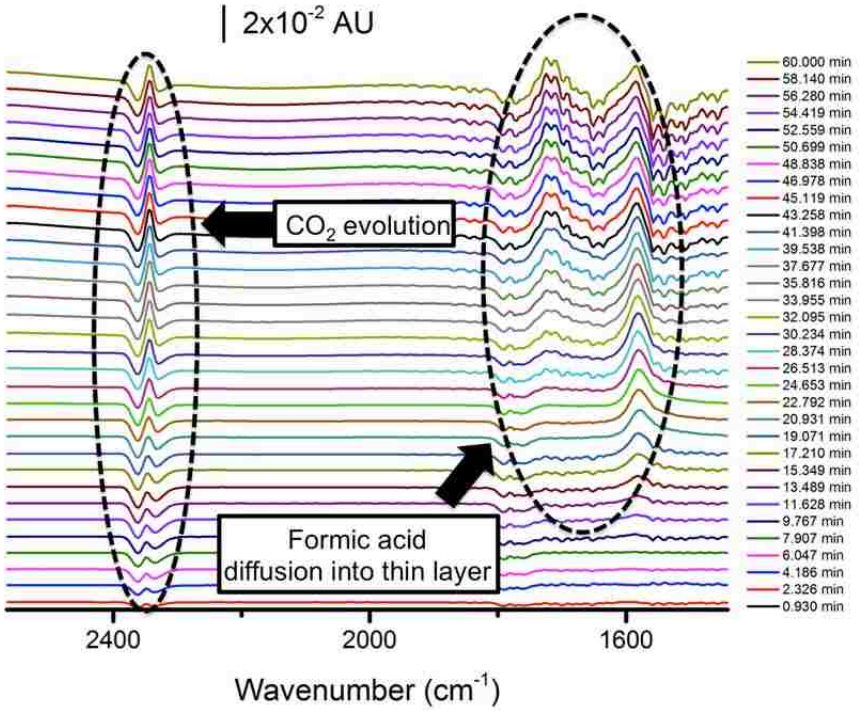
2x10-2 AU
CO2 evolution
Formic acid
diffusion into thin layer
60.000 min
58.140 min
56.280 min
54.419 min
52.559 min
50.699 min
48.838 min
46.978 min
45.119 min
43.258 min
41.398 min
39.538 min
37.677 min
35.816 min
33.955 min
32.095 min
30.234 min
28.374 min
26.513 min
24.653 min
22.792 min
20.931 min
19.071 min
17.210 min
15.349 min
13.489 min
11.628 min
9.767 min
7.907 min
6.047 min
4.186 min
2.326 min
0.930 min
2400
2000
1600
Wavenumber (cm-1)

Figure 7.5: (Top) Relative absorbance of CO_2 (2341cm^{-1}) after additions of methanol, formaldehyde and formic acid. CO_2 production was at a maximum once all three fuels are present, correlating to the polarization curves. (Bottom) FTIR spectra taken during formic acid diffusion into thin layer

Upon addition of formic acid, the level of CO_2 in the system increased. This result matches the polarization data presented earlier as well. When all three fuels are present, the current produced is at a maximum, and CO_2 evolution is also maximized.

We have successfully demonstrated complete oxidation of methanol using a fully enzymatic cascade. The maximum current generation was achieved when the electrolyte contained methanol, formaldehyde, and formic acid; fuels for each of the three enzymes. CO_2 was detected from the electrode when all three fuels were present. This work solidifies the feasibility of enzymatic fuel cells for deep oxidation of alcohol fuels.

Chapter 8 - Hybrid nano-structured platinum-based catalyst/enzyme anode for oxidation of ethanol and ethylene glycol

8.1 - Introduction

Complete oxidation of fuels to extract the maximum amount of energy while minimizing reaction byproducts is the goal of successful anode design for a fuel cell. Platinum and platinum-based metals are commonly used to catalyze oxidation of hydrogen for polymer electrolyte membrane (PEM) fuel cells, and alcohols in direct alcohol fuel cells (DAFCs). Hydrogen is a non-polluting fuel, but essential widespread infrastructure does not exist to safely distribute compressed hydrogen for commercial applications[170, 171]. Power sources based on DAFCs using ethanol, ethylene glycol and glycerol show greater promise because the fuels used are biorenewable, safe to transport handle and store, and are compatible with existing distribution infrastructure[64, 172]. Unfortunately, long electrode lifetimes and complete oxidation of these fuels has been difficult to realize, mainly due to catalyst fouling and difficulty in C-C bond scission.

Enzymatic biofuel cells are a promising technology for low power devices. Enzymes harvested from bacteria or other sources are capable of oxidizing a wide variety of fuels for power generation[88, 173]. These operate at near neutral pHs with temperatures ranging between 20 and 37°C in order to preserve the enzyme's secondary and tertiary structure. Due to their high specificity for their substrate, enzymes are ideal catalysts because they do not become passivated or inhibited by impurities or reaction byproducts in the fuel. Enzymes however are fragile, sometimes require complex immobilization schemes for longer lifetimes and can operate in a limited temperature and pH range. Alone, they are usually only capable of single two electron oxidation steps, and require multiple enzymes for deep or complete fuel oxidation. Several

schemes have been developed to allow enzyme based fuel cells to increase the degree of oxidation including constructing enzyme cascades that duplicate part or all of the Krebs cycle and metabolon structures that mimick living systems[94, 96, 163, 165, 174-177].

A recent report by our group has demonstrated complete oxidation of ethylene glycol and glycerol using a nanostructured PtRu electrocatalyst in neutral media[178]. Although CO_2 was detected during oxidation, the presence of reaction byproducts indicated a low conversion. The presence of these byproducts is indicative of energy that is not harvested from the fuel. In order to increase the conversion, enzymes could be used for co-catalysis. To realize this, an immobilization scheme that satisfies enzyme stability and lifetime requirements must be developed that enables the metal catalysts to operate efficiently.

We present a hybrid anode consisting of a nanostructured PtRu electrocatalyst with NAD-dependent alcohol dehydrogenase (ADH) from *Saccharomyces cerevisiae* immobilized in a conductive chitosan scaffold[179-181]. The combination of the inorganic and biological catalysts served to enhance oxidation of ethanol, and ethylene glycol fuel. NAD^+ was regenerated by using a polymerized polymethylene green (PMG) film on the electrode. Cyclic voltammetry was used to initially evaluate the system to determine if both catalysts were working in concert. Steady state polarization was used to determine the feasibility of constructing a hybrid inorganic/organic anode. A concentration calibration curve was constructed to determine the enzymatic activity and performance.

8.2 - Methods and Materials

Ethanol, ethylene glycol, alcohol dehydrogenase from *Saccharomyces cerevisiae* and chitosan were purchased from Sigma. Methylene green, and NAD^+ were purchased from Fluka, and

multi-walled carbon nanotubes (MWCNTs) (20-30nm OD, 10-30um length, 95 wt% purity) were purchased from www.cheaptubesinc.com. Chitosan was pretreated before use to achieve a final deacetylation degree of 95% by autoclaving for 20 min at 121°C in 40 wt% NaOH solution, filtrated, washed with DI water and phosphate buffer pH 8.0 and dried in a vacuum oven at 50°C for 24h[182]. A 1 wt% chitosan stock solution was prepared in 0.25 M acetic acid and its pH was then adjusted to 5.8 with concentrated NaOH and stored at room temperature with stirring. A MWCNTs/Chitosan solution was prepare from this stock solution with a final concentration of 2.5 wt% of MWCNTs. NAD^+ stock solutions were prepared with phosphate buffer, pH 7.01. Electrochemical measurements were carried out in standard three-electrode electrochemical cell containing platinum wire as the counter electrode, an Ag/AgCl reference electrode (CH Instruments), and a glassy carbon electrode with a diameter of 3 mm. All potential values are given against Ag/AgCl. Prior to use, the GC electrode was polished with alumina slurry (Electron Microscopy Sciences) to a mirror finish.

Polymethylene green (Poly-MG) was electrochemically polymerized on the glassy carbon electrodes by cyclic voltammetry as previously reported[179, 183, 184]. The electropolymerization of MG was carried out by cyclic voltammetry under a scan rate of 50 mV/s from -0.5 V to 1.3V vs. Ag/AgCl. The methylene green monomer concentration in the polymerization solution was 0.5 mM with 0.1 M KNO_3 in 50 mM phosphate buffer pH 7.01 depleted of oxygen by bubbling nitrogen for 15 minutes before polymerization, and bubbling during polymerization for 20 cycles.

Chitosan polymeric scaffolds for enzyme immobilization were prepared following methods described previously with several modifications[90, 112]. Nanostructured PtRu catalyst synthesis has been reported previously[68], and was used to create nanostructured $Pt_{30}Ru_{70}$ unsupported

catalysts. A 3mg/mL catalyst ink was created by adding 6 mg of catalyst powder with 60 µL of 5 wt% Nafion and 1940 µL of 4:1 DI:IPA. Surface areas were measured by the N_2-BET method using a Micrometrics 2360 Gemini Analyzer.

GC electrodes were prepared by electropolymerization of Poly-MG, followed by drop casting 2 µL of PtRu ink, followed by drop casting 5 µL of a combination of MWCNTs-chitosan/NAD^+/ADH (2.5 µL MWCNTs-chitosan : 2.5 µL DI: 0.165 mg NAD^+: 0.3 mg ADH).

Cyclic voltammetry experiments were performed from -0.5 V to 0.5 V at a scan rate of 10 mV/s in 5 mL 0.2 M ethylene glycol or 0.1 M ethanol in 0.1 M potassium phosphate buffer solution pH 7. Buffer solutions were deaerated in nitrogen for 15 minutes prior to initiating an experiment. Steady state polarization curves were constructed by polarizing the electrode from -0.2 V to 0.8 V with step increments of 0.1 V for 15 minutes each. The last 10 percent (90 points) were averaged to obtain each data point. A calibration curve was formed by polarizing the assembled electrode at 0.1 V while adding fuel incrementally until a 3 M concentration was reached. The current was recorded after the electrode reached steady state following incremental addition of fuel. Each steady state current was graphed against its corresponding fuel concentration.

8.3 - Results

PMG, PtRu, and ADH were assembled on the electrode as shown in Figure 8.1. PMG was polymerized first on the electrode surface, followed by the MWCNTs/NAD^+/ADH layer or catalyst ink as needed. Due to the solubility of PMG in alcohols, caution was taken to add an appropriate amount of the Nafion-containing catalyst ink so as not to dissolve the PMG layer.

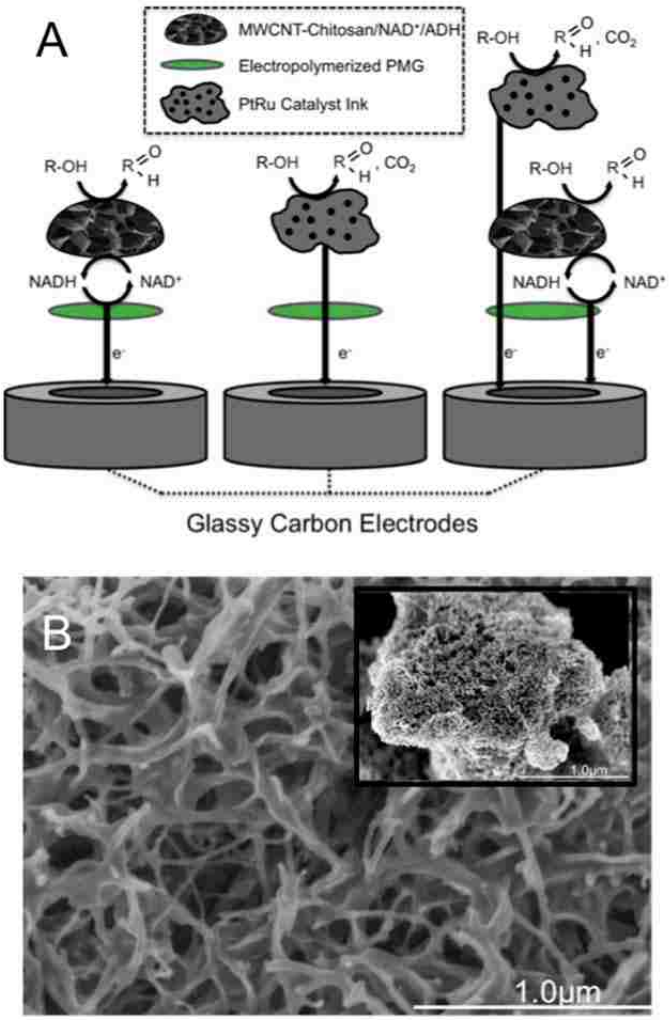

Figure 8.1: Electrode assembly. GC with PMG and MWNT-Chitosan/NAD^+/ADH layer (A, left). GC with PMG and PtRu ink (A, middle). Hybrid electrode with PMG on GC, PtRu ink, and MWNT-Chitosan/NAD^+/ADH layer (A, right). Hybrid electrocatalyst consisting of PMG, and ADH over PtRu electrocatalyst (B). PtRu electrocatalyst (B, insert)

Cyclic voltammetry of the assembled electrodes shows an increase in current when both the enzyme and metal catalyst layers are present on the electrode surface compared to the metal catalyst or enzyme alone (Figure 8.2).

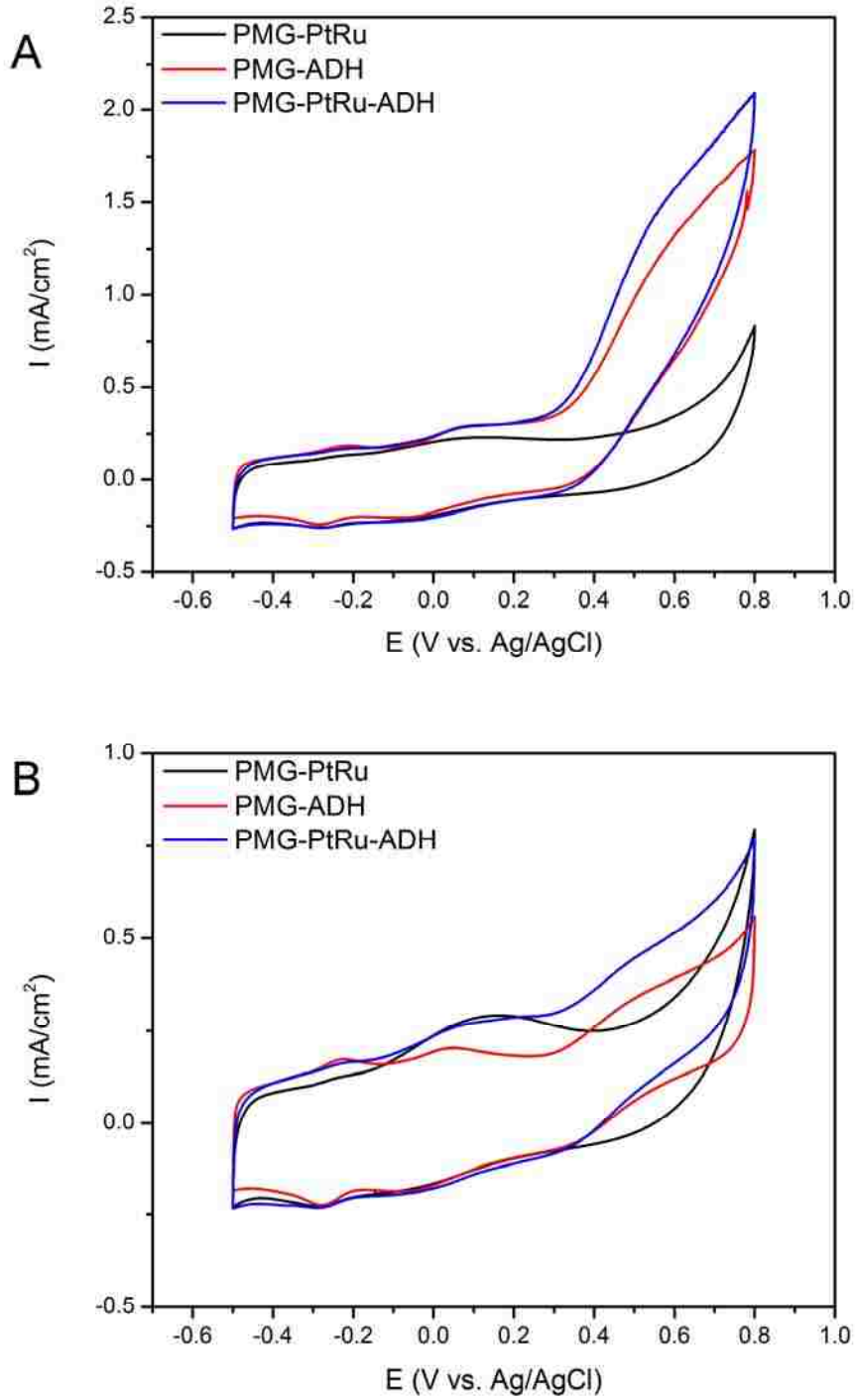

Figure 8.2: Cyclic voltammetry of assembled electrodes with ADH (red), PtRu (black), or both (blue) with 0.1 M ethanol (A) or 0.2 M ethylene glycol (B) fuel. 20mV/s vs Ag/AgCl reference electrode in 0.1 M phosphate buffered solution, 50 mM NAD^+ with no rotation

The enzymatic CVs (PMG-ADH and PMG-PtRu-ADH) show the polymethylene green catalyzed oxidation of NAD^+ typical double redox couples at app. -0.26 V and +0.08 V[183, 185], indicating an enzymatic catalytic oxidation of ethanol and the PMG mediated re-oxidation of NADH to NAD^+. Yeast ADH is known to also oxidize ethylene glycol[186] but with much lower activity which is reflected by the much lower catalytic currents in Figure 8.2 B. The enzymatic (PMG-ADH) as well as the hybrid (PMG-PtRu-ADH) anode show a significant oxidative current starting at onset potentials +0.24 V and +0.3 V for ethanol and ethylene glycol, respectively. The fact that this anodic current does not appear for the PMG-PtRu modified electrode suggest a purely enzymatic oxidation of the fuels and/or their reaction products. This hypothesis is underlined by the facts that (i) the enhanced anodic wave shows no reversible cathodic peak in the backward sweep and (ii) the anodic current is much higher for ethanol oxidation, the favored enzymatic substrate.

To test this hypothesis amperometric curves were obtained by measuring the current response of each system during consecutive additions of fuel at an applied potential of 0.1 V vs. Ag/AgCl (Figure 8.3).

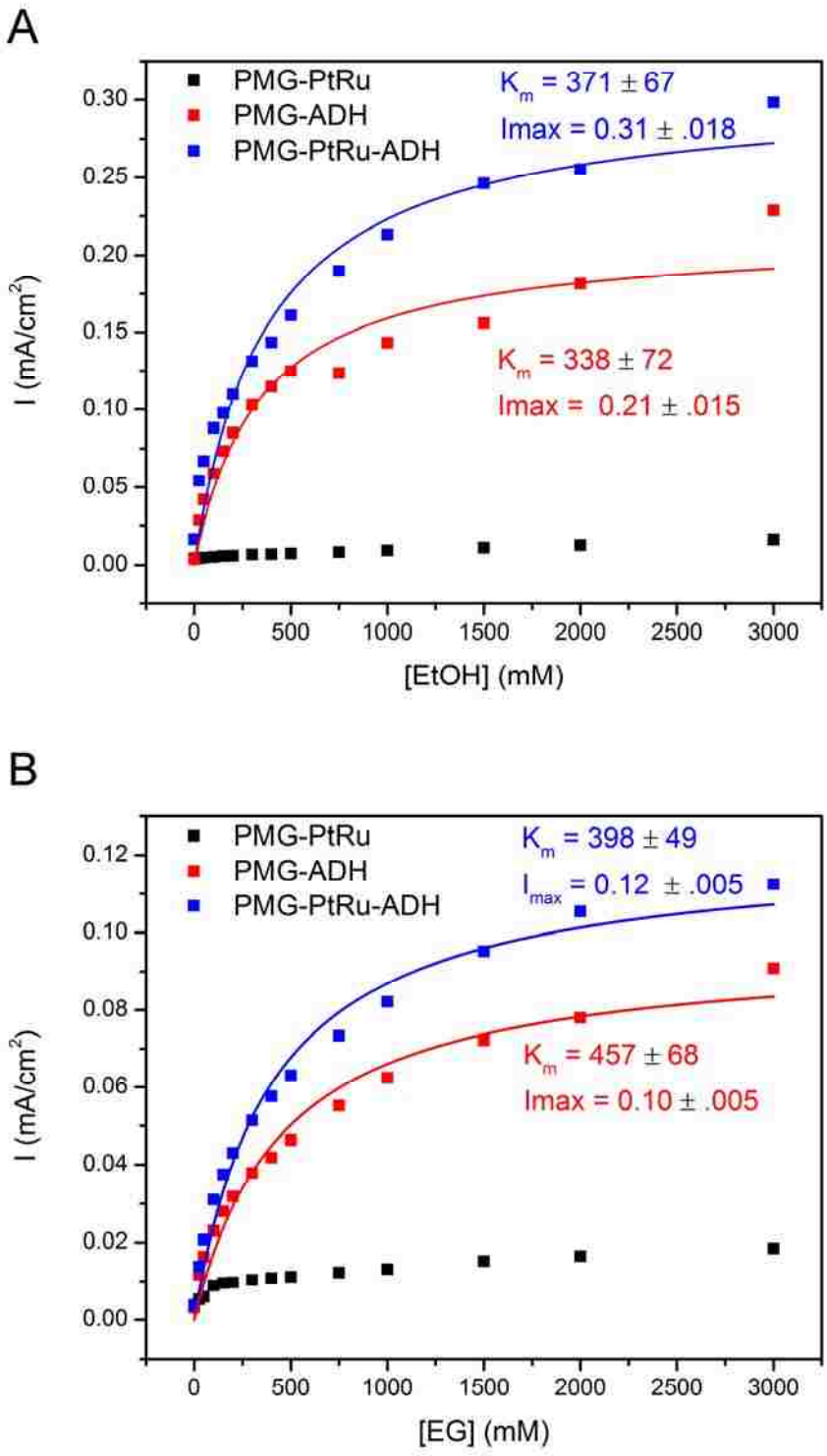

Figure 8.3: Amperometric response of assembled electrodes during consecutive additions of ethanol (A) and ethylene glycol (B) taken at 0.1 V vs. Ag/AgCl

A current density vs. concentration calibration curve was constructed that showed Michaelis-Menten dependence typical of enzymes. The K_M values for the enzymatic (PMG-ADH) and the hybrid anode were very similar for the same oxidized fuel: 338 ± 72 mM (PMG-ADH) and 371 ± 67 mM for ethanol oxidation and 457 ± 68 mM (PMG-ADH) and 398 ± 49 mM (PMG-PtRu-ADH) for ethylene glycol oxidation, representing a dominating enzymatic fuel oxidation. Also, the slightly higher K_M constant for ethylene glycol oxidation accounts for the lower substrate affinity of ADH. For both fuels the catalytic currents for the hybrid (PMG-PtRu-ADH) anodes are significantly higher than the metal (PMG-PtRu) anode, and displayed 1.48 and 1.2 times higher current densities than the enzyme (PMG-ADH) anode for ethanol and ethylene glycol oxidation, respectively. The metal catalyst works as co-catalyst for the oxidation of the fed organic fuels and/or their byproducts by contributing an additional amperometric current to the overall oxidation.

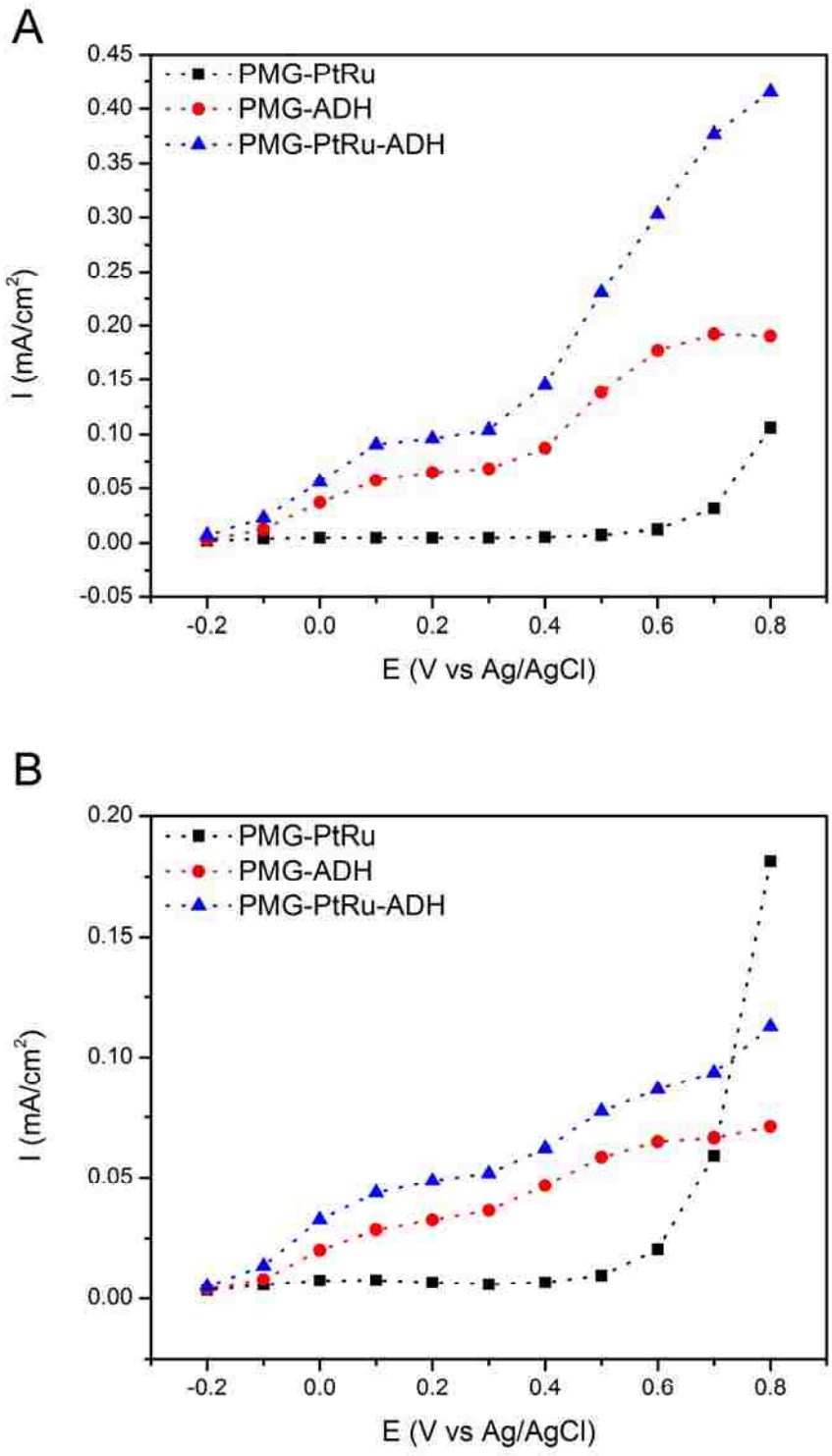

Figure 8.4: Polarization curves of assembled electrodes consisting of ADH (red), PtRu (black), or both (blue) with 0.1 M ethanol (A) or 0.2 M ethylene glycol (B) fuel.

Hydrostatic polarization (Figure 8.4) of the assembled electrodes illustrates the performance gains achieved by utilizing both enzyme and metal catalyst. Using either ethanol or ethylene glycol as fuel, the hybrid PMG-PtRu-ADH anode had higher currents at each potential step, except at the final potential at +0.8 V with ethylene glycol as the fuel. The PMG-ADH anode consistently outperformed the PMG-PtRu anode with a wide separation through most of the potential range from -0.2 V to +0.6 V for both fuels. The difference in current density between the hybrid anode and the PMG-ADH anode grew through the potential range, with the largest separation at higher currents when oxidizing ethanol. It also maintained a higher current density of approximately 250 μA/ cm^2 over the PMG-ADH anode through most of the entire potential range, growing slightly at currents past +0.6 V with ethylene glycol as fuel. A closer look at the polarization curves reveals clearly two catalytic processes: (i) the enzymatic NAD+ mediated oxidation of both alcohols starting at an open circuit potential of app. -0.2 V and (ii) a second co-catalytic oxidation staring at a higher overpotentials of approximately +0.3 V.

8.4 - Conclusions

A hybrid anode based on nano-structured PtRu and NADH-dependant ADH was constructed for the oxidation of ethanol and ethylene glycol. Increased performance of the hybrid anode demonstrates the feasibility of co-catalysis with organic and inorganic catalysts. Optimization of the system by using different platinum based catalysts such as Pt-Sn or Pt-Ru-Sn, or increasing the amount of catalyst deposited without damaging the PMG layer should result in even higher current densities. Overall, this work opens up the possibility of completely oxidizing very complex, high energy density fuels such as sugars and complex alcohols.

Chapter 9 - Conclusions

9.1 - Electrochemical and in situ IR characterization of PtRu catalysts for complete oxidation of ethylene glycol and glycerol

Unsupported nanostructured PtRu electrocatalysts were synthesized using a spray pyrolysis process with varying atomic compositions. A ruthenium rich and platinum rich PtRu were compared to supported E-Tek PtRu on Vulcan XC-72 at a pH range from 5 – 8 for the oxidation of ethylene glycol and glycerol. Oxalic acid is also evaluated as a fuel because is it a terminal oxidation product of glycerol oxidation that enzymes cannot successfully oxidize electrochemically. The nanostructured catalysts were evaluated by SEM and exhibited a sponge-like morphology that helped to increase the metal utilization despite its low surface area. In situ FTIR spectroscopy was used to probe the reaction to determine if complete oxidation occurred by monitoring the production of CO_2. The nanostructured catalyst successfully oxidized each fuel (oxalic acid, ethylene glycol, glycerol) to CO_2 with no indication of CO formation. This presents an interesting opportunity to combine enzymatic catalysts with metallic Pt-based catalysts for oxidation of more complex fuels, due to the ability of enzymes to oxidize complex fuels, and metal catalysts efficiency at oxidizing small organic molecules.

9.2 - Electrooxidation of Ethylene Glycol and Glycerol by Platinum-Based Binary and Ternary Nano-structured Catalysts

Spray pyrolysis of metal precursors was used to synthesize binary and ternary nano-structured Pt-based catalysts. Characterization of the catalysts was performed using SEM, TEM, and EDS to determine morphology, purity and composition. The electrochemical performance of synthesized $Pt_{84}Ru_{16}$, $Pt_{96}Sn_4$, and $Pt_{88}Ru_6Sn_6$ was evaluated via cyclic voltammetry and steady

state polarization for oxidation of ethylene glycol and glycerol. The binary $Pt_{84}Ru_{16}$ and $Pt_{96}Sn_4$ catalysts had higher maximum currents and better stability than a templated Pt catalyst and templated ternary $Pt_{88}Ru_6Sn_6$ catalyst. All binary and ternary catalysts had less adsorbed reaction products during potential cycling than the templated platinum electrocatalyst. *In situ* infrared reflection absorption spectroscopy (IRRAS) analysis showed complete oxidation of ethylene glycol and glycerol with the binary and ternary catalysts by CO_2 generation. This work emphasizes the benefits provided by adding Ru and Sn to Pt catalysts for oxidation of complex alcohols.

9.3 - Hybrid nano-structured platinum-based catalyst/enzyme anode for oxidation of ethanol and ethylene glycol

A hybrid anode based on nano-structured PtRu metal catalyst and NAD-dependent alcohol dehydrogenase was constructed to oxidize ethanol and ethylene glycol. Co-catalysis of each fuel was evident in oxidative peaks by cyclic voltammetry, and increased current density as shown by steady state polarization. When oxidizing ethanol and ethylene glycol, the hybrid anode demonstrated higher current densities at concentrations up to 3 M than anodes comprised of enzyme or metal catalyst alone. This work can potentially lead the way to oxidation of more complex molecules such as sugars and other polyols.

9.4 - Future outlook

The work presented here lays the groundwork for construction of anodes capable of deep oxidation of complex fuels. In addition to PtRu electrocatalysts, other binary and ternary catalysts should be explored that will have higher activity in media conducive to extended enzyme lifetimes. Optimization of catalyst to Nafion ratio in the catalyst ink should be

investigated to minimize the damage to the methylene green layer required for enzyme electron transfer. Furthermore, enzymatic cascades and metabolon structures could be integrated to a hybrid fuel cell to allow for complex polyol oxidation. The anode design techniques presented in this work demonstrates a framework for improved energy generation from varied and complex fuels.

References

1. US, E. I. A. *Annual Energy Outlook 2011, With Projections to 2035*; U.S. Energy Information Administration: 2011.
2. Stambouli, A.; Traversa, E., Fuel cells, an alternative to standard sources of energy. *Renewable and Sustainable Energy Reviews* **2002,** *6* (3), 295-304.
3. Chou, J. Electro-oxidation of Glycerin: Utilization of glycerin as a fuel cell fuel. Carnegie Mellon University.
4. Bard, A. J.; Faulkner, L. R., *Electrochemical methods: Fundamentals and Applications*. 2 ed.; John Wiley & Sons Inc: 2001; p 833.
5. Hogarth, M.; Ralph, T., Catalysis for low temperature fuel cells. *Platinum Metals Review* **2002,** *46* (4), 146-164.
6. Wang, J., *Analytical Electrochemistry*. 2 ed.; John Wiley & Sons: 2004; p 1-223.
7. Mauritz, K. A.; Moore, R. B., State of Understanding of Nafion. *Chemical Reviews* **2004,** *104* (10), 4535-4585.
8. Sopian, K.; Daud, W., Challenges and future developments in proton exchange membrane fuel cells. *Renewable Energy* **2006,** *31* (5), 719-727.
9. Lin, B. Y. S.; Kirk, D. W.; Thorpe, S. J., Performance of alkaline fuel cells: A possible future energy system? *J. Power Sources* **2006,** *161* (1), 474-483.
10. Gülzow, E., Alkaline fuel cells: a critical view. *J. Power Sources* **1996,** *61* (1-2), 99-104.
11. Vogel, W.; Lundquist, J., Reduction of Oxygen on Teflon-Bonded Platinum Electrodes. *Journal of The Electrochemical Society* **1970,** *117* (12), 1512-1516.
12. Burchardt, T.; Gouérec, P.; Sanchez-Cortezon, E.; Karichev, Z.; Miners, J., Alkaline fuel cells: contemporary advancement and limitations. *Fuel* **2002,** *81* (17), 2151-2155.
13. Kiros, Y.; Lindstrom, O.; Kaimakis, T., Cobalt and Cobalt-Based Macrocycle Blacks as Oxygen-Reduction Catalysts in Alkaline Fuel Cells. *J. Power Sources* **1993,** *45* (2), 219-227.
14. Kiros, Y.; Schwartz, S., Pyrolyzed Macrocycles on High Surface-Area Carbons for the Reduction of Oxygen in Alkaline Fuel Cells. *J. Power Sources* **1991,** *36* (4), 547-555.
15. Varcoe, J.; Slade, R., Prospects for Alkaline Anion‐Exchange Membranes in Low Temperature Fuel Cells. *Fuel Cells* **2005,** *5* (2), 187-200.
16. Matsuoka, K.; Iriyama, Y.; Abe, T.; Matsuoka, M.; Ogumi, Z., Alkaline direct alcohol fuel cells using an anion exchange membrane. *J. Power Sources* **2005,** *150*, 27-31.
17. Agel, E.; Bouet, J.; Fauvarque, J., Characterization and use of anionic membranes for alkaline fuel cells. *J. Power Sources* **2001,** *101* (2), 267-274.
18. Yu, E.; Scott, K., Direct methanol alkaline fuel cells with catalysed anion exchange membrane electrodes. *J. Appl. Electrochem.* **2005,** *35* (1), 91-96.
19. Wang, Y.; Li, L.; Hu, L.; Zhuang, L.; Lu, J.; Xu, B., A feasibility analysis for alkaline membrane direct methanol fuel cell: thermodynamic disadvantages versus kinetic advantages. *Electrochem. Commun.* **2003,** *5* (8), 662-666.
20. Piela, P.; Zelenay, P., Researchers redefine the DMFC roadmap. *The Fuel Cell Review* **2004,** *1* (2), 17-23.
21. Lamy, C.; Leger, J.-M.; Srinivasan, S., Modern Aspects of Electrochemistry. In *Modern Aspects of Electrochemistry*, Bockris, J. O. M.; Conway, B. E.; White, R. E., Eds. Springer US: 2002; Vol. 34, pp 53-118.

22. Nordlund, J.; Lindbergh, G., Temperature-dependent kinetics of the anode in the DMFC. *Journal of The Electrochemical Society* **2004,** *151* (9), A1357-A1362.
23. Jiang, R.; Chu, D., Comparative studies of methanol crossover and cell performance for a DMFC. *Journal of The Electrochemical Society* **2004,** *151* (1), A69-A76.
24. Watanabe, M.; Motoo, S., Electrocatalysis by ad-atoms. Part II. Enhancement of the oxidation of methanol on platinum by ruthenium ad-atoms. *J. Electroanal. Chem.* **1975,** *60* (3), 267-273.
25. Antolini, E., Catalysts for direct ethanol fuel cells. *J. Power Sources* **2007,** *170* (1), 1-12.
26. Antolini, E.; Gonzalez, E. R., Alkaline direct alcohol fuel cells. *J. Power Sources* **2010,** *195* (11), 3431-3450.
27. Huber, G. W.; Iborra, S.; Corma, A., Synthesis of transportation fuels from biomass: Chemistry, catalysts, and engineering. *Chemical Reviews* **2006,** *106* (9), 4044-4098.
28. Martinot, E. Renewables 2009 Global Status Report. http://www.ren21.net/globalstatusreport/g2009.asp.
29. Mann, J.; Yao, N.; Bocarsly, A. B., Characterization and analysis of new catalysts for a direct ethanol fuel cell. *Langmuir* **2006,** *22* (25), 10432-10436.
30. Vigier, F.; Coutanceau, C.; Perrard, A.; Belgsir, E.; Lamy, C., Development of anode catalysts for a direct ethanol fuel cell. *J. Appl. Electrochem.* **2004,** *34* (4), 439-446.
31. Kim, J. H.; Choi, S. M.; Nam, S. H.; Seo, M. H.; Choi, S. H.; Kim, W. B., Influence of Sn content on PtSn/C catalysts for electrooxidation of C1-C3 alcohols: Synthesis, characterization, and electrocatalytic activity. *Applied Catalysis B: Environmental* **2008,** *82*, 89-102.
32. Wang, L.; Meng, H.; Shen, P. K.; Bianchini, C.; Vizza, F.; Wei, Z., In situ FTIR spectroelectrochemical study on the mechanism of ethylene glycol electrocatalytic oxidation at a Pd electrode. *Phys. Chem. Chem. Phys.* **2011,** *13* (7), 2667-2673.
33. Wieland, B.; Lancaster, J. P.; Hoaglund, C. S.; Holota, P.; Tornquist, W. J., Electrochemical and infrared spectroscopic quantitative determination of the platinum-catalyzed ethylene glycol oxidation mechanism at CO adsorption potentials. *Langmuir* **1996,** *12* (10), 2594-2601.
34. Roquet, L.; Belgsir, E.; Leger, J.; Lamy, C., Kinetics and Mechanisms of the Electrocatalytic Oxidation of Glycerol as Investigated by Chromatographic Analysis of the Reaction-Products - Potential and Ph Effects. *Electrochim. Acta* **1994,** *39* (16), 2387-2394.
35. Kwon, Y.; Schouten, K. J. P.; Koper, M. T. M., Mechanism of the Catalytic Oxidation of Glycerol on Polycrystalline Gold and Platinum Electrodes. *Chemcatchem* **2011,** *3* (7), 1176-1185.
36. Carrettin, S.; McMorn, P.; Johnston, P.; Griffin, K.; Kiely, C. J.; Hutchings, G. J., Oxidation of glycerol using supported Pt, Pd and Au catalysts. *Phys. Chem. Chem. Phys.* **2003,** *5* (6), 1329-1336.
37. Xia, X.; Iwasita, T.; Ge, F.; Vielstich, W., Structural effects and reactivity in methanol oxidation on polycrystalline and single crystal platinum. *Electrochim. Acta* **1996,** *41* (5), 711-718.
38. Herrero, E.; Franaszczuk, K.; Wieckowski, A., Electrochemistry of Methanol at Low-Index Crystal Planes of Platinum - an Integrated Voltammetric and Chronoamperometric Study. *J Phys Chem* **1994,** *98* (19), 5074-5083.

39. Juanto, S.; Beden, B.; Hahn, F.; Leger, J.; Lamy, C., Infrared Spectroscopic Study of the Methanol Adsorbates at a Platinum-Electrode Part II. the Pt (100) Surface in an Acid Medium. *J. Electroanal. Chem.* **1987,** *237* (1), 119-129.
40. Tripkovic, A.; Popovic, K.; Lovic, J., The influence of the oxygen-containing species on the electrooxidation of the C-1-C-4 alcohols at some platinum single crystal surfaces in alkaline solution. *Electrochim. Acta* **2001,** *46*, 3163-3173.
41. Herrero, E.; Chrzanowski, W.; Wieckowski, A., Dual Path Mechanism in Methanol Electrooxidation on a Platinum-Electrode. *J Phys Chem* **1995,** *99* (25), 10423-10424.
42. Watanabe, M.; Saegusa, S.; Stonehart, P., High Platinum Electrocatalyst Utilizations for Direct Methanol Oxidation. *J. Electroanal. Chem.* **1989,** *271*, 213-220.
43. Beden, B.; Juanto, S.; Leger, J.; Lamy, C., Infrared Spectroscopic Study of the Methanol Adsorbates at a Platinum Electrode Part III. Structural Effects and Behavior of a Polycrystalline Surface. *J. Electroanal. Chem.* **1987,** *238*, 323-331.
44. Morin, M.; Lamy, C.; Leger, J.; Vasquez, J.; Aldaz, A., Structural Effects in Electrocatalysis - Oxidation of Ethanol on Platinum Single-Crystal Electrodes - Effect of Ph. *J. Electroanal. Chem.* **1990,** *283*, 287-302.
45. Shin, J.; Tornquist, W.; Korzeniewski, C.; Hoaglund, C., Elementary steps in the oxidation and dissociative chemisorption of ethanol on smooth and stepped surface planes of platinum electrodes. *Surface Science* **1996,** *364* (2), 122-130.
46. Lai, S.; Koper, M., Electro-oxidation of ethanol and acetaldehyde on platinum single-crystal electrodes. *Faraday Discussions* **2008,** *140*, 399-416.
47. Colmati, F.; Tremiliosi-Filho, G.; Gonzalez, E. R.; Berná, A.; Herrero, E.; Feliu, J. M., Surface structure effects on the electrochemical oxidation of ethanol on platinum single crystal electrodes. *Faraday Discussions* **2008,** *140*, 379-397.
48. Platinum Price Charts. http://platinum.matthey.com/pgm-prices/price-charts/.
49. Chen, A.; Holt-Hindle, P., Platinum-Based Nanostructured Materials: Synthesis, Properties, and Applications. *Chemical Reviews* **2010,** *110* (6), 3767-3804.
50. Selvaraj, V.; Vinoba, M.; Alagar, M., Electrocatalytic oxidation of ethylene glycol on Pt and Pt-Ru nanoparticles modified multi-walled carbon nanotubes. *J. Colloid Interface Sci.* **2008,** *322* (2), 537-544.
51. Selvaraj, V.; Alagar, M., Ethylene glycol oxidation on Pt and Pt–Ru nanoparticle decorated polythiophene/multiwalled carbon nanotube composites for fuel cell applications. *Nanotechnology* **2008,** *19*, 045504.
52. Yamazaki, S.-i.; Fujiwara, N.; Yasuda, K., A catalyst that uses a rhodium phthalocyanin for oxalic acid oxidation and its application to an oxalic acid sensor. *Electrochim. Acta* **2010,** *55* (3), 753-758.
53. Kowal, A.; Li, M.; Shao, M.; Sasaki, K.; Vukmirovic, M. B.; Zhang, J.; Marinkovic, N. S.; Liu, P.; Frenkel, A. I.; Adzic, R., Ternary Pt/Rh/SnO2 electrocatalysts for oxidizing ethanol to CO2. *Nature Materials* **2009,** *8* (4), 325-330.
54. Yang, L.; Allen, R.; Scott, K.; Christenson, P.; Roy, S., A comparative study of PtRu and PtRuSn thermally formed on titanium mesh for methanol electro-oxidation. *J. Power Sources* **2004,** *137* (2), 257-263.
55. Jusys, Z.; Schmidt, T.; Dubau, L.; Lasch, K.; Jorissen, L.; Garche, J.; Behm, R., Activity of PtRuMeOx (Me = W, Mo or V) catalysts towards methanol oxidation and their characterization. *J. Power Sources* **2002,** *105* (2), 297-304.

56. Liu, H.; Song, C.; Zhang, L.; Zhang, J.; Wang, H.; Wilkinson, D. P., A review of anode catalysis in the direct methanol fuel cell. *J. Power Sources* **2006,** *155* (2), 95-110.
57. Deffernez, A.; Hermans, S.; Devillers, M., Bimetallic Bi-Pt, Ru-Pt and Ru-Pd and trimetallic catalysts for the selective oxidation of glyoxal into glyoxalic acid in aqueous phase. *Applied Catalysis A: General* **2005,** *282* (1-2), 303-313.
58. Ralph, T.; Hogarth, M., Catalysis for low temperature fuel cells. *Platinum Metals Review* **2002,** *46* (3), 117-135.
59. Chu, Y. H.; Shul, Y. G., Combinatorial investigation of Pt-Ru-Sn alloys as an anode electrocatalysts for direct alcohol fuel cells. *International Journal of Hydrogen Energy* **2010,** *35* (20), 11261-11270.
60. Neto, A.; Vasconcelos, T.; Da Silva, R.; Linardi, M.; Spinace, E., Electro-oxidation of ethylene glycol on PtRu/C and PtSn/C electrocatalysts prepared by alcohol-reduction process. *J. Appl. Electrochem.* **2005,** *35* (2), 193-198.
61. Oliveira Neto, A.; Dias, R. R.; Tusi, M. M.; Linardi, M.; Spinace, E. V., Electro-oxidation of methanol and ethanol using PtRu/C, PtSn/C and PtSnRu/C electrocatalysts prepared by an alcohol-reduction process. *J. Power Sources* **2007,** *166* (1), 87-91.
62. Vigier, F.; Rousseau, S.; Coutanceau, C.; Leger, J.; Lamy, C., Electrocatalysis for the direct alcohol fuel cell. *Topics in Catalysis* **2006,** *40* (1), 111-121.
63. Zhu, J.; Cheng, F.; Tao, Z.; Chen, J., Electrocatalytic methanol oxidation of Pt0.5Ru0.5-xSnx/C (x=0-0.5). *The Journal of Physical Chemistry C* **2008,** *112* (16), 6337-6345.
64. Lamy, C.; Belgsir, E.; Leger, J., Electrocatalytic oxidation of aliphatic alcohols: Application to the direct alcohol fuel cell (DAFC). *J. Appl. Electrochem.* **2001,** *31* (7), 799-809.
65. Matsuoka, K.; Iriyama, Y.; Abe, T.; Matsuoka, M.; Ogumi, Z., Electrocatalytic oxidation of ethylene glycol in alkaline solution. *Journal of The Electrochemical Society* **2005,** *152* (4), A729-A731.
66. Gasteiger, H.; Markovic, N.; Ross Jr, P.; Cairns, E., Methanol electrooxidation on well-characterized platinum-ruthenium bulk alloys. *The Journal of Physical Chemistry* **1993,** *97* (46), 12020-12029.
67. Nitani, H.; Nakagawa, T.; Daimon, H.; Kurobe, Y.; Ono, T.; Honda, Y.; Koizumi, A.; Seino, S.; Yamamoto, T. A., Methanol oxidation catalysis and substructure of PtRu bimetallic nanoparticles. *Applied Catalysis A: General* **2007,** *326* (2), 194-201.
68. Switzer, E. E.; Datye, A. K.; Atanassov, P. B., Nanostructured Anode Pt–Ru Electrocatalysts for Direct Methanol Fuel Cells. *Topics in Catalysis* **2007,** *46* (3), 334-338.
69. Switzer, E. E.; Olson, T.; Datye, A.; Atanassov, P. B.; Hibbs, M.; Cornelius, C., Templated Pt-Sn electrocatalysts for ethanol, methanol and CO oxidation in alkaline media. *Electrochim. Acta* **2009,** *54* (3), 989-995.
70. Jiang, L.; Hsu, A.; Chu, D.; Chen, R., Ethanol electro-oxidation on Pt/C and PtSn/C catalysts in alkaline and acid solutions. *International Journal of Hydrogen Energy* **2010,** *35* (1), 365-372.
71. Zhou, W.; Song, S.; Li, W.; Zhou, Z.; Sun, G.; Xin, Q.; Douvartzides, S.; Tsiakaras, P., Direct ethanol fuel cells based on PtSn anodes: the effect of Sn content on the fuel cell performance. *J. Power Sources* **2005,** *140* (1), 50-58.
72. Koper, M.; Shubina, T.; van Santen, R., Periodic density functional study of CO and OH adsorption on Pt-Ru alloy surfaces: Implications for CO tolerant fuel cell catalysts. *Journal of Physical Chemistry B* **2002,** *106* (3), 686-692.

73. Lei, Z.; An, L.; Dang, L.; Zhao, M.; Shi, J.; Bai, S.; Cao, Y., Highly dispersed platinum supported on nitrogen-containing ordered mesoporous carbon for methanol electrochemical oxidation. *Microporous and Mesoporous Materials* **2009,** *119* (1-3), 30-38.
74. Carroll, N. J.; Pylypenko, S.; Atanassov, P. B.; Petsev, D., Microparticles with Bimodal Nanoporosity Derived by Microemulsion Templating. *Langmuir* **2009,** *25* (23), 13540-13544.
75. Pylypenko, S.; Olson, T. S.; Carroll, N. J.; Petsev, D. N.; Atanassov, P. B., Templated Platinum/Carbon Oxygen Reduction Fuel Cell Electrocatalysts. *The Journal of Physical Chemistry C* **2010,** *114* (9), 4200-4207.
76. Ding, J.; Chan, K.; Ren, J.; Xiao, F., Platinum and platinum-ruthenium nanoparticles supported on ordered mesoporous carbon and their electrocatalytic performance for fuel cell reactions. *Electrochim. Acta* **2005,** *50* (15), 3131-3141.
77. Zhao, D.; Huo, Q.; Feng, J.; Chmelka, B.; Stucky, G., Nonionic triblock and star diblock copolymer and oligomeric surfactant syntheses of highly ordered, hydrothermally stable, mesoporous silica structures. *J. Am. Chem. Soc.* **1998,** *120* (24), 6024-6036.
78. Zhao, D.; Feng, J.; Huo, Q.; Melosh, N.; Fredrickson, G.; Chmelka, B.; Stucky, G., Triblock copolymer syntheses of mesoporous silica with periodic 50 to 300 angstrom pores. *Science* **1998,** *279* (5350), 548-552.
79. Lee, J.; Kim, J.; Hyeon, T., Recent progress in the synthesis of porous carbon materials. *Advanced Materials* **2006,** *18* (16), 2073-2094.
80. Ambrosio, E. P.; Francia, C.; Manzoli, M.; Penazzi, N.; Spinelli, P., Platinum catalyst supported on mesoporous carbon for PEMFC. *International Journal of Hydrogen Energy* **2008,** *33* (12), 3142-3145.
81. Nam, J.; Jang, Y.; Kwon, Y.; Nam, J., Direct methanol fuel cell Pt-carbon catalysts by using SBA-15 nanoporous templates. *Electrochem. Commun.* **2004,** *6* (7), 737-741.
82. Antolini, E.; Perez, J., The renaissance of unsupported nanostructured catalysts for low-temperature fuel cells: from the size to the shape of metal nanostructures. *Journal of Materials Science* **2011,** *46* (13), 4435-4457.
83. Liu, L.; Pu, G.; Viswanathan, R.; Fan, Q.; Liu, R.; Smotkin, E., Carbon supported and unsupported Pt-Ru anodes for liquid feed direct methanol fuel cells. *Electrochim. Acta* **1998,** *43* (24), 3657-3663.
84. Arico, A.; Shukla, A.; El-Khatib, K.; Cretì, P.; Antonucci, V., Effect of carbon-supported and unsupported Pt-Ru anodes on the performance of solid-polymer-electrolyte direct methanol fuel cells. *J. Appl. Electrochem.* **1999,** *29* (6), 671-676.
85. Ren, X.; Wilson, M. S.; Gottesfeld, S., High performance direct methanol polymer electrolyte fuel cells. *Journal of The Electrochemical Society* **1996,** *143* (1).
86. Choi, W.; Woo, S., Bimetallic Pt-Ru nanowire network for anode material in a direct-methanol fuel cell. *J. Power Sources* **2003,** *124* (2), 420-425.
87. Moehlenbrock, M. J.; Minteer, S. D., Extended lifetime biofuel cells. *Chemical Society Reviews* **2008,** *37* (6), 1188-1196.
88. Atanassov, P. B.; Apblett, C.; Banta, S.; Brozik, S.; Calabrese Barton, S. A. C.; Cooney, M. J.; Liaw, B.; Mukerjee, S.; Minteer, S. D., Enzymatic biofuel cells. *Electrochem. Soc. Interface* **2007,** *16* (2), 28-31.
89. Moore, C.; Akers, N.; Hill, A.; Johnson, Z.; Minteer, S. D., Improving the environment for immobilized dehydrogenase enzymes by modifying Nafion with tetraalkylammonium bromides. *Biomacromolecules* **2004,** *5* (4), 1241-1247.

90. Cooney, M. J.; Lau, C.; Windmeisser, M.; Liaw, B.; Klotzbach, T.; Minteer, S. D., Design of chitosan gel pore structure: towards enzyme catalyzed flow-through electrodes. *J. Mater. Chem.* **2008,** *18* (6), 667-674.
91. Dai, Z. H.; Liu, F. X.; Lu, G. F.; Bao, J. C., Electrocatalytic detection of NADH and ethanol at glassy carbon electrode modified with electropolymerized films from methylene green. *Journal of Solid State Electrochemistry* **2008,** *12* (2), 175-180.
92. Blaedel, W. J.; Jenkins, R. A., Study of the Electrochemical Oxidation of Reduced Nicotinamide Adenine Dinucleotide. *Analytical Chemistry* **1975,** *47* (8), 1337-1343.
93. Karyakin, A.; Ivanova, Y.; Revunova, K.; Karyakina, E., Electropolymerized flavin adenine dinucleotide as an advanced NADH transducer. *Analytical Chemistry* **2004,** *76* (7), 2004-2009.
94. Arechederra, R. L.; Minteer, S. D., Complete Oxidation of Glycerol in an Enzymatic Biofuel Cell. *Fuel Cells* **2009,** *9* (1), 63-69.
95. Treu, B.; Minteer, S. D., Isolation and purification of PQQ-dependent lactate dehydrogenase from Gluconobacter and use for direct electron transfer at carbon and gold electrodes. *Bioelectrochemistry* **2008,** *74* (1), 73-77.
96. Arechederra, R. L.; Treu, B.; Minteer, S. D., Development of glycerol/O2 biofuel cell. *J. Power Sources* **2007,** *173* (1), 156-161.
97. Laurinavicius, V.; Razumiene, J.; Ramanavicius, A.; Ryabov, A., Wiring of PQQ-dehydrogenases. *Biosensors and Bioelectronics* **2004,** *20* (6), 1217-1222.
98. Ivnitski, D.; Atanassov, P.; Apblett, C., Direct bioelectrocatalysis of PQQ-dependent glucose dehydrogenase. *Electroanalysis* **2007,** *19* (15), 1562-1568.
99. Treu, B. L.; Minteer, S. D., Isolation and purification of PQQ-dependent lactate dehydrogenase from Gluconobacter and use for direct electron transfer at carbon and gold electrodes. *Bioelectrochemistry* **2008,** *74* (1), 73-77.
100. Treu, B. L.; Arechederra, R.; Minteer, S. D., Bioelectrocatalysis of Ethanol via PQQ-Dependent Dehydrogenases Utilizing Carbon Nanomaterial Supports. *Journal of Nanoscience and Nanotechnology* **2009,** *9* (4), 2374-2380.
101. Friedrich, J. M.; Ponce-De-Leon, C.; Reade, G. W.; Walsh, F. C., Reticulated vitreous carbon as an electrode material. *Journal of Electroanalytical Chemistry* **2004,** *561* (1-2), 203-217.
102. Cooney, M. J.; Lau, C.; Windmeisser, M.; Liaw, B. Y.; Klotzbach, T.; Minteer, S. D., Design of chitosan gel pore structure: towards enzyme catalyzed flow-through electrodes. *Journal of Materials Chemistry* **2008,** *18* (6), 667-674.
103. Lau, C.; Cooney, M. J.; Atanassov, P., Conductive macroporous composite chitosan-carbon nanotube scaffolds. *Langmuir* **2008,** *24* (13), 7004-7010.
104. Sun, D. M.; Scott, D.; Cooney, M. J.; Liaw, B. Y., A promising reconstitution platform for PQQ-dependent apo-enzymes in chitosan-carbon nanotube matrices. *Electrochemical and Solid State Letters* **2008,** *11* (6), B101-B104.
105. Cai, C. X.; Chen, J., Direct electron transfer of glucose oxidase promoted by carbon nanotubes. *Analytical Biochemistry* **2004,** *332* (1), 75-83.
106. Cai, C. X.; Chen, J.; Lu, T. H., Direct electron transfer of glucose oxidase on the carbon nanotube electrode. *Science in China Series B-Chemistry* **2004,** *47* (2), 113-119.
107. Iijima, S., Helical Microtubules of Graphitic Carbon. *Nature* **1991,** *354* (6348), 56-58.
108. Saito, Y., Carbon nanotubes produced by arc discharge. *New Diamond and Frontier Carbon Technology* **1999,** *9* (1), 1-30.

109. Thess, A.; Lee, R.; Nikolaev, P.; Dai, H. J.; Petit, P.; Robert, J.; Xu, C. H.; Lee, Y. H.; Kim, S. G.; Rinzler, A. G.; Colbert, D. T.; Scuseria, G. E.; Tomanek, D.; Fischer, J. E.; Smalley, R. E., Crystalline ropes of metallic carbon nanotubes. *Science* **1996,** *273* (5274), 483-487.
110. Moore, C. M.; Akers, N. L.; Hill, A. D.; Johnson, Z. C.; Minteer, S. D., Improving the Environment for Immobilized Dehydrogenase Enzymes by Modifying Nafion with Tetraalkylammonium Bromides. *Biomacromolecules* **2004,** *5* (4), 1241-1247.
111. Cooney, M. J.; Svoboda, V.; Lau, C.; Martin, G.; Minteer, S. D., Enzyme catalysed biofuel cells. *Energy & Environmental Science* **2008,** *1* (3), 320-337.
112. Cooney, M. J.; Petermann, J.; Lau, C.; Minteer, S. D., Characterization and evaluation of hydrophobically modified chitosan scaffolds: Towards design of enzyme immobilized flow-through electrodes. *Carbohydrate Polymers* **2009,** *75* (3), 428-435.
113. Lu, Y.; Fan, H.; Stump, A.; Ward, T.; Rieker, T.; Brinker, C., Aerosol-assisted self-assembly of mesostructured spherical nanoparticles. *Nature* **1999,** *398* (6724), 223-226.
114. Brinker, C.; Lu, Y.; Sellinger, A.; Fan, H., Evaporation-induced self-assembly: Nanostructures made easy. *Advanced Materials* **1999,** *11* (7), 579-+.
115. Bore, M. T.; Rathod, S. B.; Ward, T. L.; Datye, A. K., Hexagonal mesostructure in powders produced by evaporation-induced self-assembly of aerosols from aqueous tetraethoxysilane solutions. *Langmuir* **2003,** *19*, 256-264.
116. Rathod, S. B.; Ward, T. L., Hierarchical porous and composite particle architectures based on self assembly and phase separation in droplets. *J. Mater. Chem.* **2007,** *17*, 2329-2335.
117. Goldstein, J. I.; Newbury, D. E.; Joy, D. C.; Lyman, C. E.; Echlin, P.; Lifshin, E.; Sawyer, L.; Michael, J. R., *Scanning Electron Microscopy and X-Ray Microanalysis*. Third Edition ed.; Springer: p 689.
118. Arenz, M.; Stamenkovic, V.; Ross, P. N.; Markovic, N. M., ScienceDirect - Electrochemistry Communications : Preferential oxidation of carbon monoxide adsorbed on Pd submonolayer films deposited on Pt(1 0 0). *Electrochem. Commun.* **2003,** *5* (9), 809-813.
119. Li, H.; Guarr, T., Electrocatalytic oxidation of oxalic acid at electrodes coated with polymeric metallophthalocyanines. *J. Electroanal. Chem.* **1991,** *317* (1-2), 189-202.
120. Martins, C. A.; Giz, M. J.; Camara, G. A., Generation of carbon dioxide from glycerol: Evidences of massive production on polycrystalline platinum. *Electrochim. Acta* **2011,** *56* (12), 4549-4553.
121. De Lima, R.; Paganin, V.; Iwasita, T.; Vielstich, W., On the electrocatalysis of ethylene glycol oxidation. *Electrochim. Acta* **2003,** *49* (1), 85-91.
122. Gomes, J. F.; Tremiliosi-Filho, G., Spectroscopic Studies of the Glycerol Electro-Oxidation on Polycrystalline Au and Pt Surfaces in Acidic and Alkaline Media. *Electrocatalysis* **2011,** *2* (2), 96-105.
123. Kwon, Y.; Lai, S. C. S.; Rodriguez, P.; Koper, M. T. M., Electrocatalytic Oxidation of Alcohols on Gold in Alkaline Media: Base or Gold Catalysis? *J. Am. Chem. Soc.* **2011,** *133* (18), 6914-6917.
124. Watanabe, M.; Uchida, M., Preparation of highly dispersed Pt+ Ru alloy clusters and the activity for the electrooxidation of methanol. *J. Electroanal. Chem.* **1987,** *229*, 395-406.
125. Berná, A.; Manuel Delgado, J.; Manuel Orts, J.; Rodes, A.; Miguel Feliu, J., In-situ infrared study of the adsorption and oxidation of oxalic acid at single-crystal and thin-film gold electrodes: A combined external reflection infrared and ATR-SEIRAS approach. *Langmuir* **2006,** *22* (17), 7192-7202.

126. Konopka, D. A.; Li, M.; Artyushkova, K.; Marinkovic, N.; Sasaki, K.; Adzic, R.; Ward, T. L.; Atanassov, P. B., Platinum Supported on NbRuyOz as Electrocatalyst for Ethanol Oxidation in Acid and Alkaline Fuel Cells. *The Journal of Physical Chemistry C* **2011,** *115* (7), 3043-3056.
127. Cabaniss, S.; Leenheer, J.; McVey, I., Aqueous infrared carboxylate absorbances: aliphatic di-acids. *Spectrochim Acta A* **1998,** *54* (3), 449-458.
128. Gisbert, R.; Garcia, G.; Koper, M. T. M., Adsorption of phosphate species on poly-oriented Pt and Pt(111) electrodes over a wide range of pH. *Electrochim. Acta* **2010,** *55* (27), 7961-7968.
129. Ye, S.; Kita, H.; Aramata, A., Hydrogen and Anion Adsorption at Platinum Single-Crystal Electrodes in Phosphate Solutions Over a Wide-Range of Ph. *J. Electroanal. Chem.* **1992,** *333*, 299-312.
130. Abdel Rahim, M.; Abdel Hameed, R.; Khalil, M., Nickel as a catalyst for the electro-oxidation of methanol in alkaline medium. *J. Power Sources* **2004,** *134* (2), 160-169.
131. Xu, C.; Shen, P.; Liu, Y., Ethanol electrooxidation on Pt/C and Pd/C catalysts promoted with oxide. *J. Power Sources* **2007,** *164* (2), 527-531.
132. Feng, Y.; Yin, W.; Li, Z.; Huang, C.; Wang, Y., Ethylene glycol, 2-propanol electrooxidation in alkaline medium on the ordered intermetallic PtPb surface. *Electrochim. Acta* **2010,** *55* (23), 6991-6999.
133. Verma, A.; Basu, S., Evaluation of an alkaline fuel cell for multifuel system. *Journal of Fuel Cell Science and Technology* **2005,** *2* (4), 234-238.
134. Bianchini, C.; Shen, P. K., Palladium-Based Electrocatalysts for Alcohol Oxidation in Half Cells and in Direct Alcohol Fuel Cells. *Chemical Reviews* **2009,** *109* (9), 4183-4206.
135. Serov, A.; Kwak, C., Recent achievements in direct ethylene glycol fuel cells (DEGFC). *Applied Catalysis B: Environmental* **2010,** *97* (1-2), 1-12.
136. Delime, F.; Leger, J.-M.; Lamy, C., Enhancement of the electroxidation of ethanol on a Pt-PEM electrode modified by tin. Part I: Half cell study. *J. Appl. Electrochem.* **1999,** *29*, 1249-1254.
137. Kawaguchi, T.; Rachi, Y.; Sugimoto, W.; Murakami, Y.; Takasu, Y., Performance of ternary PtRuRh/C electrocatalyst with varying Pt : Ru : Rh ratio for methanol electro-oxidation. *J. Appl. Electrochem.* **2006,** *36* (10), 1117-1125.
138. Girishkumar, G.; Hall, T. D.; Vinodgopal, K.; Kamat, P. V., Single wall carbon nanotube supports for portable direct methanol fuel cells. *The Journal of Physical Chemistry B* **2006,** *110*, 107-114.
139. Kim, H. J.; Choi, S. M.; Green, S.; Tompsett, G. A.; Lee, S. H.; Huber, G. W.; Kim, W. B., Highly active and stable PtRuSn/C catalyst for electrooxidations of ethylene glycol and glycerol. *Applied Catalysis B: Environmental* **2011,** *101*, 366-375.
140. Livshits, V.; Philosoph, M.; Peled, E., Direct ethylene glycol fuel-cell stack--Study of oxidation intermediate products. *J. Power Sources* **2008,** *178* (2), 687-691.
141. Livshits, V.; Peled, E., Progress in the development of a high-power, direct ethylene glycol fuel cell (DEGFC). *J. Power Sources* **2006,** *161* (2), 1187-1191.
142. Peled, E.; Livshits, V.; Duvdevani, T., High-power direct ethylene glycol fuel cell (DEGFC) based on nanoporous proton-conducting membrane (NP-PCM). *J. Power Sources* **2002,** *106*, 245-248.
143. Peled, E.; Duvdevani, T.; Aharon, A.; Melman, A., New fuels as alternatives to methanol for direct oxidation fuel cells. *Electrochemical And Solid State Letters* **2001,** *4* (4), A38-A41.

144. Chetty, R.; Scott, K., Catalysed titanium mesh electrodes for ethylene glycol fuel cells. *J. Appl. Electrochem.* **2007,** *37* (9), 1077-1084.
145. Faguy, P.; Marinkovic, N., Design and performance of a new infrared reflection accessory for spectroelectrochemical studies. *Applied Spectroscopy* **1996,** *50* (3), 394-400.
146. Shen, P.; Xu, C., Alcohol oxidation on nanocrystalline oxide Pd/C promoted electrocatalysts. *Electrochem. Commun.* **2006,** *8* (1), 184-188.
147. Christensen, P.; Hamnett, A., The Oxidation of Ethylene-Glycol at a Platinum-Electrode in Acid and Base - an Insitu Ftir Study. *J. Electroanal. Chem.* **1989,** *260* (2), 347-359.
148. Chang, S.; Ho, Y.; Weaver, M., Applications of Real-Time FTIR Spectroscopy to the Elucidation of Complex Electroorganic Pathways: Electrooxidation of Ethylene Glycol on Gold, Platinum, and Nickel in Alkaline Solution. *J. Am. Chem. Soc.* **1991,** *113* (25), 9506-9513.
149. Lide, D. R., CRC handbook of chemistry and physics: a ready-reference book of chemical and physical data. 91 ed.; CRC Press: 2004.
150. Demarconnay, L.; Brimaud, S.; Coutanceau, C.; Leger, J.-M., Ethylene glycol electrooxidation in alkaline medium at multi-metallic Pt based catalysts. *J. Electroanal. Chem.* **2007,** *601*, 169-180.
151. Simões, M.; Baranton, S., Enhancement of catalytic properties for glycerol electrooxidation on Pt and Pd nanoparticles induced by Bi surface modification. *Applied Catalysis B: Environmental* **2011**.
152. Avramov-Ivic, M.; Leger, J.; Beden, B.; Hahn, F.; Lamy, C., Adsorption of Glycerol on Platinum in Alkaline-Medium - Effect of the Electrode Structure. *J. Electroanal. Chem.* **1993,** *351*, 285-297.
153. Korzeniewski, C., Infrared spectroscopy in electrochemistry: New methods and connections to UhV surface science. *Critical Reviews in Analytical Chemistry* **1997,** *27* (2), 81-102.
154. Lu, H. D.; Wheeldon, I. R.; Banta, S., Catalytic biomaterials: engineering organophosphate hydrolase to form self-assembling enzymatic hydrogels. *Protein Engineering Design & Selection* **2010,** *23* (7), 559-566.
155. Wheeldon, I. R.; Campbell, E.; Banta, S., A Chimeric Fusion Protein Engineered with Disparate Functionalities-Enzymatic Activity and Self-assembly. *Journal of Molecular Biology* **2009,** *392* (1), 129-142.
156. Wheeldon, I. R.; Gallaway, J. W.; Barton, S. C.; Banta, S., Bioelectrocatalytic hydrogels from electron-conducting metallopolypeptides coassembled with bifunctional enzymatic building blocks. *Proceedings Of The National Academy Of Sciences Of The United States Of America* **2008,** *105* (40), 15275-15280.
157. Wheeldon, I. R.; Calabrese Barton, S. A. C.; Banta, S., Bioactive proteinaceous hydrogels from designed bifunctional building blocks. *Biomacromolecules* **2007,** *8* (10), 2990-2994.
158. Kim, Y.; Banta, S., Complete Oxidation of Methanol in an Enzymatic Biofuel Cell by a Self-Assembling Hydrogel Created from Three Modified Dehydrogenases. *Angew. Chem. Int. Ed. Article In press*.
159. Sheehan, M. C.; Bailey, C. J.; Dowds, B. C.; McConnell, D. J., A New Alcohol-Dehydrogenase, Reactive Towards Methanol, From Bacillus-Stearothermophilus. *Biochemical Journal* **1988,** *252* (3), 661-666.
160. Klyosov, A., Kinetics and specificity of human liver aldehyde dehydrogenases toward aliphatic, aromatic, and fused polycyclic aldehydes. *Biochemistry* **1996,** *35* (14), 4457-4467.

161. Glatt, H.; Rost, K.; Frank, H.; Seidel, A.; Kollock, R., Detoxification of promutagenic aldehydes derived from methylpyrenes by human aldehyde dehydrogenases ALDH2 and ALDH3A1. *Archives Of Biochemistry And Biophysics* **2008,** *477* (2), 196-205.
162. Serov, A.; Popova, A.; Fedorchuk, V.; Tishkov, V., Engineering of coenzyme specificity of formate dehydrogenase from Saccharomyces cerevisiae. *Biochemical Journal* **2002,** *367*, 841-847.
163. Palmore, G.; Bertschy, H.; Bergens, S.; Whitesides, G., A methanol/dioxygen biofuel cell that uses NAD(+)-dependent dehydrogenases as catalysts: application of an electro-enzymatic method to regenerate nicotinamide adenine dinucleotide at low overpotentials. *J. Electroanal. Chem.* **1998,** *443* (1), 155-161.
164. Akers, N.; Moore, C.; Minteer, S., Development of alcohol/O-2 biofuel cells using salt-extracted tetrabutylammonium bromide/Nafion membranes to immobilize dehydrogenase enzymes. *Electrochim. Acta* **2005,** *50* (12), 2521-2525.
165. Addo, P. K.; Arechederra, R. L.; Minteer, S. D., Evaluating Enzyme Cascades for Methanol/Air Biofuel Cells Based on NAD(+)-Dependent Enzymes. *Electroanalysis* **2010,** *22* (7-8), 807-812.
166. Wu, W.-Y.; Mee, C.; Califano, F.; Banki, R.; Wood, D. W., Recombinant protein purification by self-cleaving aggregation tag. *Nature Protocols* **2006,** *1* (5), 2257-2262.
167. Shingledecker, K.; Jiang, S.; Paulus, H., Reactivity of the cysteine residues in the protein splicing active center of the Mycobacterium tuberculosis RecA intein. *Archives Of Biochemistry And Biophysics* **2000,** *375* (1), 138-144.
168. Chong, S.; Xu, M.-Q., Harnessing Inteins for Protein Purification and Characterization. In *Homing Endonucleases and Inteins*, Belfort, M.; Wood, D.; Stoddard, B.; Derbyshire, V., Eds. Springer Berlin Heidelberg: 2005; Vol. 16, pp 273-292.
169. Mills, K.; Paulus, H., Biochemical Mechanisms of Intein-mediated Protein Splicing. In *Homing endonucleases and inteins*, Belfort, M.; Stoddard, B.; Wood, D.; Derbyshire, V., Eds. Springer Berlin Heidelberg: 2005; pp 233-255.
170. Ogden, J.; Steinbugler, M.; Kreutz, T., A comparison of hydrogen, methanal and gasoline as fuels for fuel cell vehicles: implications for vehicle design and infrastructure development. *J. Power Sources* **1999,** *79* (2), 143-168.
171. Ogden, J., Prospects for building a hydrogen energy infrastructure. *Annu. Rev. Energy Env.* **1999,** *24*, 227-279.
172. Lamy, C.; Lima, A.; LeRhun, V.; Delime, F.; Coutanceau, C.; Leger, J.-M., Recent advances in the development of direct alcohol fuel cells (DAFC). *J. Power Sources* **2002,** *105* (2), 283-296.
173. Calabrese Barton, S. A. C.; Gallaway, J. W.; Atanassov, P. B., Enzymatic biofuel cells for Implantable and microscale devices. *Chemical Reviews* **2004,** *104* (10), 4867-4886.
174. Minteer, S. D.; Liaw, B. Y.; Cooney, M. J., Enzyme-based biofuel cells. *Current opinion in biotechnology* **2007,** *18*, 228-234.
175. Moehlenbrock, M. J.; Toby, T. K.; Pelster, L. N.; Minteer, S. D., Metabolon Catalysts: An Efficient Model for Multi-enzyme Cascades at Electrode Surfaces. *Chemcatchem* **2011,** *3* (3), 561-570.
176. Moehlenbrock, M. J.; Toby, T. K.; Waheed, A.; Minteer, S. D., Metabolon Catalyzed Pyruvate/Air Biofuel Cell. *J. Am. Chem. Soc.* **2010,** *132* (18), 6288-+.
177. Sokic-Lazic, D.; Minteer, S. D., Pyruvate/Air Enzymatic Biofuel Cell Capable of Complete Oxidation. *Electrochemical And Solid State Letters* **2009,** *12* (9), F26-F28.

178. Falase, A.; Garcia, K.; Lau, C.; Atanassov, P. B., Electrochemical and in situ IR characterization of PtRu catalysts for complete oxidation of ethylene glycol and glycerol. *Electrochem. Commun.* **2011**.
179. Rincon, R. A.; Lau, C.; Garcia, K. E.; Atanassov, P. B., Flow-through 3D biofuel cell anode for NAD(+)-dependent enzymes. *Electrochim. Acta* **2011,** *56* (5), 2503-2509.
180. Rincon, R. A.; Lau, C.; Luckarift, H. R.; Garcia, K. E.; Adkins, E.; Johnson, G. R.; Atanassov, P. B., Enzymatic fuel cells: integrating flow-through anode and air-breathing cathode into a membrane-less biofuel cell design. *Biosensors and Bioelectronics* **2011,** *27*, 132-136.
181. Villarrubia, C. W. N.; Rincon, R. A.; Radhakrishnan, V. K.; Davis, V.; Atanassov, P. B., Methylene Green Electrodeposited on SWNTs-Based "Bucky" Papers for NADH and L-Malate Oxidation. *ACS Applied Materials & Interfaces* **2011,** *3* (7), 2402-2409.
182. Sjoholm, K. H.; Cooney, M.; Minteer, S. D., Effects of degree of deacetylation on enzyme immobilization in hydrophobically modified chitosan. *Carbohydrate Polymers* **2009,** *77* (2), 420-424.
183. Svoboda, V.; Cooney, M. J.; Liaw, B. Y.; Minteer, S. D.; Piles, E.; Lehnert, D.; Calabrese Barton, S. A. C.; Rincon, R. A.; Atanassov, P. B., Standardized characterization of electrocatalytic electrodes. *Electroanalysis* **2008,** *20* (10), 1099-1109.
184. Rincon, R. A.; Artyushkova, K.; Mojica, M.; Germain, M.; Minteer, S. D.; Atanassov, P. B., Structure and electrochemical properties of electrocatalysts for NADH oxidation. *Electroanalysis* **2010,** *22* (7‐8), 799-806.
185. Blackwell, A. E.; Moehlenbrock, M. J.; Worsham, J. R.; Minteer, S. D., Comparison of Electropolymerized Thiazine Dyes as an Electrocatalyst in Enzymatic Biofuel Cells and Self Powered Sensors. *Journal of Nanoscience and Nanotechnology* **2009,** *9* (3), 1714-1721.
186. Barron, E. S. G.; Levine, S., Oxidation of alcohols by yeast alcohol dehydrogenase and by the living cell. The thiol groups of the enzyme. *Archives of Biochemistry and Biophysics* **1952,** *41* (1), 175-187.